# Multi-Scale Variability of Surface Circulation in the Chukchi Sea and Beaufort Sea: A Model-Based Analysis

A thesis submitted in partial fulfillment of the requirement
for the degree of Bachelor of Science in
Physics from the College of William and Mary in Virginia,

by

Danya E. AbdelHameid

Accepted

---

Advisor: Prof. Donglai Gong

---

Prof. Eugene Tracy

---

Prof. Irina Novikova

Williamsburg, Virginia
May 2018

# Contents

# Acknowledgments

Thank you to my advisor, Professor Donglai Gong, for his support throughout this project.

Thank you to Professor Eugene Tracy and Professor Novikova for their thoughtful feedback. And, finally, thank you to the Physics Department for a challenging but very rewarding three years.

# List of Figures

**Abstract**

The surface circulation regime in the region encompassing Barrow Canyon and extending to Mackenzie Trough in the Beaufort and Chukchi Seas is largely determined by wind-driven circulation and this circulation is highly variable in the summer-to-fall transition period spanning July to November. Previous work has identified wind-induced reversal of the Beaufort Shelf Break Jet in the presence of intensified easterly winds and the results of this work extend this observation to suggest that wind-induced reversal occurs on a spectrum and is dictated largely by a balancing of the intensification of easterly winds as well as variation in the inflow through Bering Strait. Additionally, this work has found that intensified northward and southward winds promote the presence of eddy-like features in the interior of the Beaufort Gyre. Overall, these results suggest that the local circulation regime is highly variable and driven by variation in the wind regime, and therefore varies on timescales similar to that of the prevailing wind regime.

# Chapter 1

# Introduction

The Arctic region (see Figure 1.1) , generally defined as the region encompassing the Arctic Ocean, adjacent seas, and parts of Alaska, Northern Canada, Finland, Greenland, Iceland, Norway, Russia and Sweden, is an area of critical importance to a variety of communities and stakeholders, and the dynamics of the region have far-reaching implications on a variety of social, cultural, economic, biological, and broadly, global affairs. Much of this interest is a result of the rapidly changing environmental conditions in the region, with changes and transformations occurring on both short and long time scales, ranging from weekly or monthly scales, to annual and further, decadal scales.

Further, the Arctic region is connected to and dependent on the climatic conditions occurring at lower latitudes, which implies that as the rest of the Earth undergoes rapid, complex changes in the face of a changing climate, the Arctic region will also undergo similar or related changes. We have already begun to see some of these changes, as atmospheric and oceanic temperatures have increased and sea ice volume and extent has decreased within the last 20-30 years [11]. Further, many studies have pointed to an amplification of environmental changes in the Arctic region as compared to lower latitudes, suggesting that climatic changes at lower latitudes may have profound impacts on the Arctic region.

Of particular importance are the dynamic, complex changes occurring in the Arctic Ocean and the influence of these changes on ocean circulation regimes on local (i.e. in the Arctic region) and global scales (i.e. at lower latitudes) (see Figure 1.1). The ocean circulation regime and the associated transport of various water masses in the Arctic Ocean can strongly impact global heat and freshwater budgets, making this a key area of focus in our broader understanding of the biological, physical, and environmental processes and systems in the Arctic region.


Figure 1.1: Primary Currents in the Arctic Ocean. [2]

This thesis will focus on utilizing a model-based approach to elucidate the modulating effects of the wind regime on the regional circulation regime, near Barrow

Canyon and extending downstream to Mackenzie Trough, with a particular focus on the state of circulation in the surface layer (upper 200 meters) during the summer and early fall seasons, as these transitory seasons are expected to be altered most notably in the face of a changing climate, with the extension of the summer melt season and the delay of surface ice formation due to rising temperatures. The product of this work will be a conceptual framework of the dynamics and driving forces of surface-layer circulation in the region encompassing Barrow Canyon, Mackenzie Trough, and the Beaufort Gyre, and broadly, the Beaufort and Chukchi Seas (see Figure 1.2).

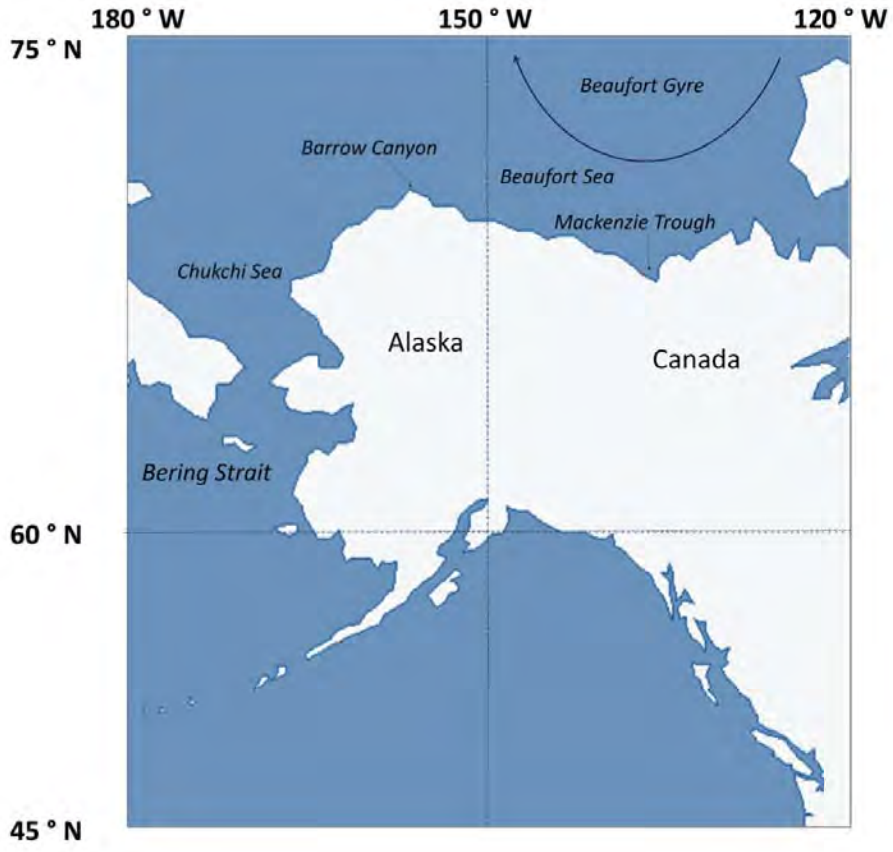


Figure 1.2: Overview of Study Area

# Chapter 2

# Overview of the Forces, Mechanisms that Drive the Transport of Water Masses

## 2.1 Equations of Motion

The forces driving the circulation of water masses can be split into two components: wind driven circulation (facilitated by tangential stress at the ocean surface due to the prevailing wind regime) and thermaline circulation, fueled by buoyancy driven convection transport. Wind driven circulation is generally considered to be the dominant mechanism of transport in the surface layer, while thermohaline circulation is considered to be the dominant mechanism of transport in the deep ocean, but this distinction is not exclusive and surface-layer circulation is also in part facilitated by the same buoyancy driven convection that drives deep-water circulation.

The surface-layer circulation regime and the associated equations of motion are given by solving the Navier Stokes equation (in three dimensions) and assuming the condition of incompressibility (i.e. the continuity equation). In cartesian coordintes (u, v, w), the full equations of motion for a parcel of fluid are given by:

$$\frac{\partial}{\partial t}(v) = -\frac{1}{\rho}\frac{\partial P}{\partial x} + A_H\left(\frac{\partial^2}{\partial x^2}(u) + \frac{\partial^2}{\partial y^2}(u)\right) + A_V\left(\frac{\partial^2}{\partial x^2}(u)\right) + fv \tag{2.1}$$

$$\frac{\partial}{\partial t}(u) = -\frac{1}{\rho}\frac{\partial P}{\partial y} + A_H\left(\frac{\partial^2}{\partial x^2}(v) + \frac{\partial^2}{\partial y^2}(v)\right) + A_V\left(\frac{\partial^2}{\partial x^2}(v)\right) + fu \tag{2.2}$$

$$\frac{\partial}{\partial t}(w) = -\frac{1}{\rho}\frac{\partial P}{\partial z} + A_H\left(\frac{\partial^2}{\partial x^2}(w) + \frac{\partial^2}{\partial y^2}(w)\right) + A_V\left(\frac{\partial^2}{\partial x^2}(w)\right) - g \tag{2.3}$$

Where,

- $\frac{1}{\rho}\frac{\partial P}{\partial z}$ = the pressure gradient force in each direction due to differential pressure fields within a fluid (in this case, in the 'z' direction. ($\rho$ is the density of the water mass)
- $fv$ = the Coriolis force due to the rotation of the earth
- $A_H\left(\frac{\partial^2}{\partial x^2}(v) + \frac{\partial^2}{\partial y^2}(v)\right) + A_V\left(\frac{\partial^2}{\partial x^2}(v)\right)$ = force due to friction in the horizontal ($A_H$) and vertical directions ($A_V$) the
- $g$ = the gravitational force
- $A_H$ is the horizontal eddy viscosity
- $A_V$ is the vertical eddy viscosity

The balance and interaction of these forces drives the acceleration of water masses in the surface layer and produce what are commonly referred to as geostrophic currents, and in a dominantly wind-driven regime, this facilitates the movement of water masses through a mechanism called Ekman Transport [citation], which will be discussed below.

## 2.2 Geostrophic Currents

In the broadest sense, the transport of water masses in the ocean is driven by the geostrophic balance, or the balancing of the pressure gradient force and coriolis force across the ocean and atmosphere. This balance assumes that frictional effects are negligent and a non-accelerating flow, an assumption that is mostly valid when considering large-scale flow on longer timescales (i.e. longer than a day). Further, if we assume a vertically homogeneous, well mixed water column, we can solely consider the horizontal geostrophic balance (i.e. we can ignore the 'w' component force balance), which is given by:

$$\frac{1}{\rho}\frac{\partial P}{\partial y} = fu \tag{2.4}$$

$$\frac{1}{\rho}\frac{\partial P}{\partial x} = fv \tag{2.5}$$

Geostrophic currents (resulting from Geostrophic balance), will yield transport that is 90 ° to the left of the Coriolis force in the Northern Hemisphere, and 90 ° to the right of the Coriolis force in the Southern Hemisphere.

## 2.3 Ekman Transport

Geostrophic currents often do not occur under conditions where we can assume that the frictional forces are neglible. If we consider the frictional component, the geostrophic balance becomes slightly modified, resulting what is called Ekman Transport and associated upwelling/downwelling within a near-surface Ekman layer.

If we assume that a homogenous, infinitely deep ocean, steady flow, no pressure gradients, no horizontal friction, constant vertical eddy viscosity (Az) and a constant wind stress at the ocean surface equation equations 2.1-2.3, reduce to a balance of

the coriolis force and the force due to vertical friction within the water column. If we assume that the solution to this second order differential equation is a linear combination of sine and cosine functions in the horizontal directions with an exponentially decaying amplitude in the vertical direction and apply the boundary conditions (i.e. at the surface w=0, the surface velocity is that of northerly wind and in the deep ocean, w=$\infty$, the velocity is 0), the equation reduces to:

$$u_E = V_0 e^{\frac{\pi}{D_E}w}\left(\cos\frac{\pi}{4} + \frac{\pi}{D_E}w\right) \tag{2.6}$$

$$v_E = V_0 e^{\frac{\pi}{D_E}w}\left(\sin\frac{\pi}{4} + \frac{\pi}{D_E}w\right) \tag{2.7}$$

Where,

- $u_E$ = the horizontal Ekman velocity
- $v_E$ = the vertical Ekman velocity
- $D_E = \pi\sqrt{\frac{A_Z}{f}}$ = the Ekman depth, where $f$ is the coriolis parameter given by $f = 2\Omega\sin\phi$ ( is the latitude of the location of interest, and $\Omega$ is the rotation rate of the Earth
- $A_H$ is the horizontal eddy viscosity

The sine and cosine components of the Ekman velocity solutions result in a flow with a vertically varying direction throughout the water column, producing a spiral flow that is maximally deflected to the right with increasing depth, known as the Ekman spiral (see Figure 2.1) . This differential deflection results in a net transport that is 90 ° to the right of the direction of flow of the prevailing wind regime in the northern hemisphere and 90 ° to the left of the the direction of flow in the southern hemisphere.

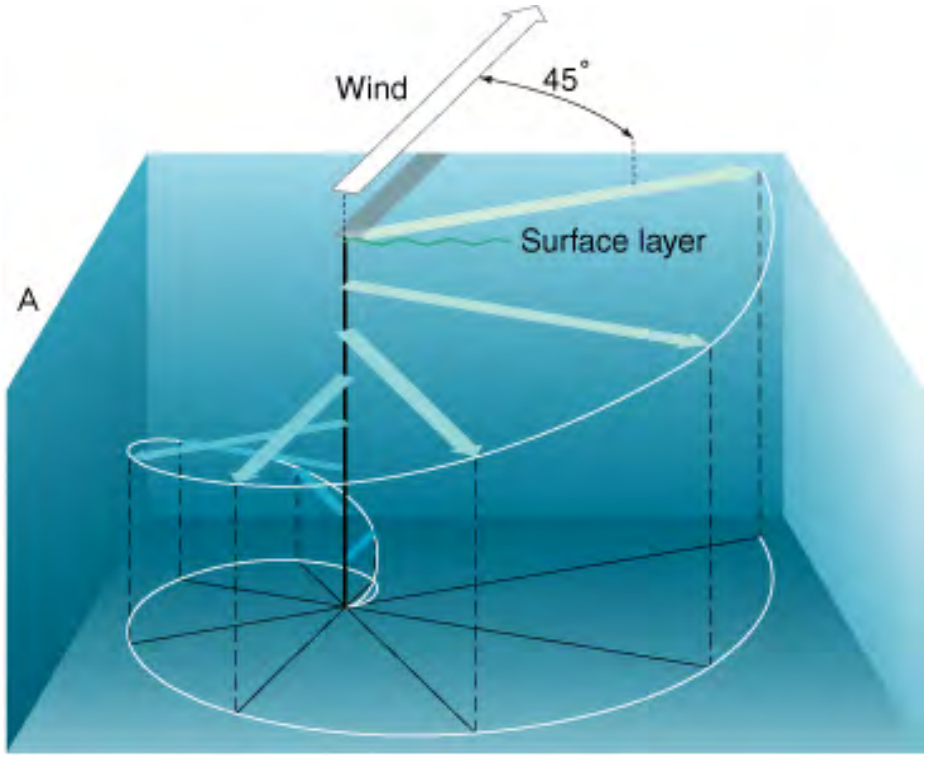


Figure 2.1: Schematic of Ekman Spiral . [12]

Within a particular region or locale, the wind regime can be incoherent, with local variance in direction, magnitude, etc. In the Northern Hemisphere, the convergence of Ekman-layer driven transport can facilitate Ekman pumping, in which water is pumped into a central junction, resulting in a mound or collection of water at the ocean surface, resulting in down welling due to the weight of the accumulated water and anticyclonic circulation, characterized by an overall surface current that is directed in a clockwise loop (see figure 2.2) .

Similarly, a divergence in the Ekman-layer driven transport can facilitate a gap or low in the sea surface, as water is pumped away from a central junction, leading to upwelling as the underlying water masses well up to fill the gap in the sea surface (this is also a consequence of the condition of incompressibility and the continuity equation). Ekman divergence or Ekman suction generally produces cyclonic circula-

tion, characterized by an overall surface current that is directed in a counterclockwise loop.

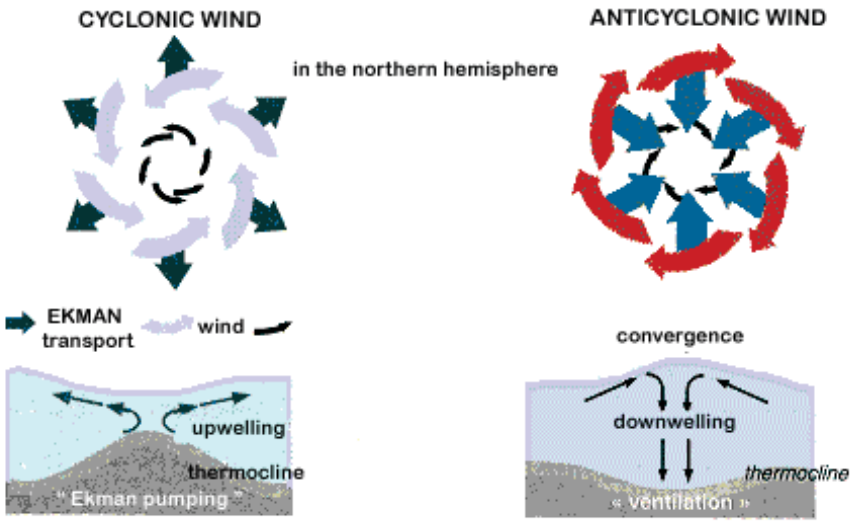


Figure 2.2: Ekman Convergence/Divergence . [12]

Overall, the surface layer circulation regime in the Beaufort/Chukchi Seas is heavily driven by the prevailing wind regime and Ekman Transport (and the associated upwelling/downwelling) is an important process in the resulting circulation regime.

# Chapter 3

# Proposed Surface-Layer Circulation Regime

On the whole, the circulation regime in the Arctic Ocean is influenced by changes in salinity (as driven by freshwater inputs/outputs and ice formation) and in the surface layer, it is dominated by the regional wind regime (as driven by the Beaufort high, a semi-permanent high pressure system that sits over the Beaufort Sea) [15]. The basin-wide temperature and salinity structure is strongly salinity stratified, allowing primarily for shallow, local-scale convection across the entirety of the basin (i.e. much of circulation in the basin occurs in smaller near, shore locales), however the circulation regime can exhibit much more variability and be significant along/near the shelf seas (i.e. the Chukchi Sea and Beaufort Sea).

The influence of wind on the surface-layer circulation regime within this region is the primary factor in determining the outcome of various water masses and Lin et al. [7] has identified that during the summer months, the wind regime is the main driver of upwelling (a primary mechanism of transport, transformation of the surface-layer), or the upwards displacement of deeper waters due to a divergence in the surface layer, along the shelf seas.

Along the shelf sea, the surface-layer circulation regime is dominated by a highly variable coastal current and dynamic Pacific-Ocean sourced offshore currents (see

Figure 3.1). Previous work has proposed that the coastal current runs parallel to the Alaskan/Canadian coast (from west to east) and along the near-coast boundary of the Beaufort Shelf and [3] has identified that the current (referred to as the Western Boundary Current, the Alaskan Coastal Current, or the Beaufort Shelf Break Jet in the literature. Here, I will hereby refer to this current as the Beaufort Shelf Break Jet (BSBJ)), and note that it is surface intensified during the summer months, making it a crucial component of summer-time/early fall-time, surface-layer circulation. Further, during the summer months, the BSBJ provides a significant flux of warm, fresh (i.e. low salinity), coastal water along the shelf and at times, offshore, towards the boundary of the Beaufort Gyre. The BSBJ is highly dependent on the wind regime, which is itself dynamic and shifting, and Lin et al. [8] have identified based on six years of mooring data from the Alaskan Beaufort Sea Slope, that the BSBJ can reverse direction under intensified, easterly winds (winds flowing from the east towards the west), thereby promoting a broader, regional surface layer circulation regime that is highly dependent on the daily, seasonal wind regime.

The Pacific-Ocean sourced, offshore currents generally are derived from the poleward transport of fresh and seasonally warm Pacific water through the Bering Strait. Previous studies have measured a mean annual transport rate of 0.8-1 Sverdrup (1 Sverdrup = $10^6 m^3 s^-1$), which equates to approximately 4-5 times the discharge rate of the Amazon River, highlighting the significance of exchange flow through this pathway in the overall circulation regime [21]. The fate of the Pacific-Ocean water flowing in through Bering Strait is highly variable and can fluctuate on the order of days, and this variability can alter the interaction and contribution of these offshore currents with the BSBJ and broadly, the regional surface-layer circulation regime.Previous work has determined that the strongest flow is in the summer months, during which the southward winds are the weakest [19].

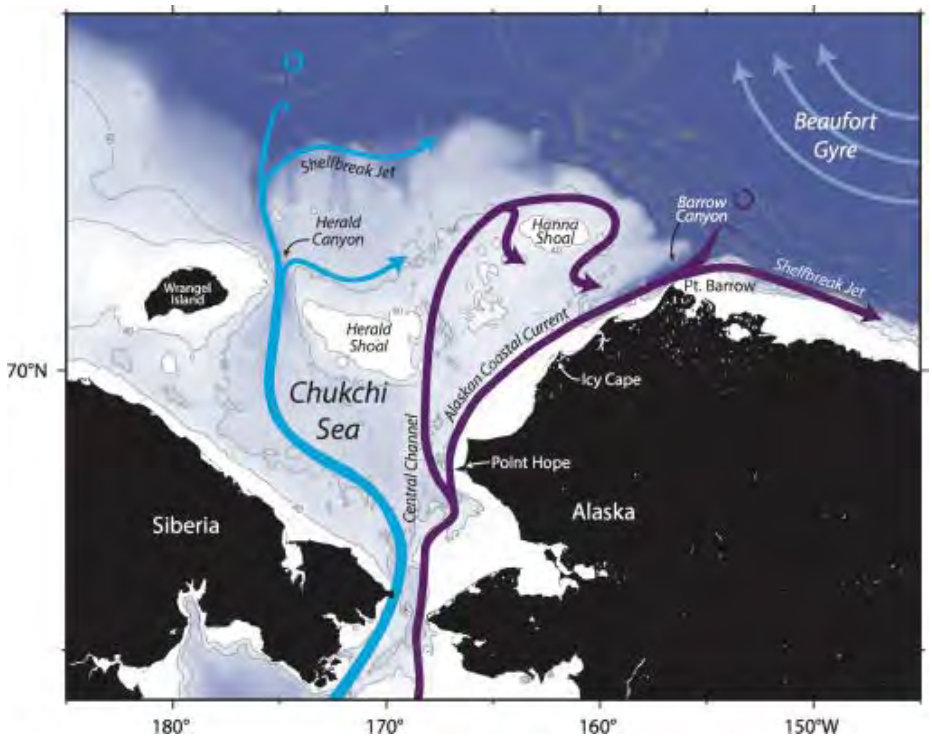


Figure 3.1: The Alaskan Coastal Current, Shelf Break Jet (referred to in this work as the Beaufort Shelf Break Jet, BSBJ) is shown in purple and is a derivative of the total inflow through Bering Strait. Gong and Pickart also identify a secondary Shelf Break jet, shown in cyan and also depicted as emanating from the total inflow through the Bering Strait and depict the anticyclonic Beaufort Gyre . [5]

In addition to the along-coast, shelf-based circulation facilitated by the BSBJ and the Pacific-Ocean sourced offshore surface currents, another crucial factor in the regional surface-layer circulation regime is the Beaufort Gyre, a mound of fresh water (FW) that accumulates in the gyre through the process of Ekman pumping [15]. The FW content of the gyre varies annually and seasonally, however previous studies have estimated that the gyre contains upwards of 45,000 km3 of FW [1].

Proshutinsky et al. [16] has suggested that the FW content of the gyre is accumulated in the winter months (defined here as November to February) and released or expelled during the summer months (defined here as June to August) (see Figure 3.2). During the winter, the wind regime is configured in such a way that drives the

ice and ocean in a clockwise rotation (hereby referred to as anticyclonic rotation), creating a system driven by Ekman pumping, wherein water is pumped towards the interior of the gyre, causing a depression of the underlying water mass and the formation of a mound of freshwater atop the sea surface. The source of the FW is varied and includes river runoff, inflow from the Atlantic and Pacific Oceans, in/outflows through Bering Strait and Fram Strait, as well as the contributions from the melting of glacial ice and the formation of sea ice [6].

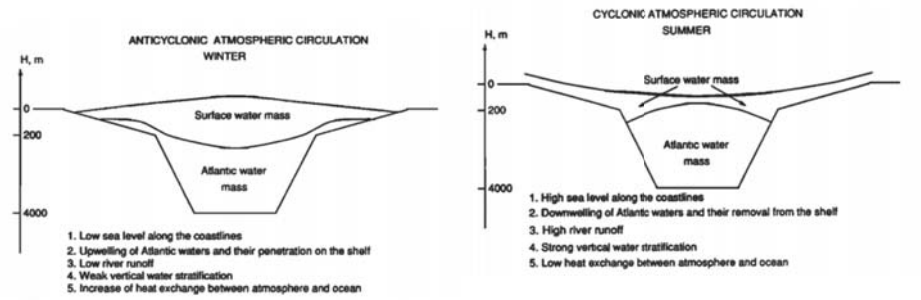


Figure 3.2: Adapted from Proshutinsky and Johnson, 1997. The panels depict the vertical water column structure of the gyre during an anticyclonic and cyclonic regime. In the upper panel, the accumulated mound atop the sea surface is evident, producing a net high in sea surface level during an anticyclonic regime, whereas a slight dip or low in sea surface level is produced during a cyclonic regime, as a portion of the freshwater that accumulated during the winter months is expelled from the gyre . [18]

Conversely, during the summer months, Proshutinsky et al. [16][17] propose that weakened anticyclonic wind conditions or full out reversal of the wind regime (i.e. shifting from anticyclonic to cyclonic rotation or clockwise rotation), promote the expulsion or release of the FW accumulated in the Beaufort gyre, creating a flux of FW that then propagates downstream of the gyre and potentially disrupting convective overturning on a global scale [1]. This cyclical oscillation from an anticyclonic, FW accumulating regime to a cyclonic, FW expelling regime is proposed to occur on a decadal timescale, however recent work by Proshutinsky et al.(2015) [17], supported

by in situ data, suggests that there is a cessation in the oscillation and transition from an anticyclonic regime to a cyclonic regime, locking the region into a prolonged anticyclonic regime. Proshutinsky et al. (2015), suggests that this cessation is possibly due to the rapidly increasing freshwater flux from the Greenland Ice Sheet (GIS), that inhibits deep convection, ultimately promoting atmospheric cooling and limiting the development of atmospheric conditions that can promote cyclonic-winds. Further, Proshutinsky et al. (2015) has suggested that in the face of a changing climate and rapidly increasing freshwater flux from the GIS due to increased melting, the oscillatory nature of the anticyclonic/cyclonic regimes will deviate from previously established trends, producing a new mode of Arctic circulation that is unprecedented.

While a detailed investigation into the mechanisms that modulate the oscillation from an anticyclonic regime to a cyclonic regime are beyond the scope of this project, Proshutinskys projection of the state of Arctic circulation and broadly, the Arctic Ocean system, highlight the importance of the Beaufort Gyre and its associated surface currents in modulating regional and global climate variations.

# Chapter 4

# Data and Methods

This thesis primarily employs a model-based approach to determining the modulatory effects of the wind regime on the regional surface-layer circulation regime in/near the Beaufort Gyre and the Alaskan/Canadian Coast. Specifically, this thesis utilizes sea surface height and surface current (defined here as the upper 200 meters) outputs from the Hybrid Ocean Coordinate Model (HYCOM) and vector wind outputs from the National Centers for Environmental Prediction (NCEP) North American Regional Reanalysis (NARR) model.

The HYCOM model is a community-based data assimilative, primitive equation model, that is,the model utilizes the Navier-Stokes equations and an 'equation of state' which relates the temperature and salinity of a fluid parcel to its density to determine ocean circulation. Further, HYCOM model is a general ocean circulation model that applies a hybrid, generalized, coordinate system, allowing for greater vertical resolution near the sea surface and along shallow, coastal regions [20]. Additionally, the HYCOM model is a data assimilative model and therefore the model is informed by sea surface height data from altimetry, sea surface temperature data derived from satellite measurements, as well as in-situ data. Model runs are executed at the Navy Department of Defense Supercomputing Resource Center and were accessed via the THREDDS protocol. More information regarding the specifications of the HYCOM

model can be accessed online at HYCOM.org.

For the purpose of this thesis, monthly averaged sea surface height (meters) and surface current (averaged for the upper 200 meters of the water column) vector HYCOM model outputs were referenced for the months of June to November from 2007 to 2017.

Similarly, the NCEP NARR model is a data assimilative atmospheric model, that provides high resolution outputs of atmospheric variables across a wide range of temporal and spatial scales. This thesis references seasonal, daily, and monthly averaged NCEP NARR vector wind output at 1000 hPa for the relevant region of interest for the months of June to November from 2007 to 2017.

Additionally, this thesis incorporates in-situ monthly mean volume transport data from the Bering Strait, compiled by the Polar Science Center, Applied Physics Laboratory at the University of Washington [21]

The model-based approach of this thesis will provide a broad perspective into the dynamics of the surface layer circulation during the summer-to-fall transition period. While there has been much work to characterize the circulation during the summer months, it is logistically and physically challenging to consider the circulation in summer-to-fall transition period and further, in the winter, as the formation of sea ice poses unique challenges to in-situ data collection. This thesis will provide a foundation for further work and data collection that seeks to investigate the dynamics of circulation during the transition from fall to winter.

# Chapter 5

# Results, Discussion, Suggestions for Future Work

## 5.1 Results

### 5.1.1 Strength, duration, dynamics of the Beaufort Gyre

The configuration of the Beaufort Gyre remains relatively stable on an annual timescale and varies considerably inter-annually in accordance with the state of the Beaufort High (the semi permanent high-pressure system established over the Beaufort Sea), the sea level pressure field, and the resulting wind regime driven by these components (see Figure 5.1). During years with a particularly strong wind regime (peak wind speeds of 4.6-8 m/s), the Gyre becomes fully formed, exhibiting a strong, and well-defined Gyre edge, characterized by the presence of a strong, unidirectional current, comprised of contributions from the previously identified BSBJ and other Bering Strait-derived currents. Alternatively, during years with a weak wind regime (peak wind speeds of 0.8-2 m/s), the Gyre edge is poorly defined and instead populated by a series of persistent, small-scale circular currents and small-scale eddies. While there is variation in Gyre strength and dynamics on a year-to-year basis, there does not appear to be significant variation in the Gyre within a particular season (i.e. July-November of a single year) and the Gyre dynamics appear to exhibit a sort

of stability or equilibrium within a season, as the Gyre conditions at the onset of the summer season (i.e. those in July), are maintained throughout the duration of the season, as they are driven primarily by the wind regime, which varies daily but remains somewhat consistent throughout the season in each year referenced in this study.

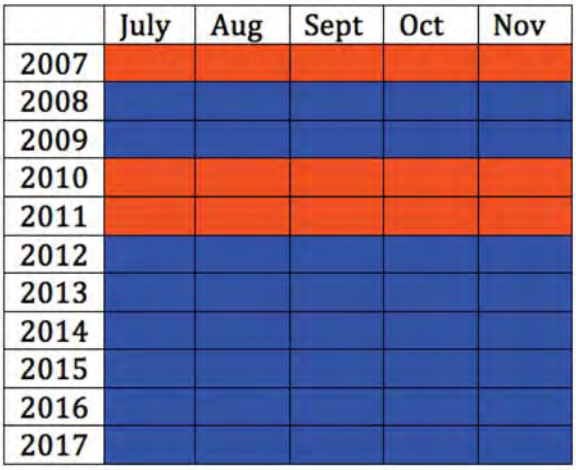


Figure 5.1: Gyre Strength - July-November, 2007-2010.'Weak' gyre conditions are denoted in blue and 'strong' gyre conditions are denoted in orange.

### 5.1.2 Reversal of the BSBJ Current

In agreement with the findings of Lin et al. (2018), this thesis has also found that under intensifying easterly winds (i.e. winds flowing from east to west), the BSBJ is susceptible to a reversal of direction and may switch directions of flow from east to west (in accordance with the prevailing wind regime), as opposed to the west to east flow catalogued by multiple previous studies [3] [5]. The reversal of BSBJ occurs most commonly (i.e. with a higher frequency) in the months of September, October, and November within the period of study (2007-2017). The exceptions to this observance are characteristically scenarios in which the easterly wind strength is insufficient to

facilitate reversal of the BSBJ (empirically determined to be 4.5-6 m/s) or all together the prevailing wind regime is dominated by westerly winds (i.e. winds flowing from west to east).

Examples of these BSBJ-reversal-limiting conditions can be found in the September (2010) and September (2016) scenarios, where the wind regime is dominated by easterly winds (albeit, weaker than the threshold required for reversal of the BSBJ) or entirely westward winds, respectively. This exception further suggests that the BSBJ reversal is strongly coupled to the strength of incoming easterly winds. A detailed catalogue of scenarios in the dataset that exhibit BSBJ reversal due to intensified easterly winds is included in Figure 5.2.

While this study did observe BSBJ reversal due to intensifying easterly winds in accordance to the results of Lin et al. (2018) [8], I extend on the characterization of this reversal to suggest that the occurrence of the BSBJ current reversal is not discrete but rather, it is continuous, with reversal occuring on a continuum (with endmembers of full reversal and no reversal). Further, my analysis suggests that the reversal of the BSBJ is highly dependent on the inflow through Bering Strait, with the quantity of inflow (and more specifically, periods of anomalously low or high inflow) exerting an influence on the outcome of the BSBJ and the overall surface layer circulation regime. Additionally, there appears to be a junction in the reversal outcome centered near Barrow Canyon, with the BSBJ exhibiting different outcomes on either side of the Canyon, dependent on the extent of intensification of the easterly-winds. I identify three possible scenarios along this spectrum: no reversal (occurring in weakly easterly wind conditions), partial reversal, and full reversal and propose that the occurence of each scenario is jointly modulated by the strength and intensity of the inflow through Bering Strait, as well as the strength and intensity of the prevailing wind regime.

The full reversal scenario occurs primarily in October and November (with one

occurence in September 2015), when the wind regime is at its peak and wind strength is maximal (see Figure 5.2). During a full reversal scenario, the BSBJ current experiences a reversal in direction (presuming that eastward flow is the default direction of flow), and is directed from east to west (i.e. a westward flow).

Conversely, the partial reversal scenario is characterized by a BSBJ that has a junction near Barrow Canyon, with the current traversing from west-east on the left hand side of the junction, and east-west on the right hand side of the junction. This scenario occurs primarily in July, with some instances of occurence in August (2010, 2014), September (2007), and November (2014).

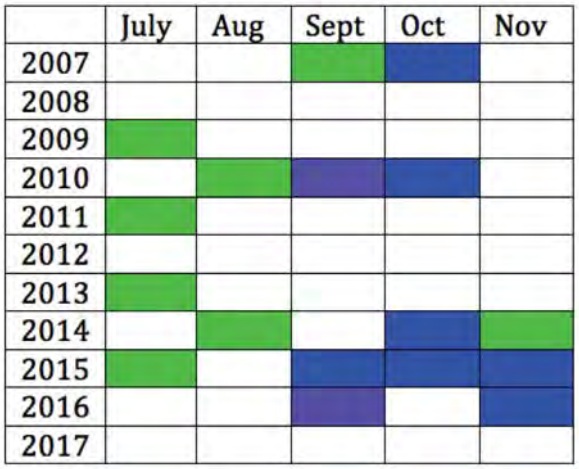


Figure 5.2: Reversal of the BSBJ - July-November, 2007-2010.'Full reversal is denoted by blue, partial reversal is denoted by green, no reversal (in the presence of intensified easterly winds) is denoted by purple.

### 5.1.3 Eddy-Inducing Wind Regimes

Various scenarios in the dataset have suggested that pole-directed (northward) and anti-pole-directed (southward) dominated wind regime promote the formation of small scale eddies (and more generally, circular circulation features) in the interior of the basin and generally within the vicinity of the Beaufort Gyre. The eddy-like features

presumably exist on weekly timescales, as they are persistent enough to be resolved through the sieve of a monthly average. The occurrence of these eddy-like features occurs primarily in October and November and are not limited by gyre strength, as eddy-like features appear in both strong and weak gyre conditions. Additionally, the presence of eddy-like features occurs earlier in the season in 2013-2017, with eddy-like features appearing in July, August (see Figure 5.3).

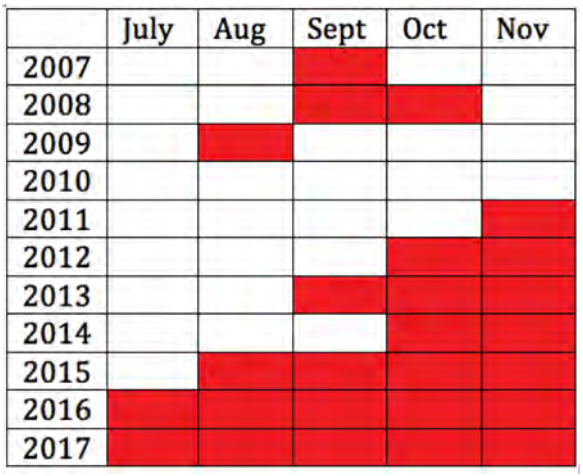


Figure 5.3: Formation of 'eddy-like' features near the boundary and interior of the Gyre - July-November, 2007-2010.The occurence of eddy-like features is denoted in red.

## 5.2 Discussion

### 5.2.1 Dynamics and Configuration of the Beaufort Gyre

While the configuration and state of the Beaufort Gyre remain relatively stable within a season, there are notable occurrences of eddy-like features and generally, complexity, within the interior of the Basin and Gyre under conditions of intensified northward and southward winds. Of particular interest is September 2008, in which the southern boundary of the Gyre experiences much instability over a very short time scale ( 1-2 months). Within this period, there is a significant change in the wind regime,

with intensification in the southward wind components, (peak wind speeds of 4.7-6 m/s) particularly near the Bering Strait. This occurrence may possibly suggest that intensified southward/northward winds promote the presence of eddy-like features, further implying that the prevailing wind regime is a primary component in the overall circulation outcome and more importantly, that the circulation is highly coupled to the wind regime and therefore, can vary on similar timescales.

### 5.2.2 Reversal of the BSBJ

The overall circulation regime in the region encompassing the Beaufort and Chukchi Seas is strongly driven by the prevailing wind regime and modulated by variation in the inflow through Bering Strait. Previous work has suggested that variation in the wind regime (particularly in the intensification of easterly winds) is likely a significant component in the reversal of the BSBJ [8]. The results of this work are in line with this finding, as reversal of the BSBJ occurs exclusively under conditions of strongly intensified easterly winds, where the threshold for sufficiently strong wind appears to be determined through a negotiation of the prevailing wind regime and the inflow through Bering Strait.

The inflow through Bering Strait is highly variable and can vary on daily to weekly time scales, with a a monthly mean inflow of 1.054 Sv (+/- 0.4238 Sv) for the months of July to November, with decreased flow (i.e. one standard deviation below the the mean) occurring in September, October and November, however the flow varies notably within a particular season and interannual. Notably, the occurrence of the full reversal scenario coincides with months of decreased inflow through Bering Strait, suggesting that there is some element of coupling and negotiation between the inflow and the prevailing wind regime that modulates the reversal outcome.

Specifically, the results of this thesis suggest that the full reversal scenario is mod-

ulated by the strength of the inflow through Bering Strait and the strength/intensity of the prevailing wind regime (as influenced by the Beaufort High) and this work proposes that full reversal occurs either in the case of a weakly intensified inflow through Bering Strait and a strongly intensified wind regime, or an averagely intensified inflow through Bering Strait and an anomalously strong wind regime.

The full reversal scenario occurs when there are significantly strong easterly winds present, creating a surface wind stress (the shear stress exerted by the wind on the water surface) that is sufficient to facilitate wind-driven transport that is anti-parallel to the pre-existing surface-layer circulation regime (which in this context, is characterized by west-to-east flow of the BSBJ). In this configuration, the sufficiently strong easterly wind strength is informed by the incoming inflow through Bering Strait, and more specifically, the quantity of volume transport and the time-scale in which it occurs. Here, the threshold for the classification of a sufficiently strong easterly wind is informed by the quantity of inflow through Bering Strait, as a stronger, intensified inflow would require a stronger, intensified wind regime to facilitate reversal. This dependence is exemplified in the August (2015), September (2015), October (2015), and November (2015) scenarios, which all exhibitfull reversal, however under vastly different inflow conditions and wind regimes, suggesting that the local balance of the transport driven by the prevailing wind regime and the inflow through Bering Strait is highly local and dependent on the local and large-scale circulation (and more importantly, the resulting pressure gradients), which may vary widely from year to year.

Additionally, in the case of partial reversal, the outcome is a segmentation of the BABJ, characterized by a west-east segment on the near-strait side of Barrow Canyon and a east-west segment on the far-strait side of Barrow Canyon. The current segments converge offshore of Barrow Canyon and are incorporated into the larger Beaufort Gyre edge current.

This segmentation of the current is most probably the result of the differential speed of the surface current, with the current being faster and intensified in the region in close proximity to the Bering Strait, that is, the left hand side of the junction, and a slowed down, calmer surface current further from the junction, on the right hand side. The differential speed and intensity of the currents facilitates two very different interactions with the incoming easterly wind, as the current on the right hand side of the junction is more readily reversed, while the left hand side of the junction is not, leading to a reversal outcome that is mirrored with respect to the junction. The partial reversal occurs most frequently in circumstances of higher than average inflow (approximately one standard deviation greater than the mean) and a generally climatologically weak wind regime (such as that seen in the months of July, August, during which the wind regime is broadly weak, with inadequate easterly winds). The coupling of an increased inflow through Begin Strait, along with a weakened wind regime facilitates a larger gradient in the surface current speed and intensity, potentially resulting in a partial reversal outcome.

While the coincidence of full reversal and partial reversal scenarios with months of decreased/increased inflow through Bering Strait may also be a product of large scale differences in the pressure gradient, as an increased easterly wind simultaneously impacts the dynamics of the flow through Bering Strait as well as the BSBJ, making it difficult to absolutely discern the modulating effects of one component on the other. However, regardless of the specifics of this coupling, the coincidence of these scenarios with months of decreased/decreased inflow further suggests that on the whole, the prevailing wind regime is a major component of the circulation in this region.

## 5.3 Suggestions for Further Work

This thesis offers a broad conceptual view of the impact of the prevailing wind regime on the regional surface circulation near the Beaufort and Chukchi Seas. While this analysis has determined that the circulation is strongly coupled to the wind regime (and more broadly, changes in atmospheric conditions) and therefore can vary on timescales that are characteristic of variation in the wind regime, there remains a larger question at hand: are we transitioning into a New Arctic? That is, is the circulation regime established through this analysis characteristic of the circulation regime that will prevail as a result of a changing climate? The preliminary results of this thesis subtly suggests that there has been a broad-scale shift of the circulation regime, however future work should establish a long-term regional climatology for the region and further probe the variation of the circulation regime from the climatological mean over coarser timescales, as it is evident that the circulation regime varies on time scales similar to that of the wind regime. Additionally, future work should extend this analysis to consider the circulation at depth, particularly near key bathymetric features, such as Barrow Canyon, Mackenzie Trough, and broadly, near the shelf break and basin interior.

# Appendix A

# HYCOM, NCEP NARR Model Outputs

## A.1 Sea Surface Height, Surface Current HYCOM Model Outputs

Note: the color bar displays sea surface height (meters), measured relative to the geoid. The vector arrows display the surface current (i.e. the upper 200 m).

## A.2 NCEP NARR Vector Wind Outputs

Note: Vector wind is displayed in m/s.

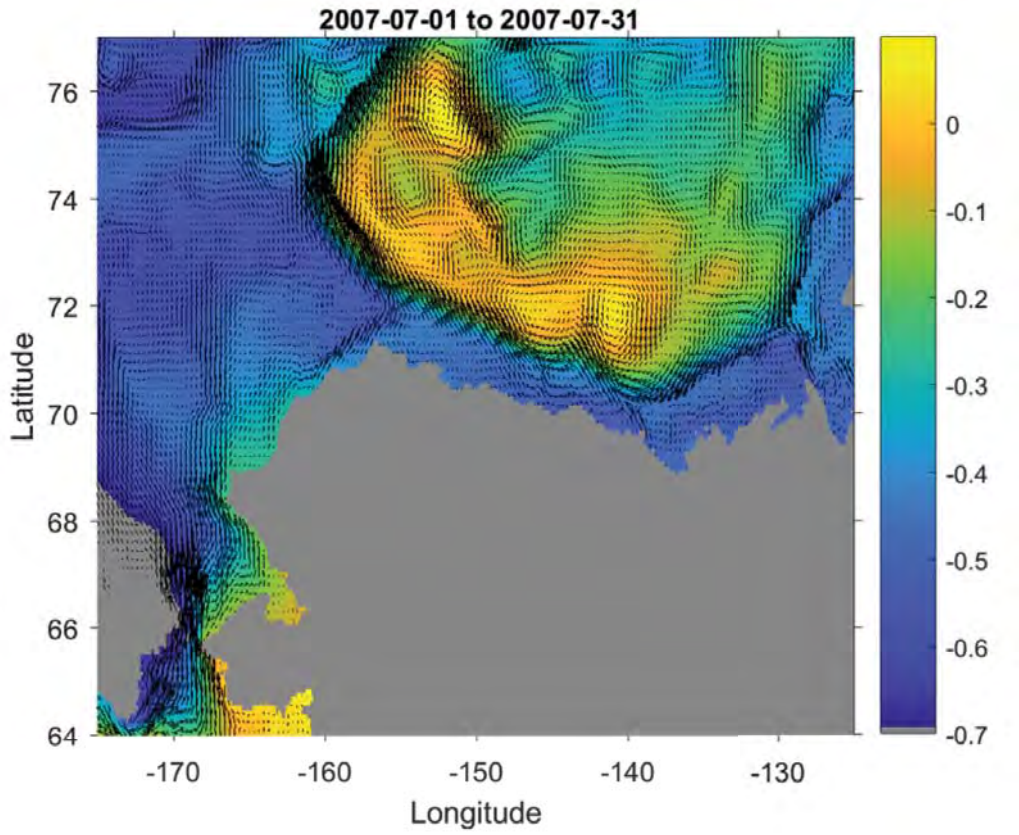


July 2007

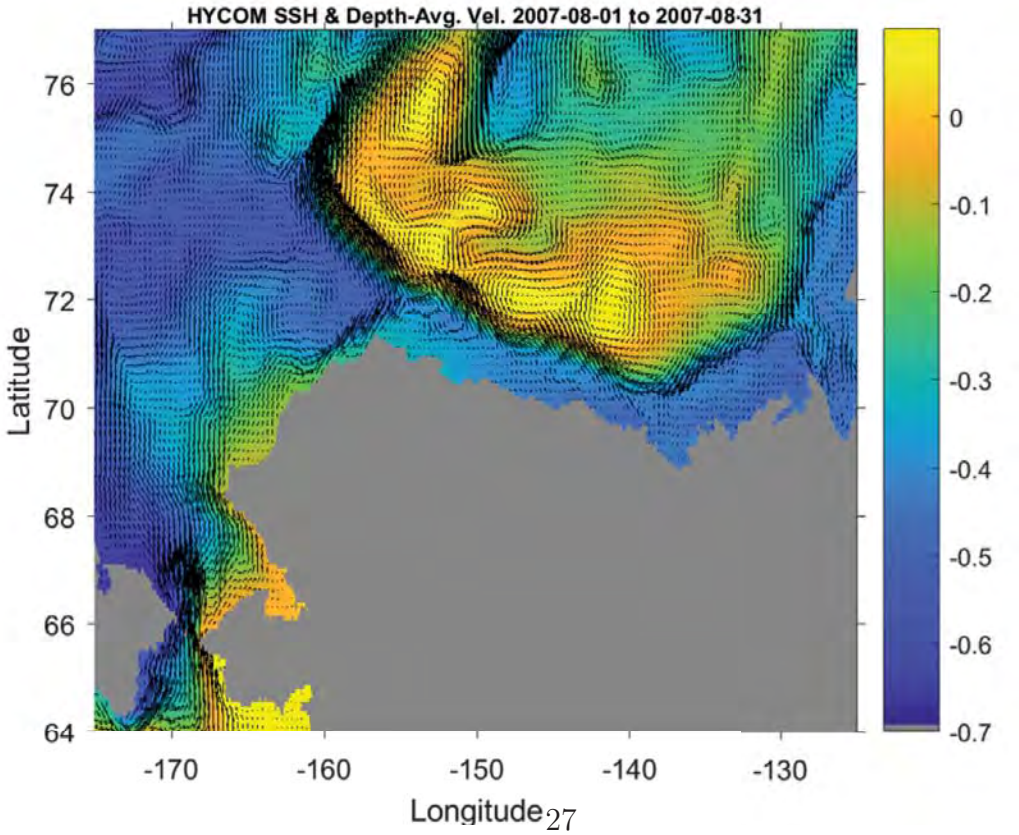


August 2007

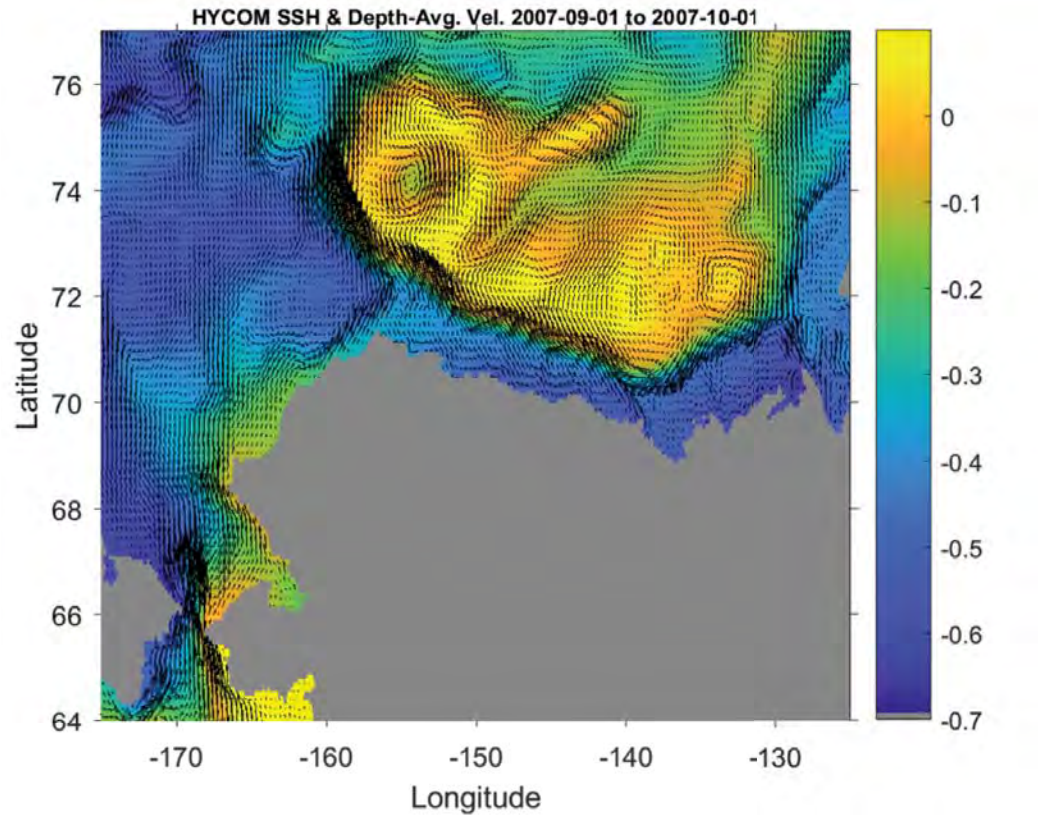


September 2007

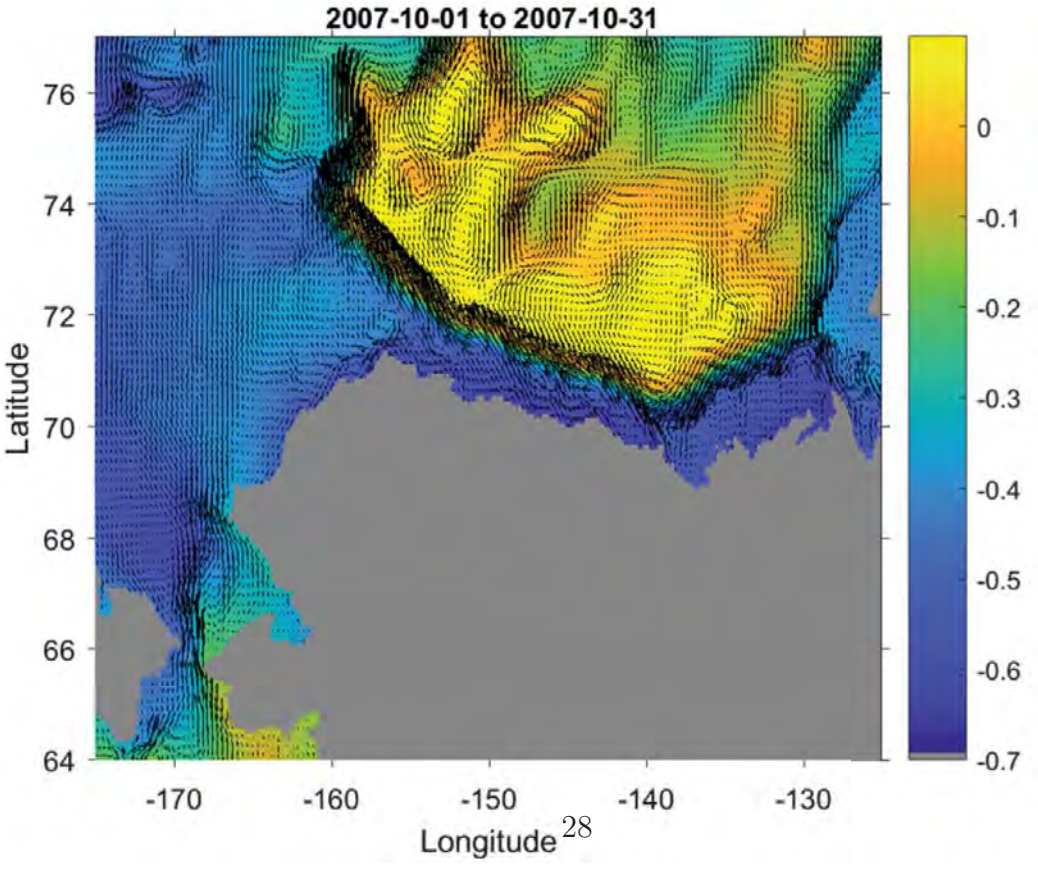


October 2007

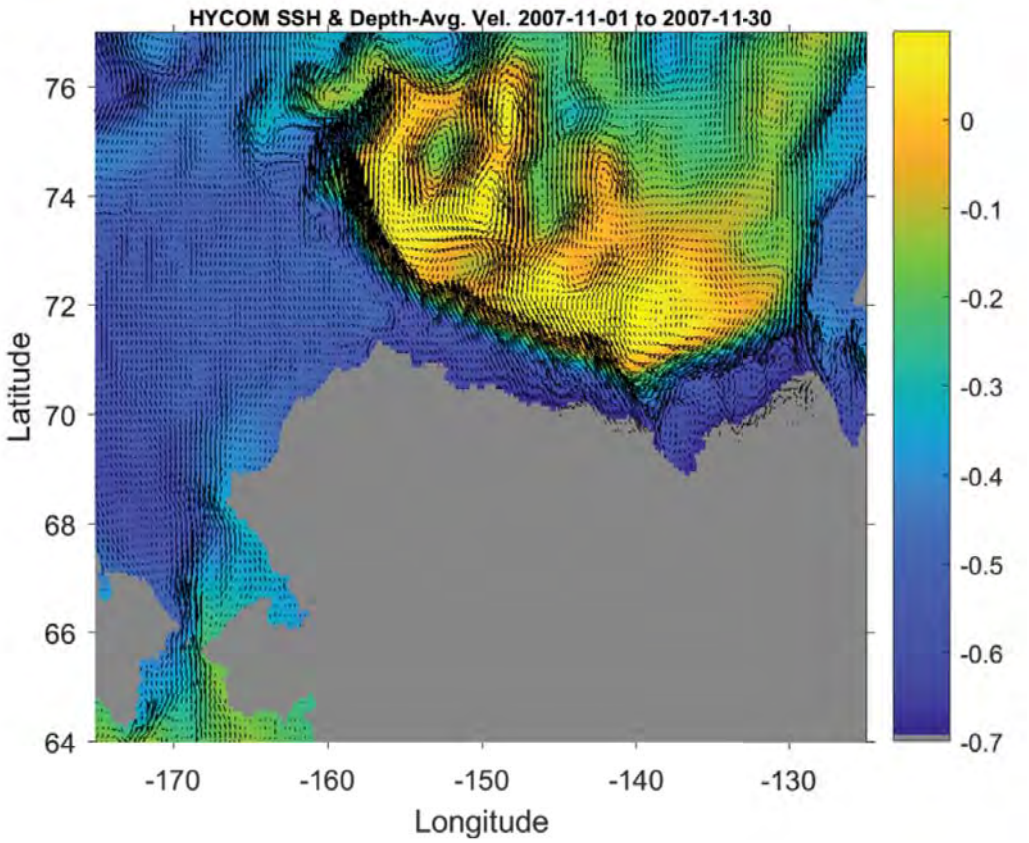


November 2007

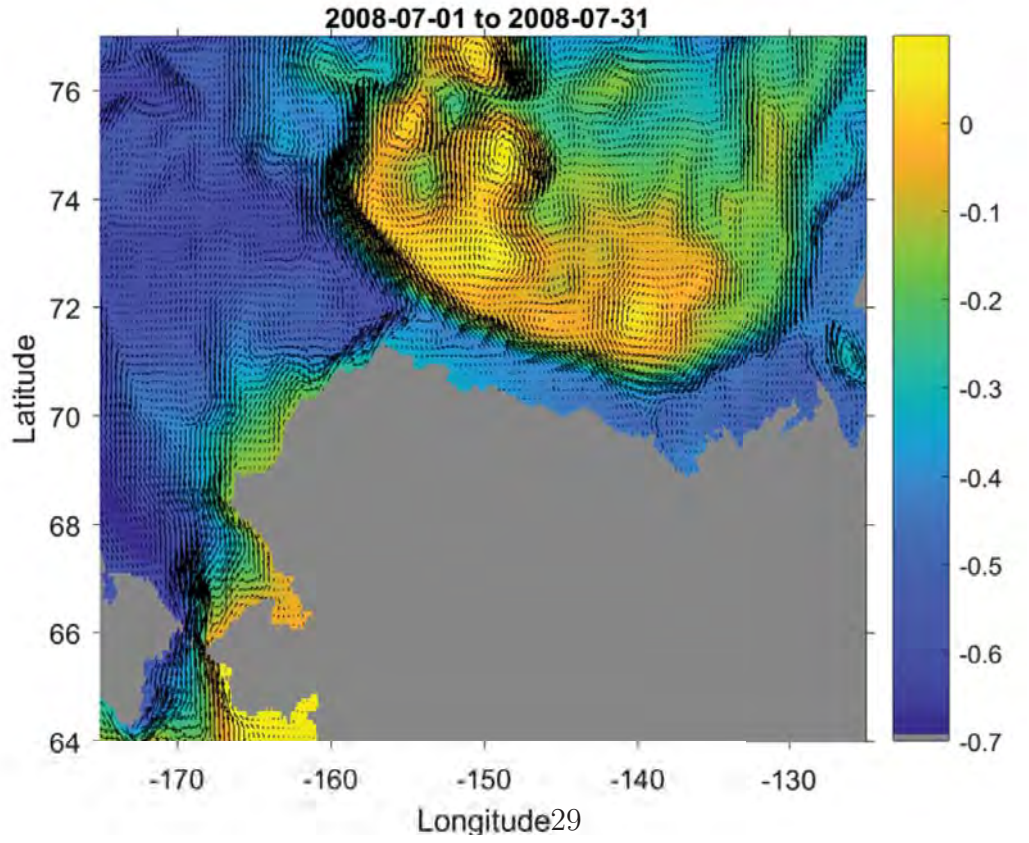




July 2008

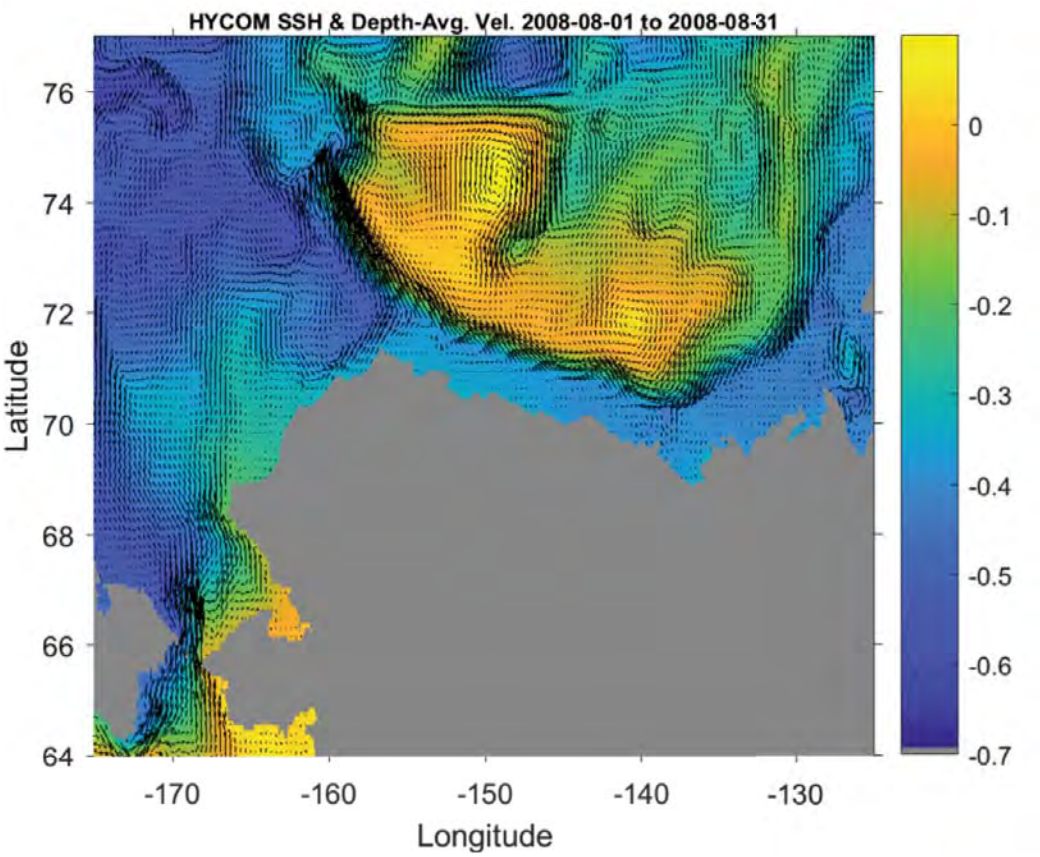


August 2008

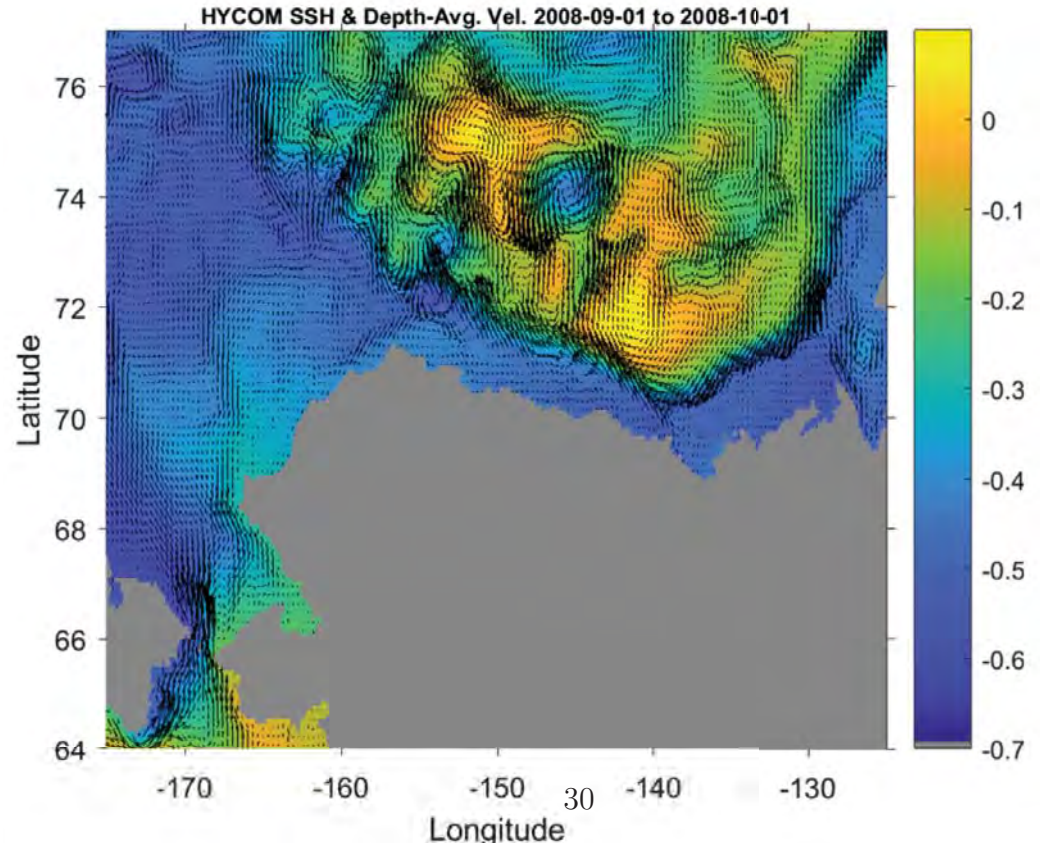




September 2008

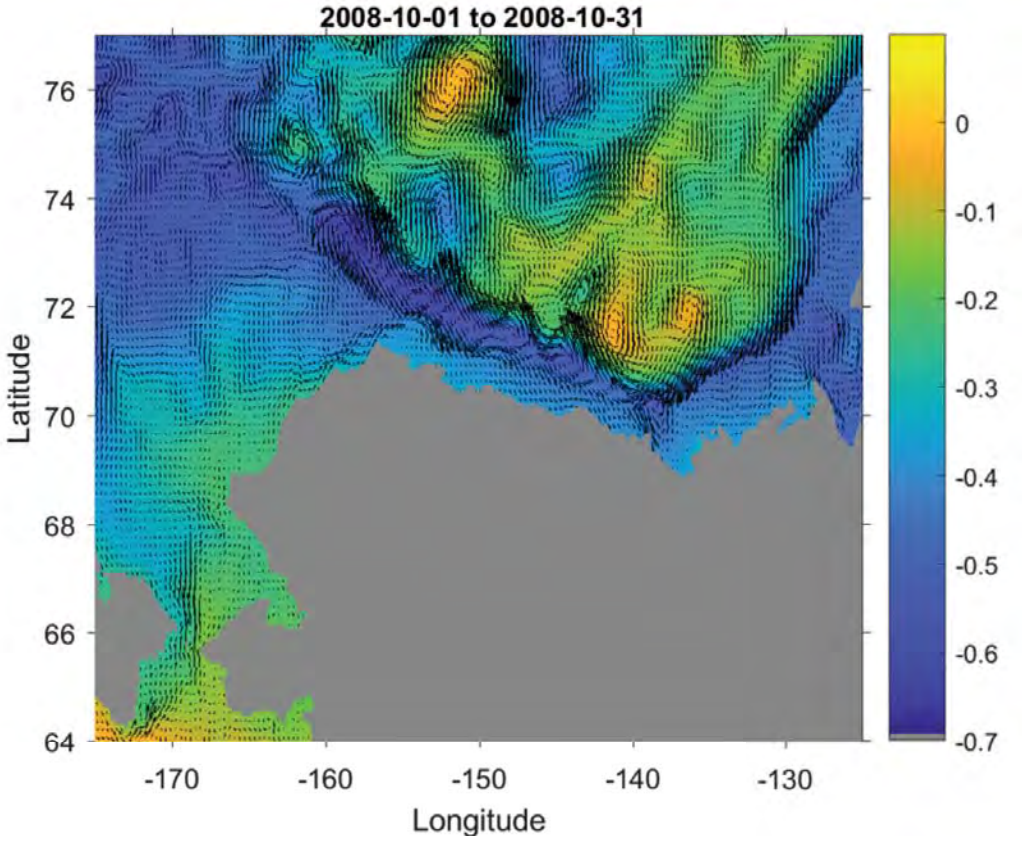


October 2008

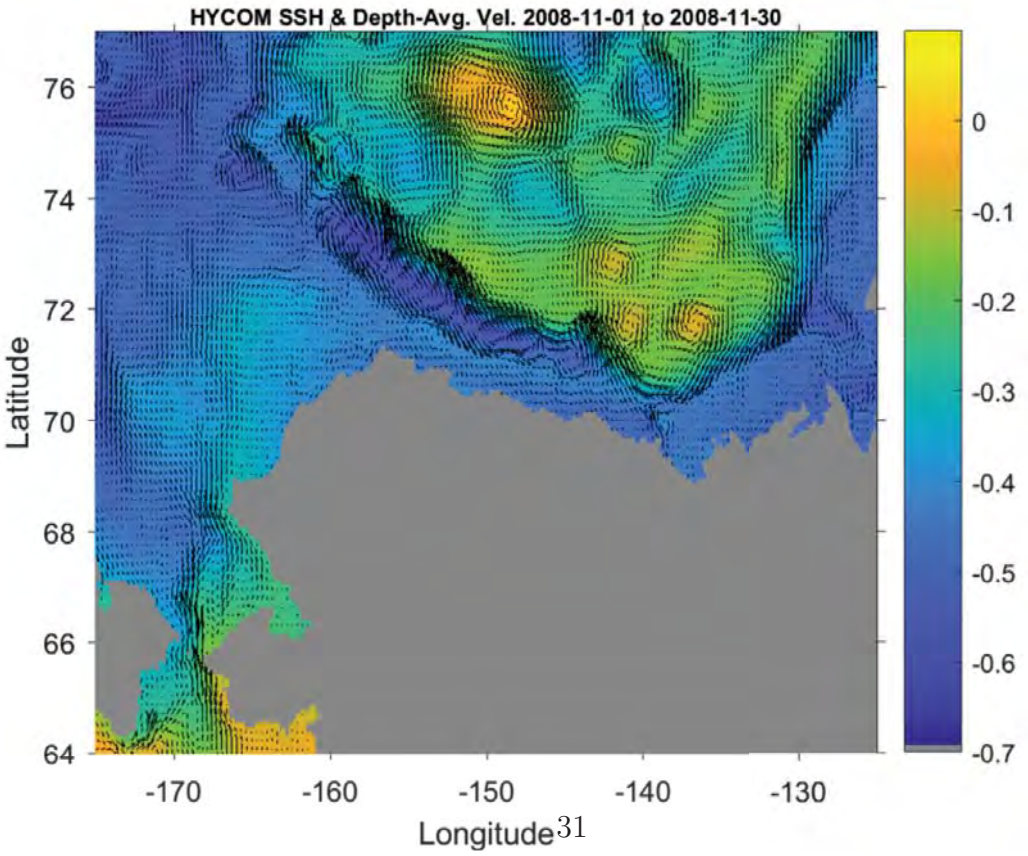




October 2008

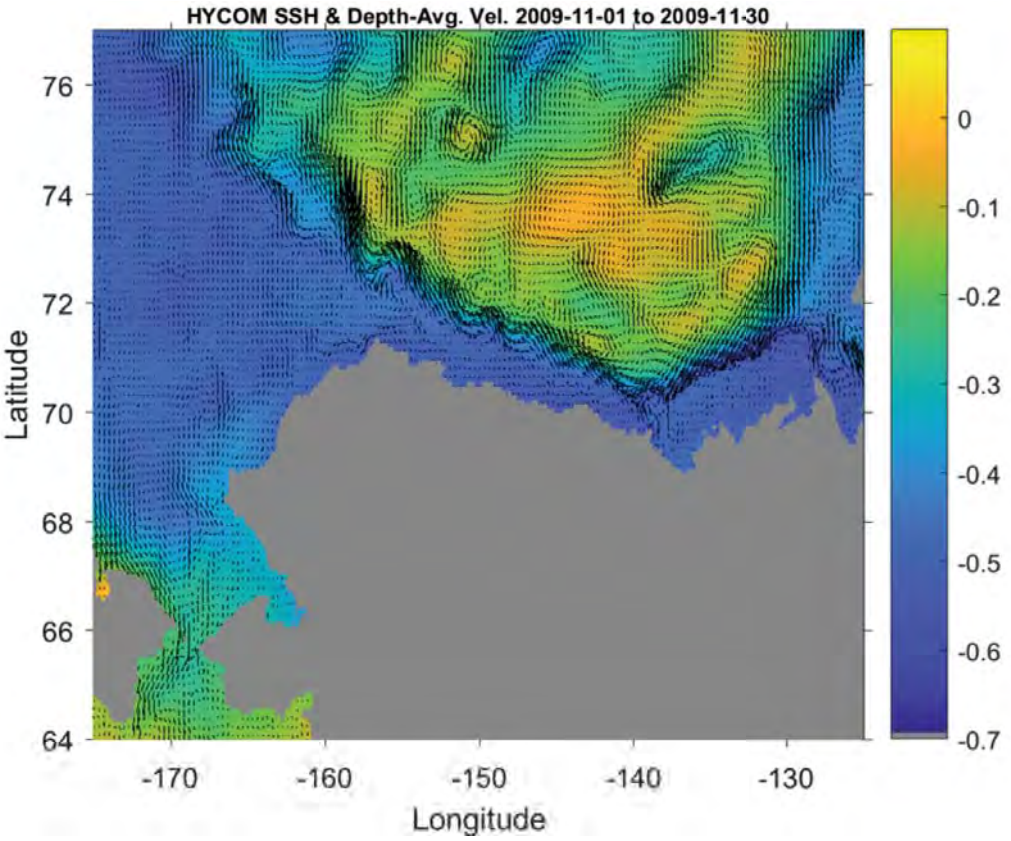


November 2009

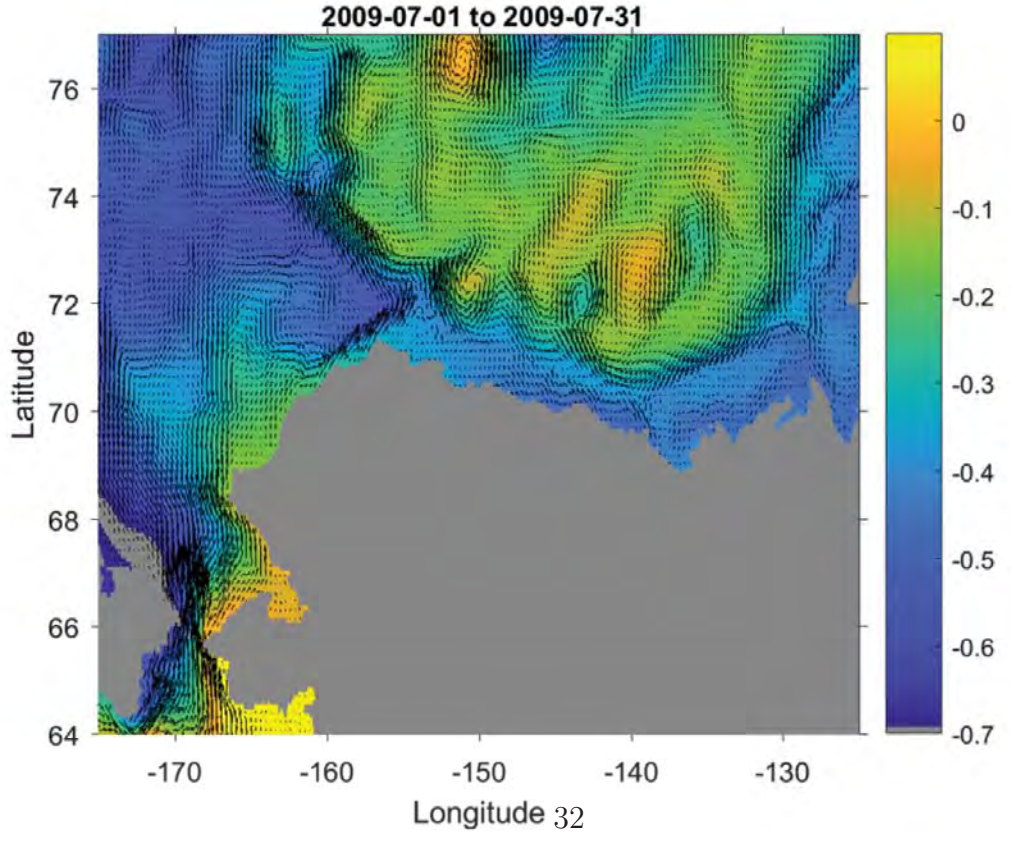




July 2009

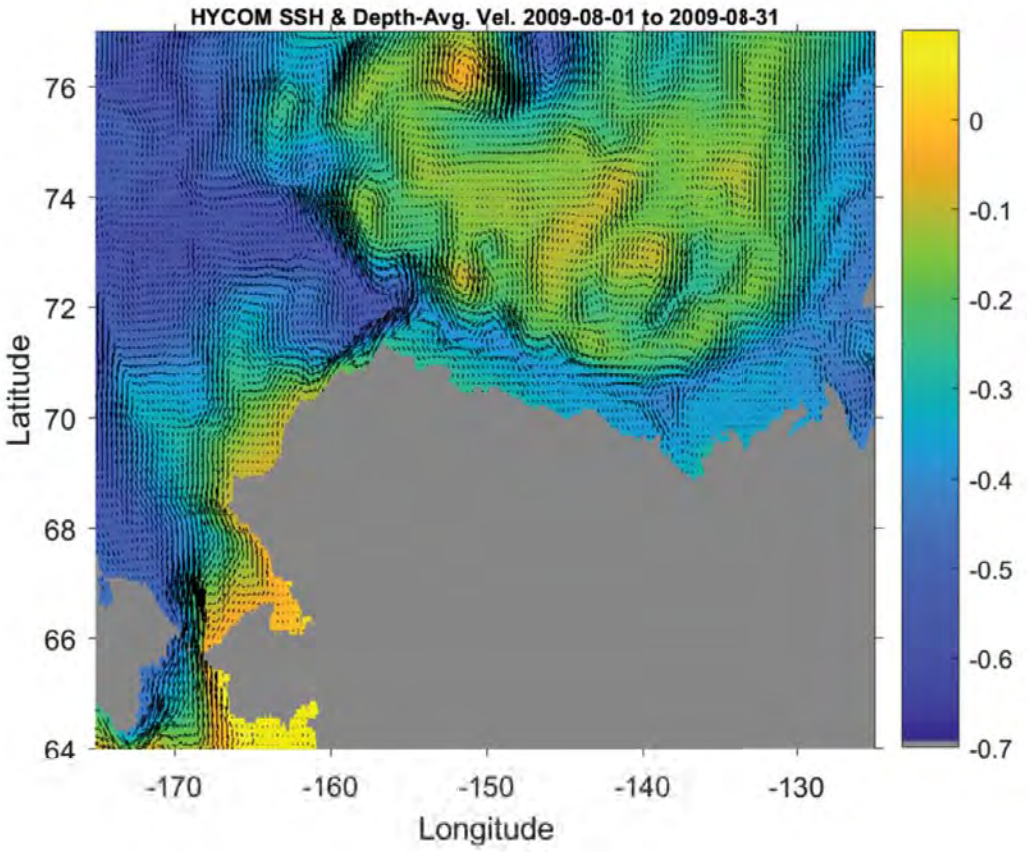


August 2009

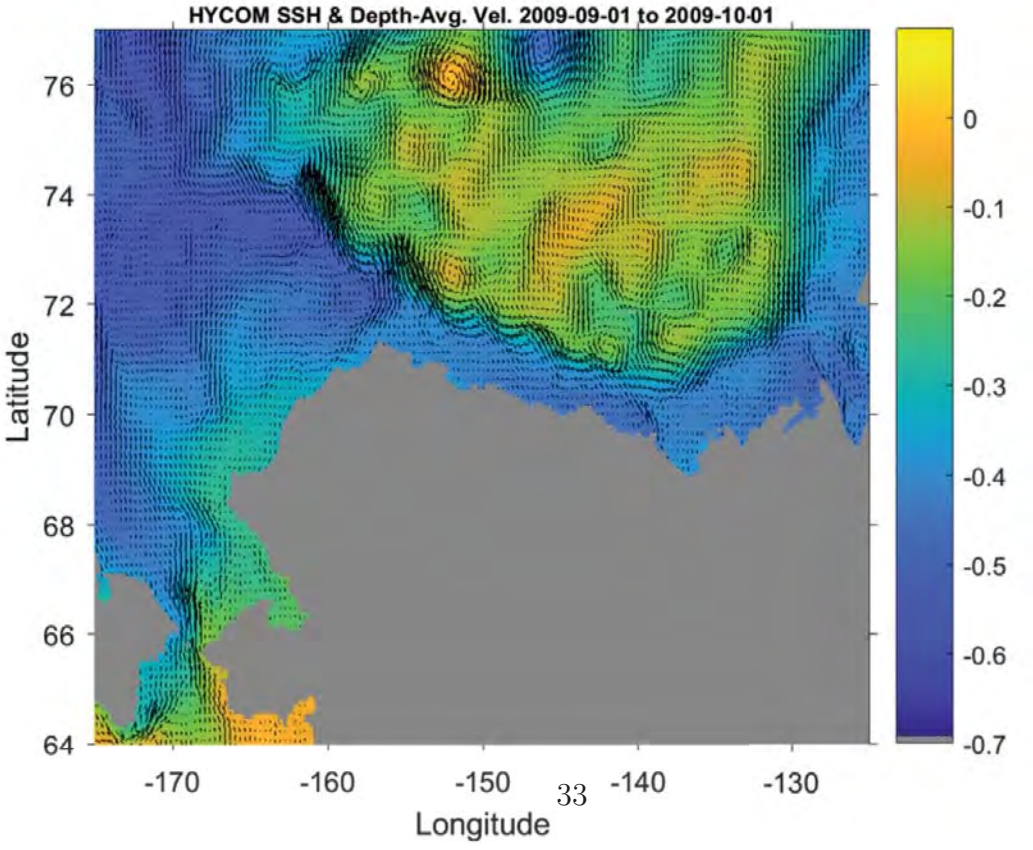




September 2009

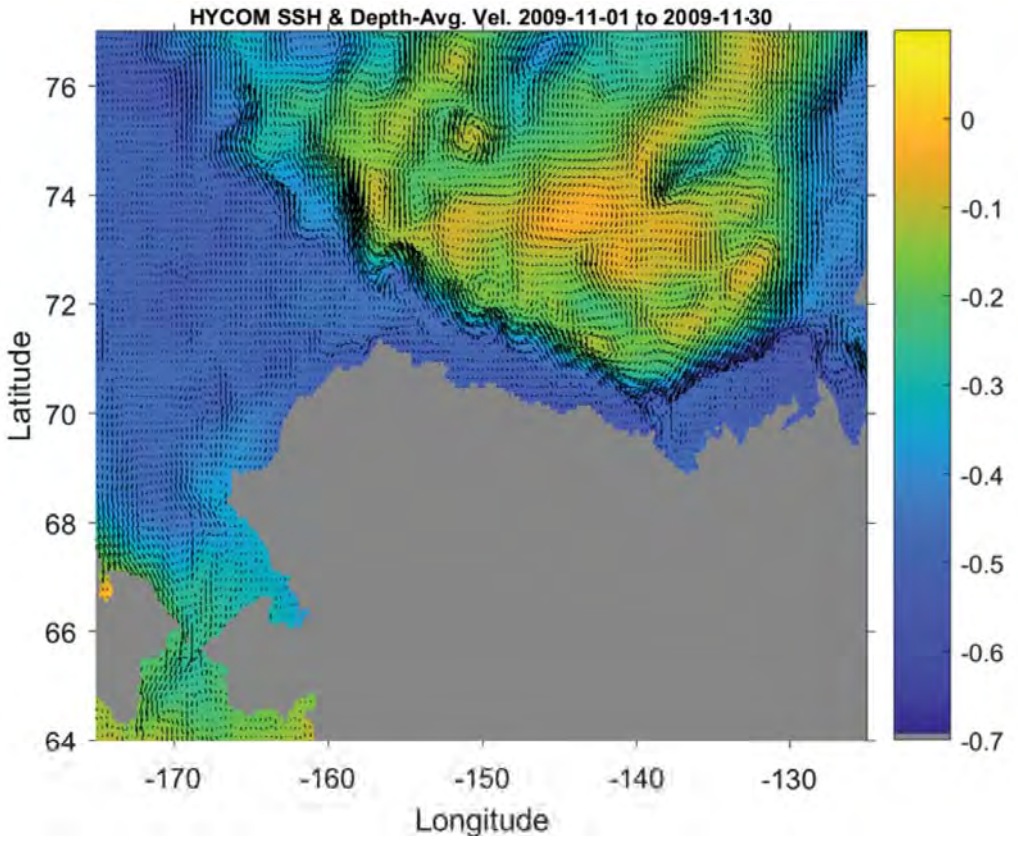


November 2009

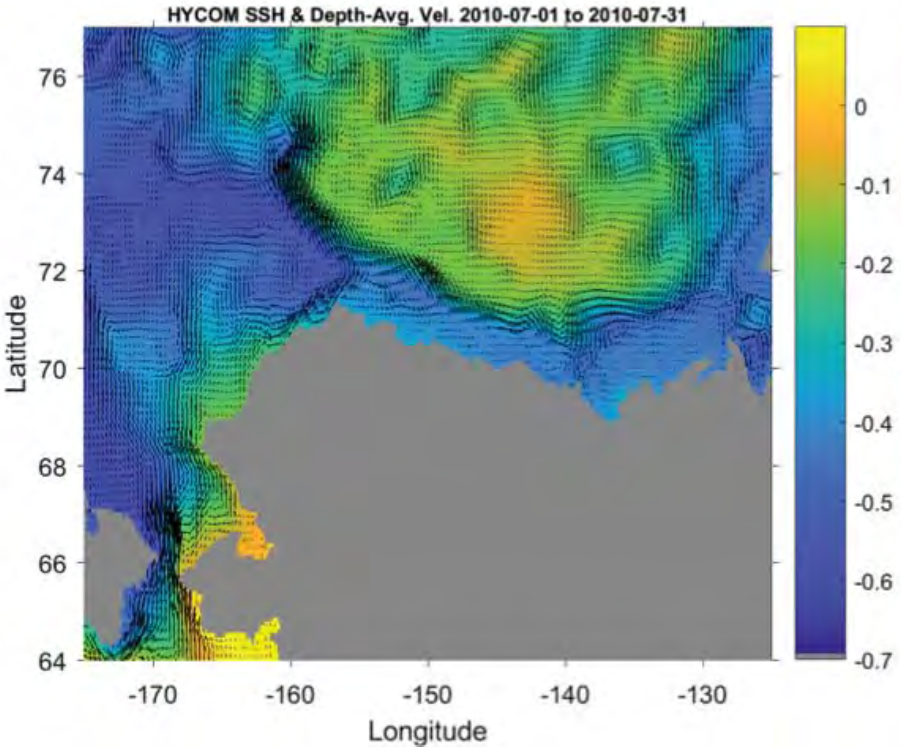


July 2010

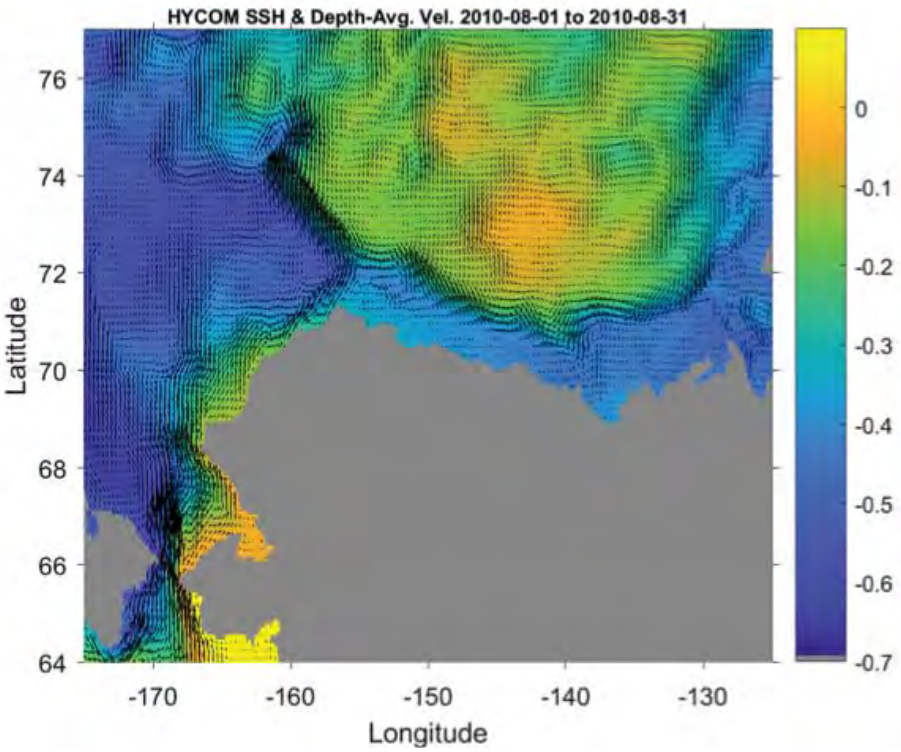


August 2010

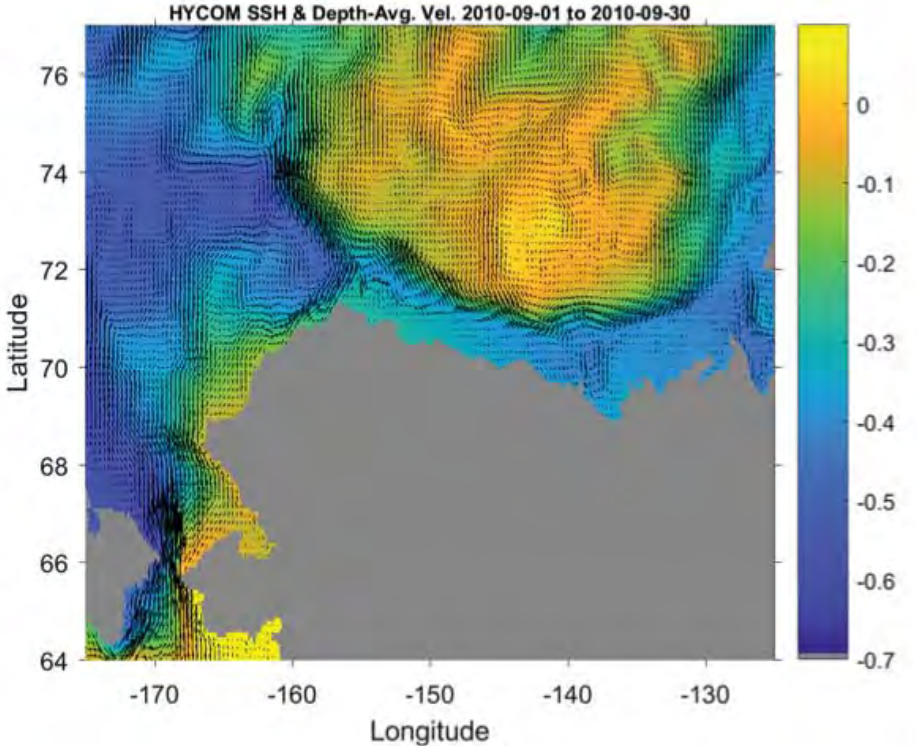


September 2010

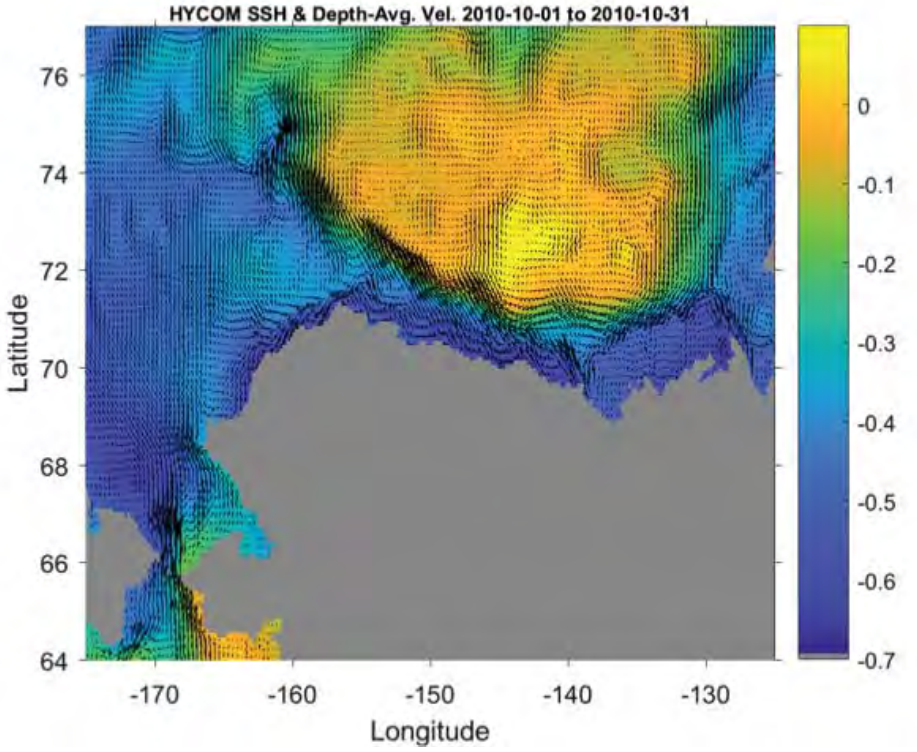


October 2010

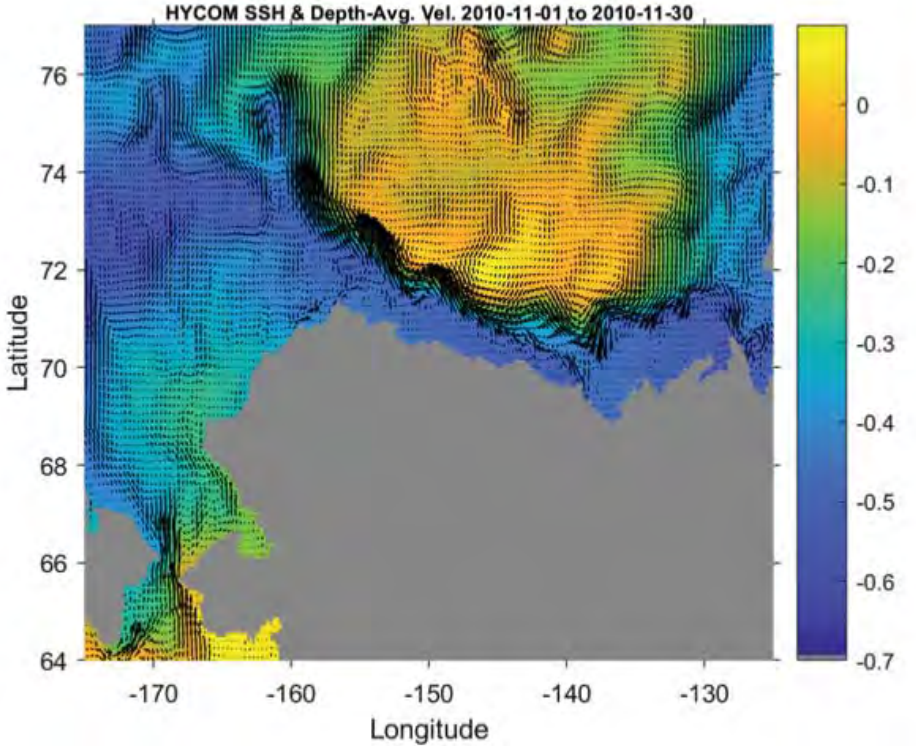


November 2010

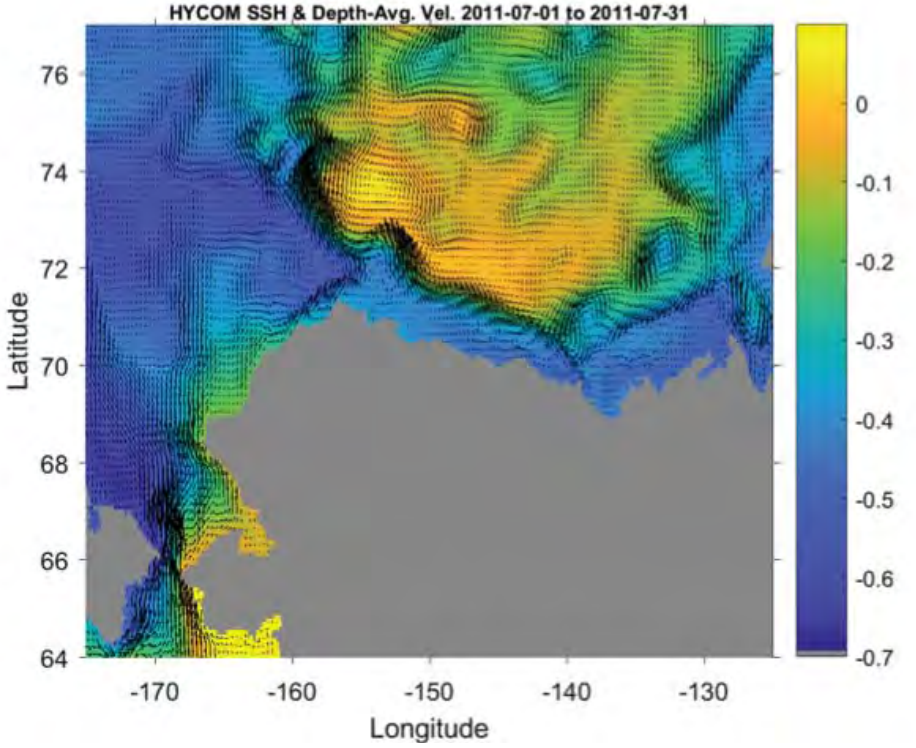


July 2011

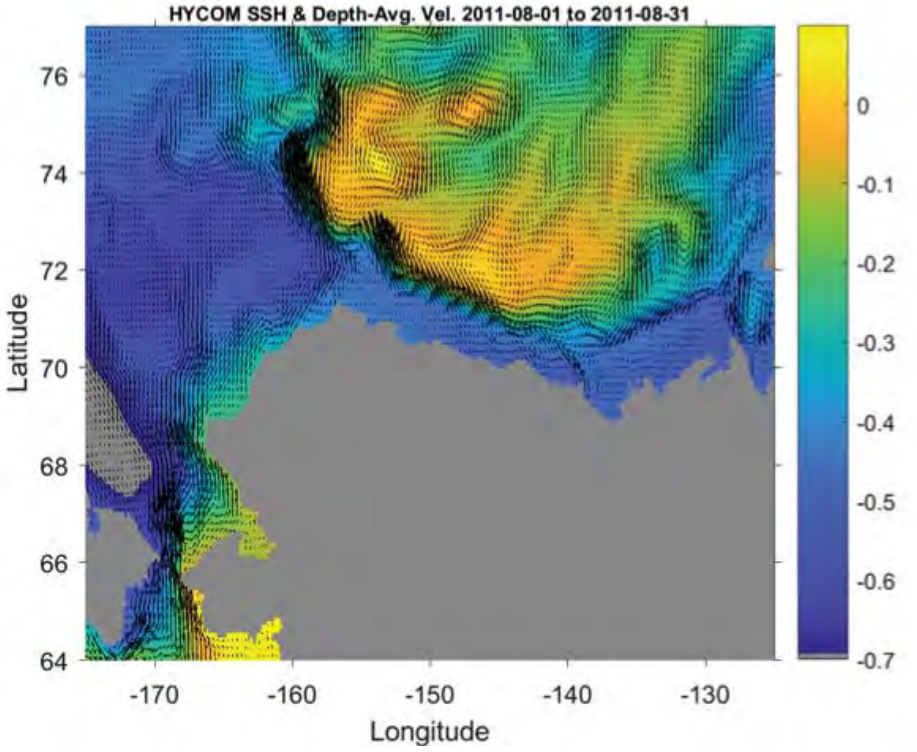


August 2011

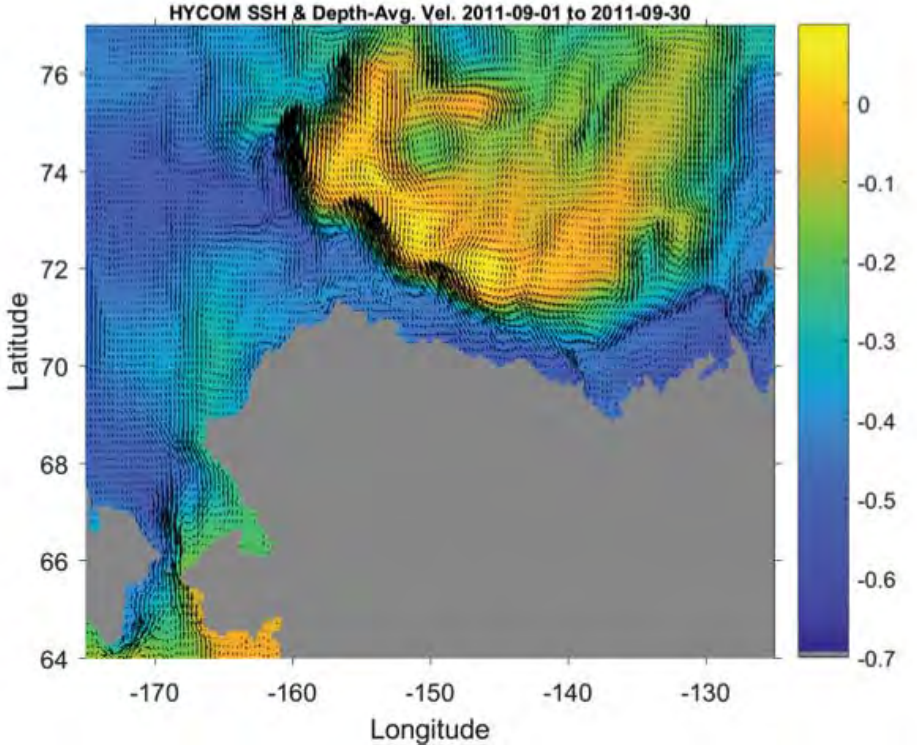


September 2011

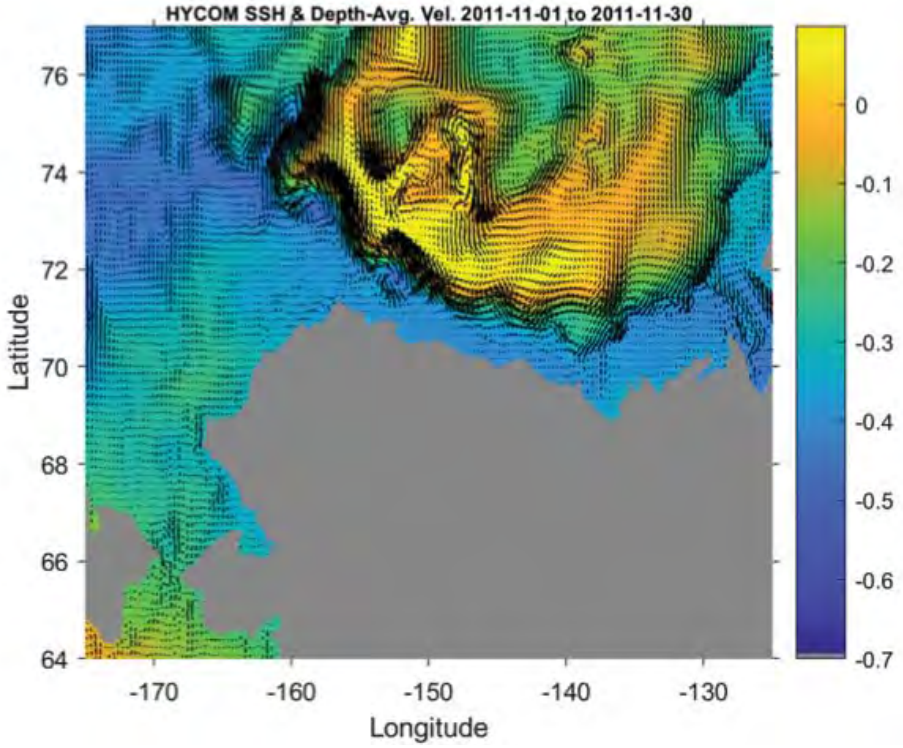


November 2011

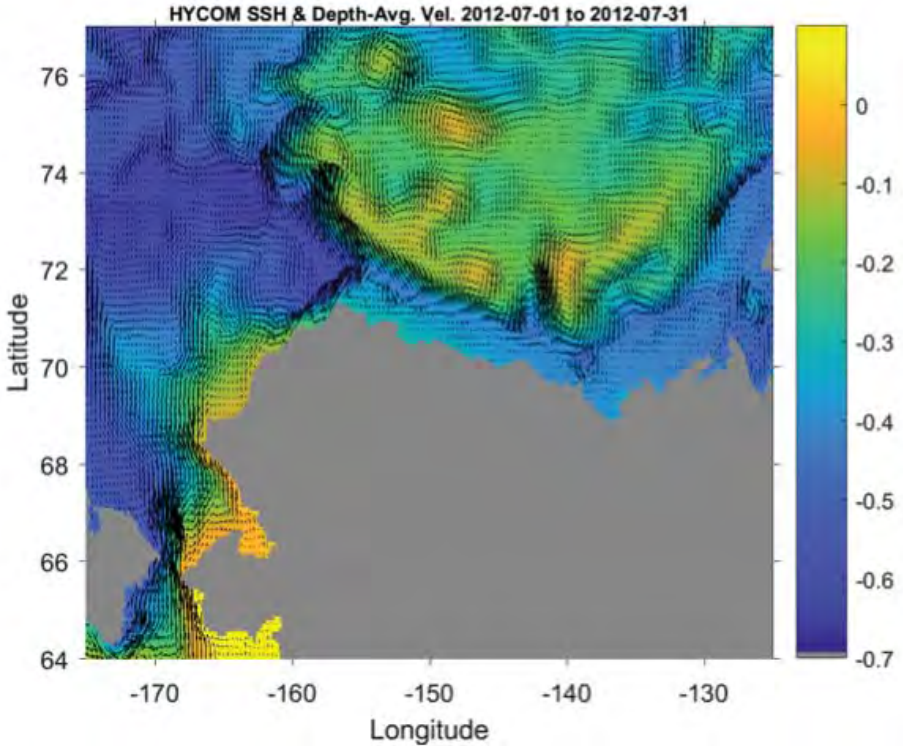


July 2012

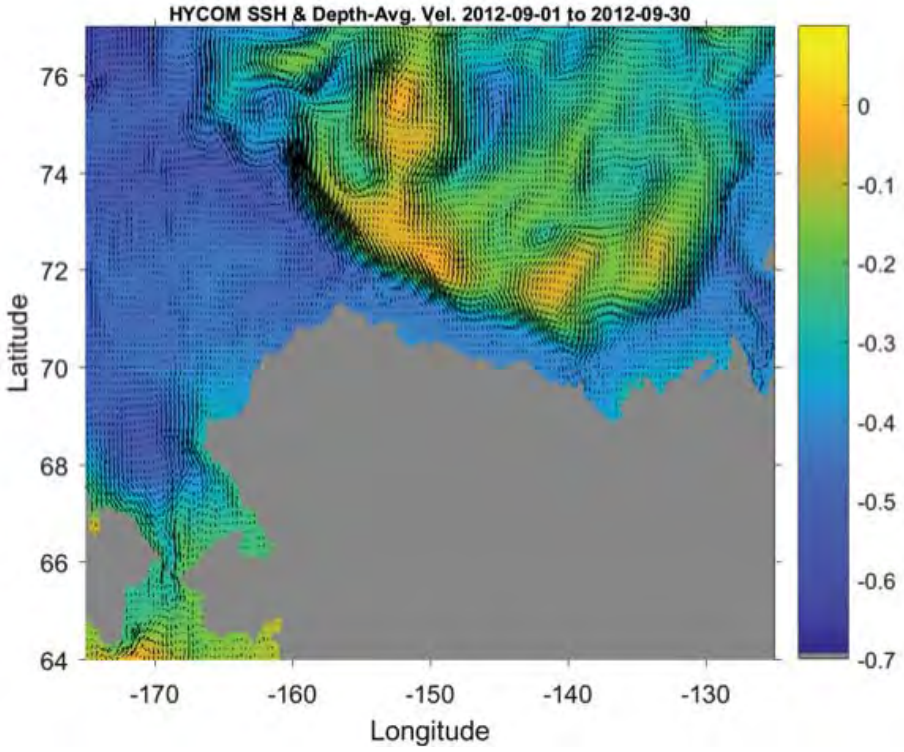


September 2012

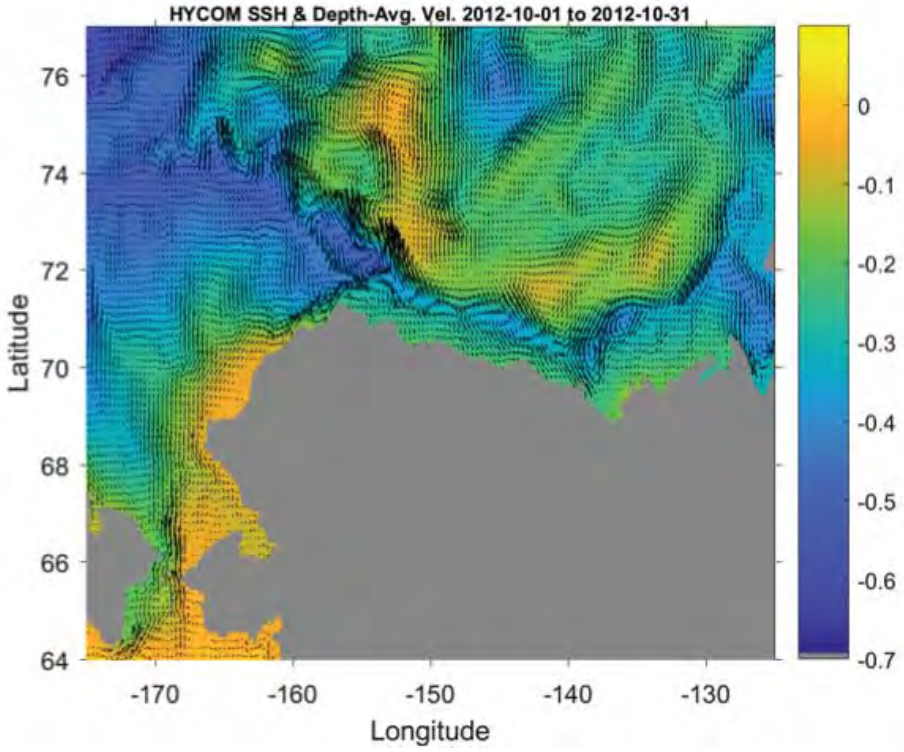


October 2012

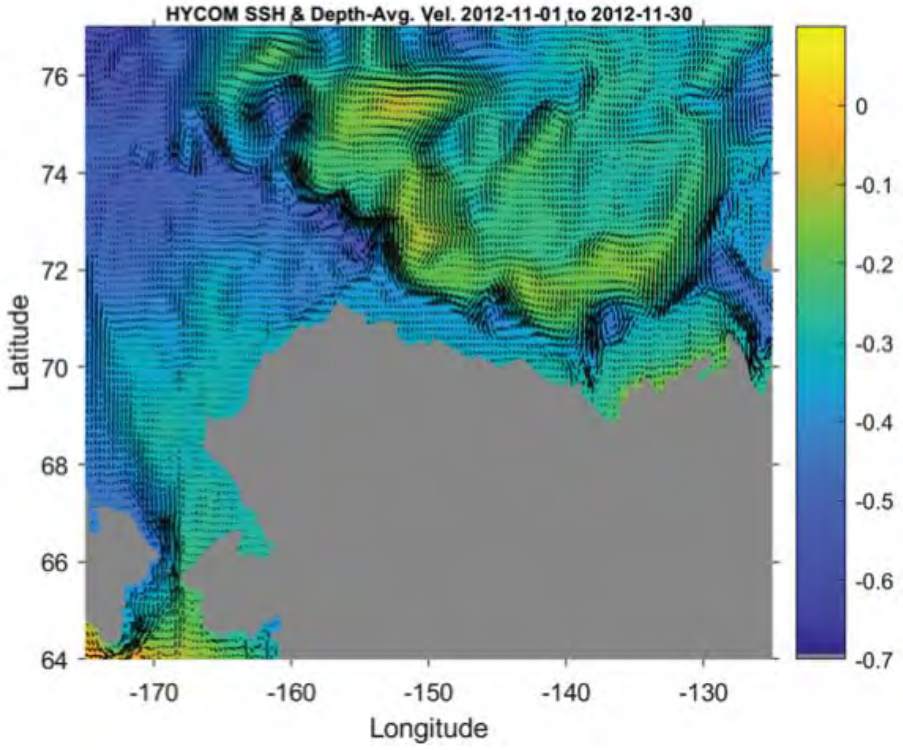


November 2012

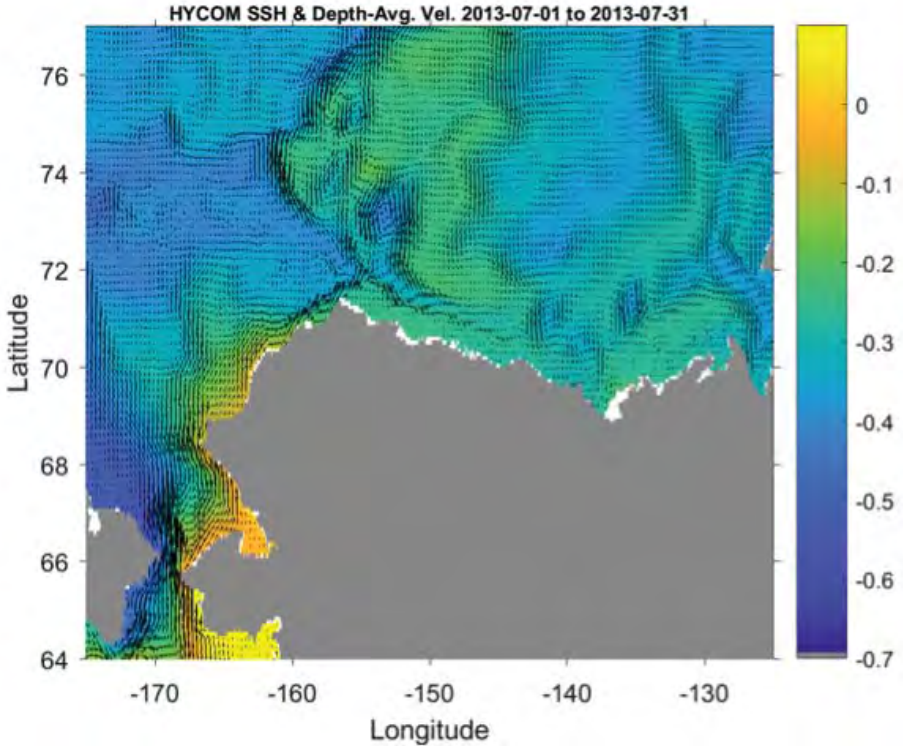


July 2013

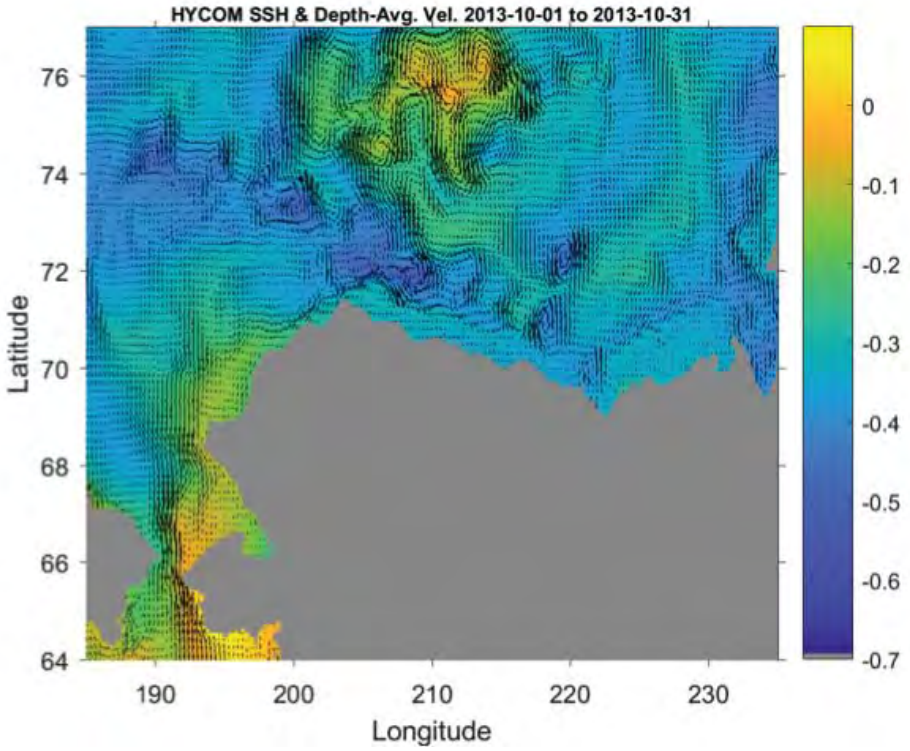


October 2013

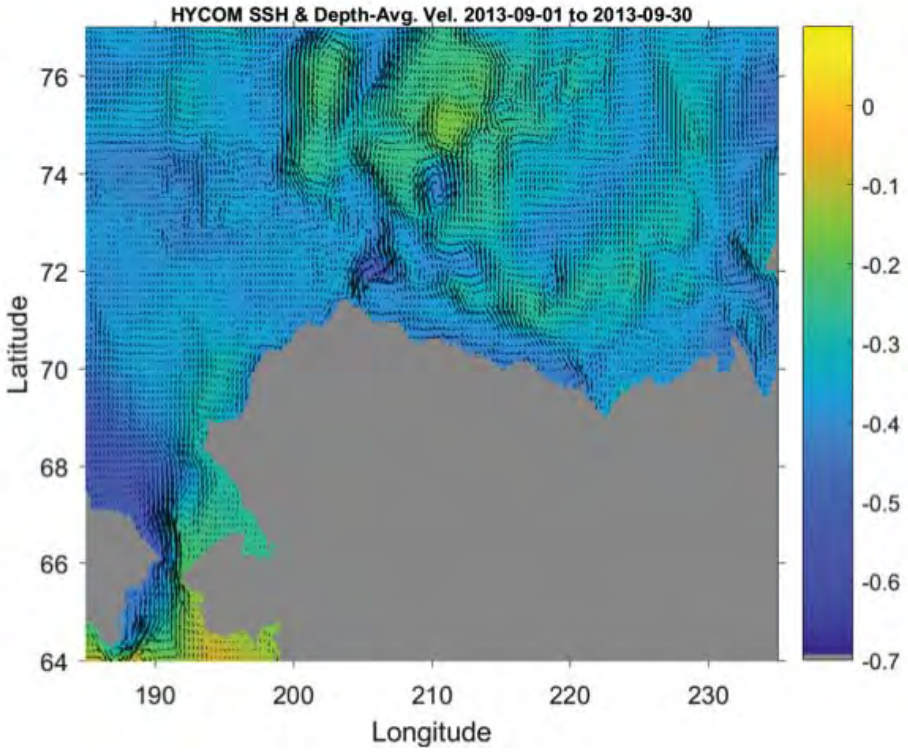


September 2013

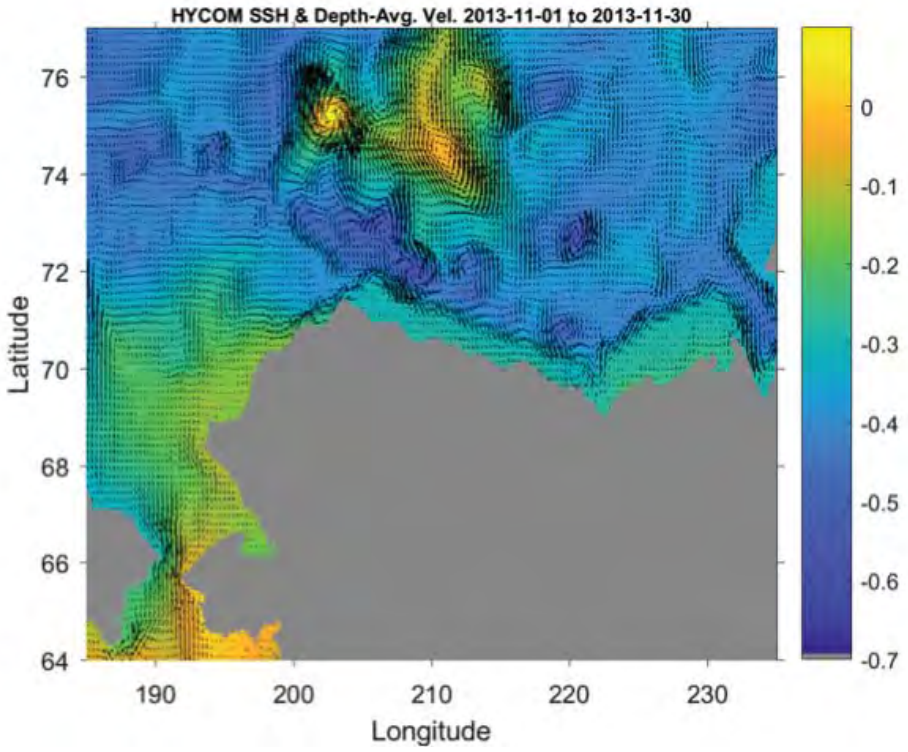


November 2013

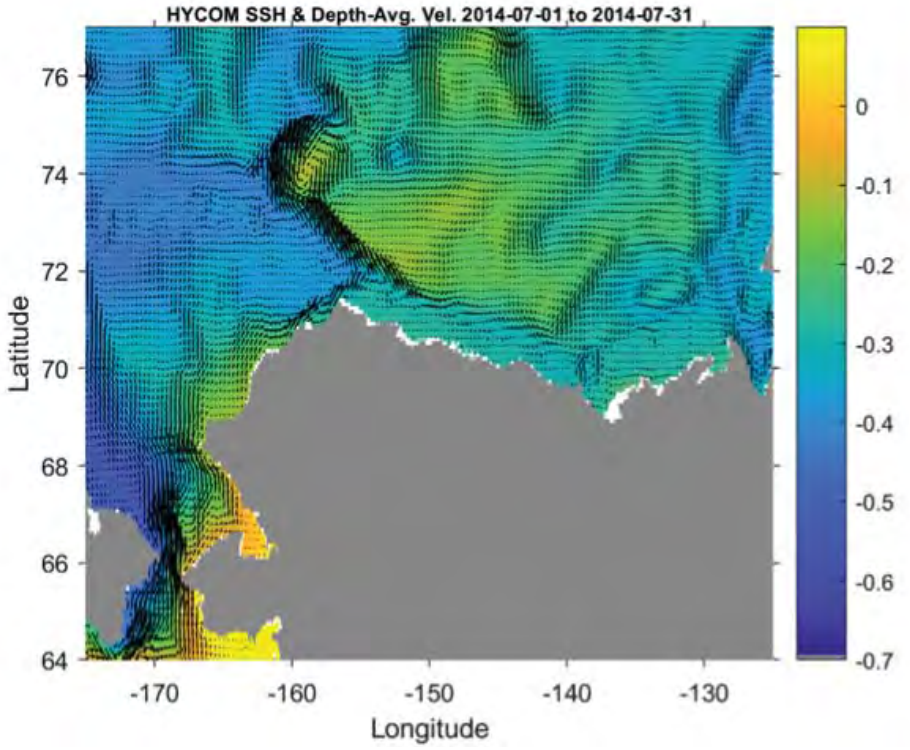


July 2014

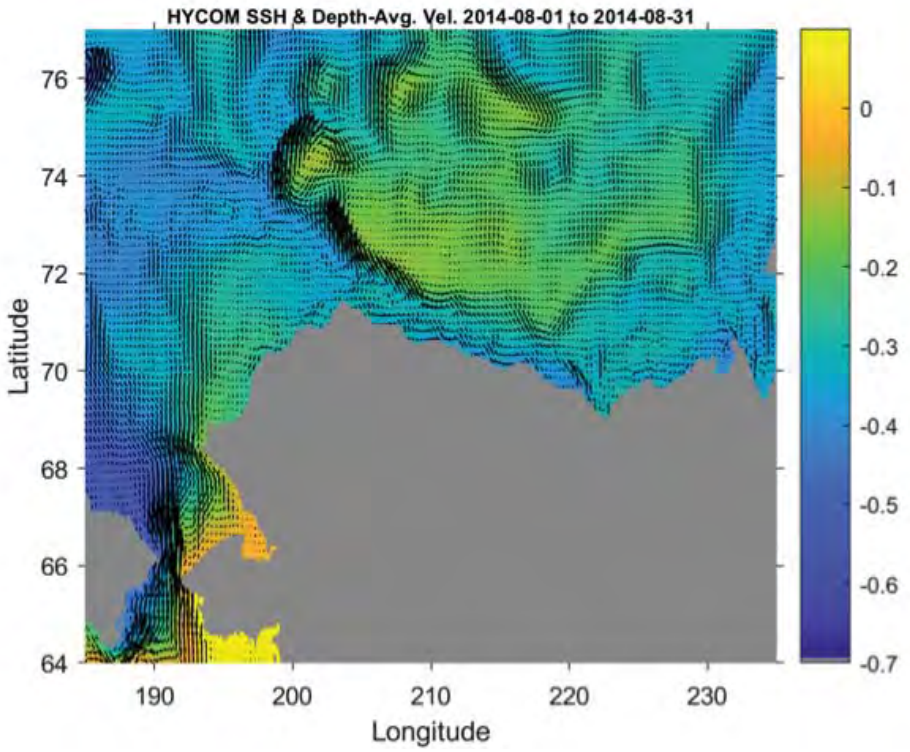


August 2014

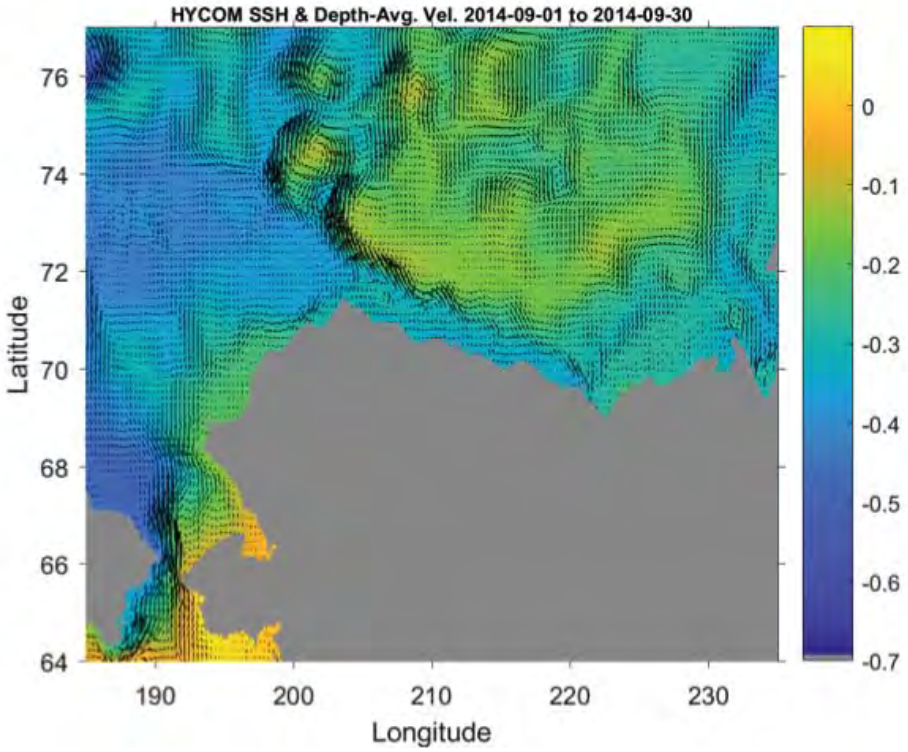


September 2014

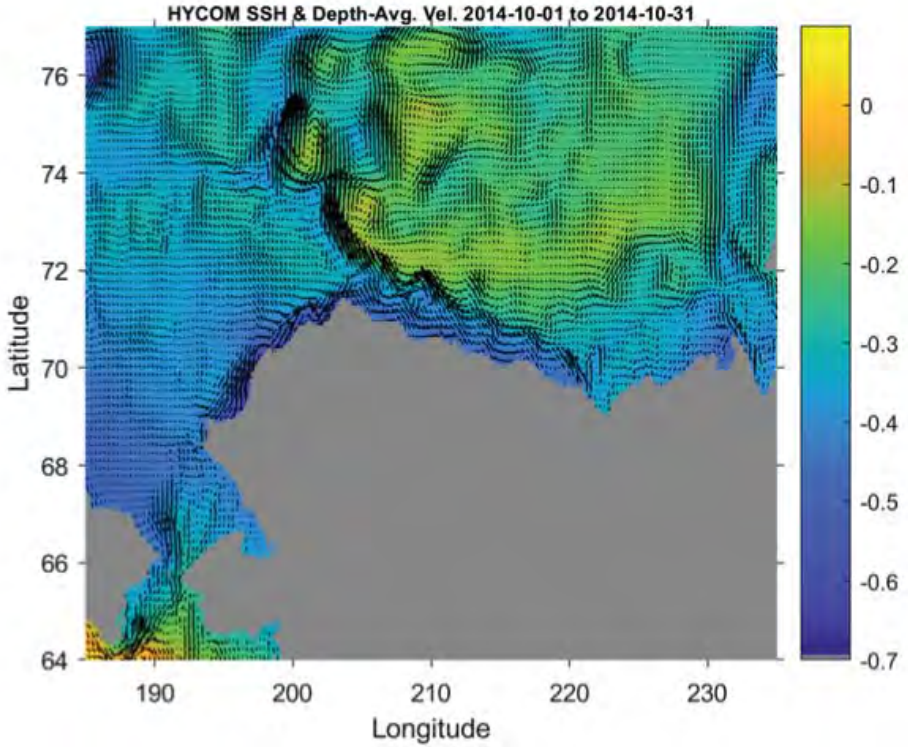


October 2014

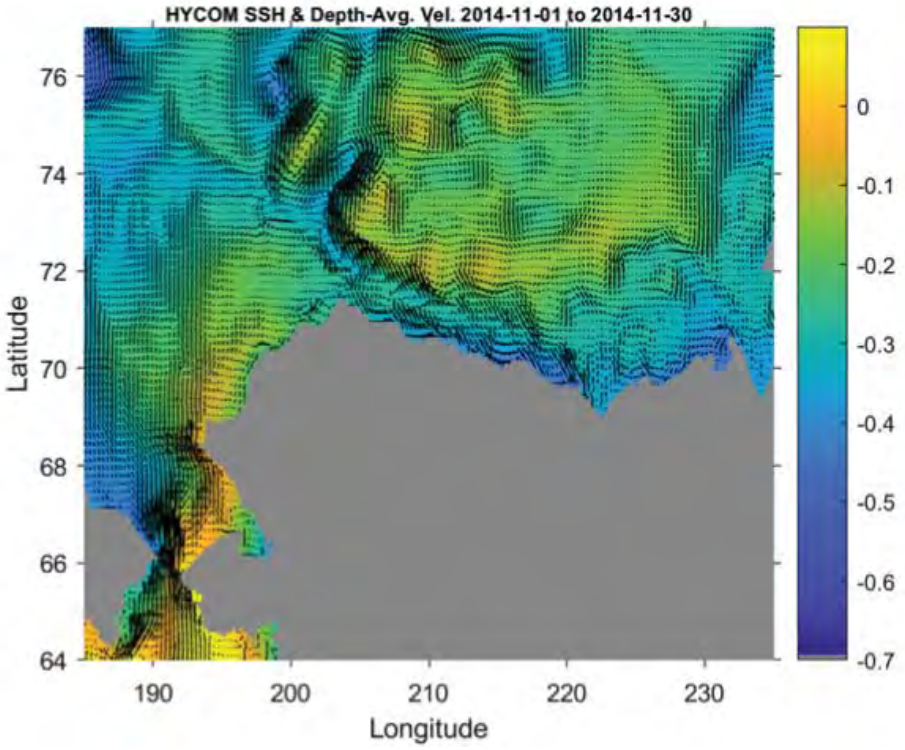


November 2014

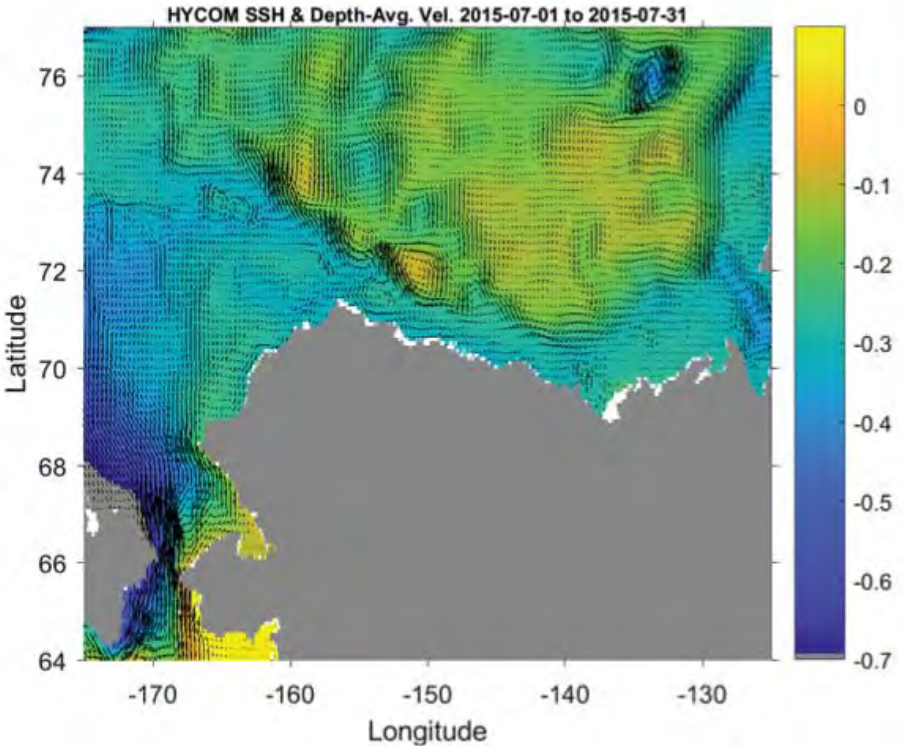


July 2014

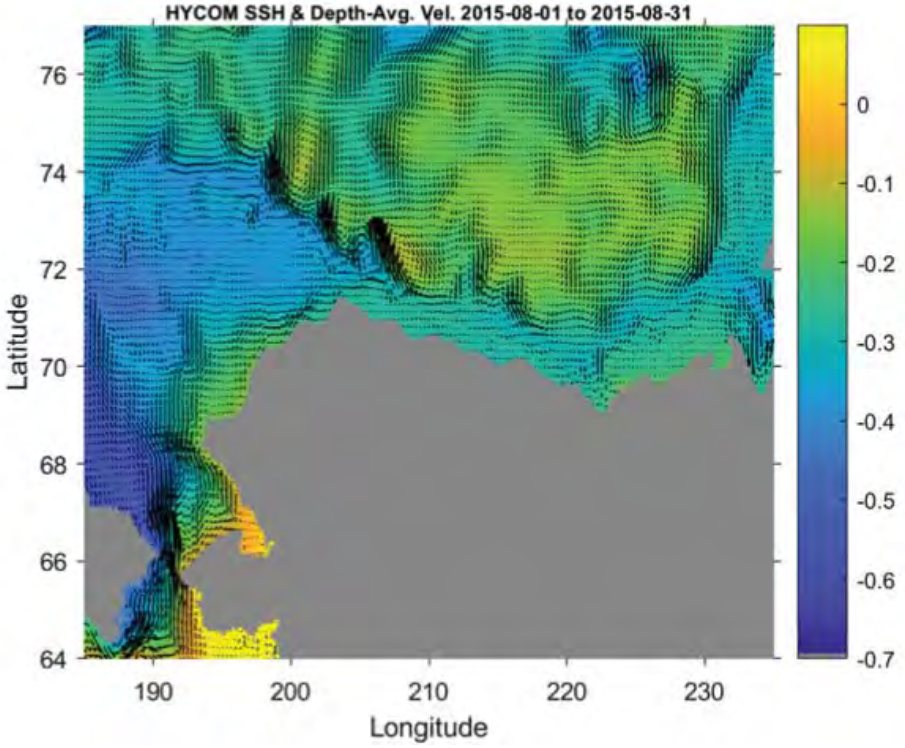


August 2015

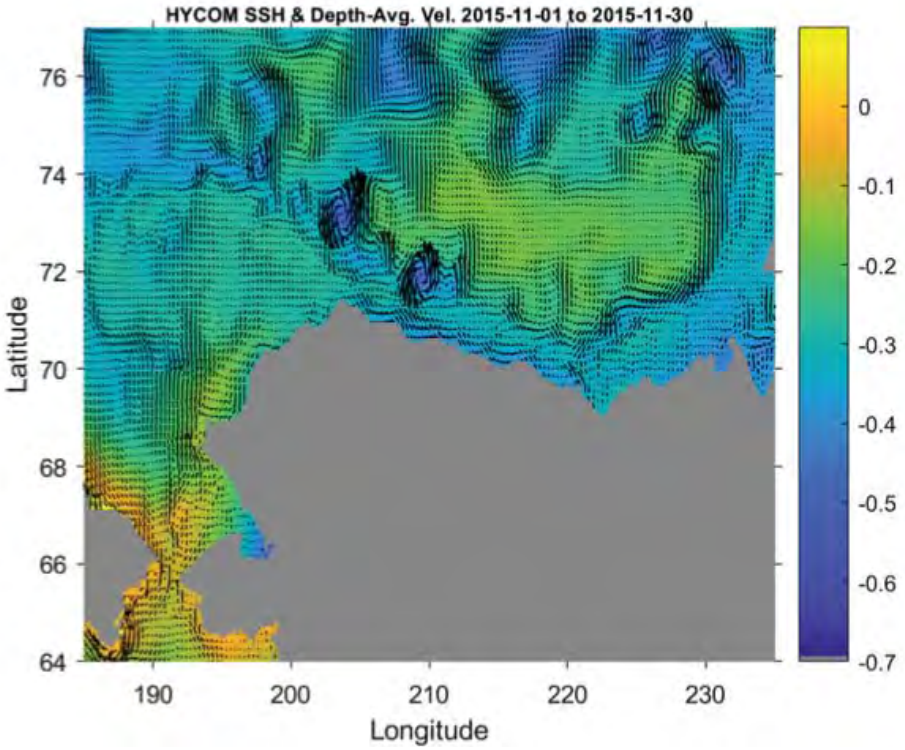


November 2015

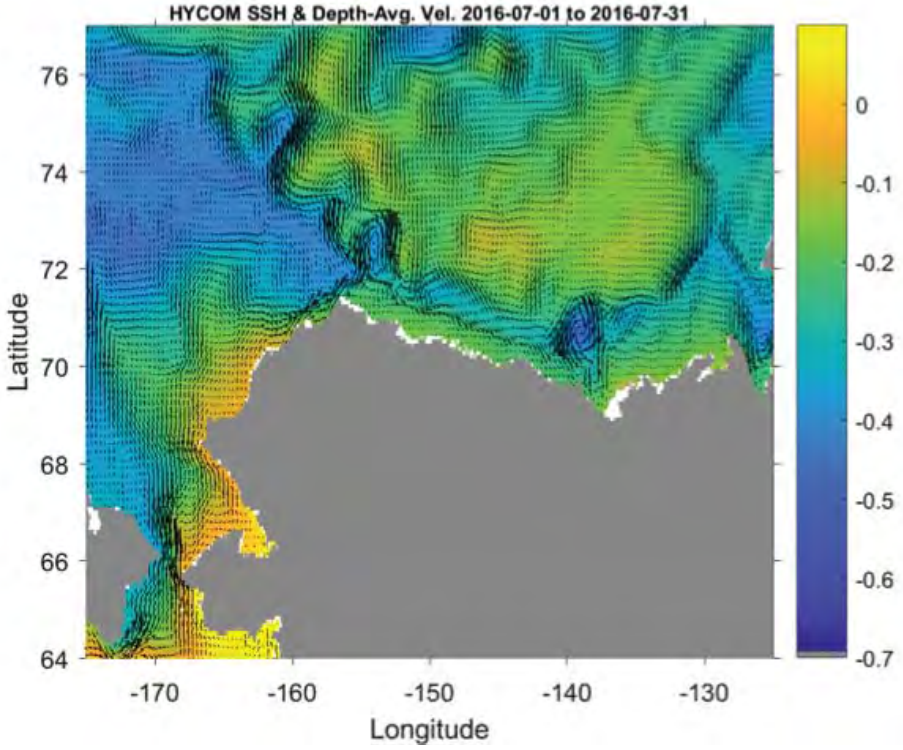


July 2016

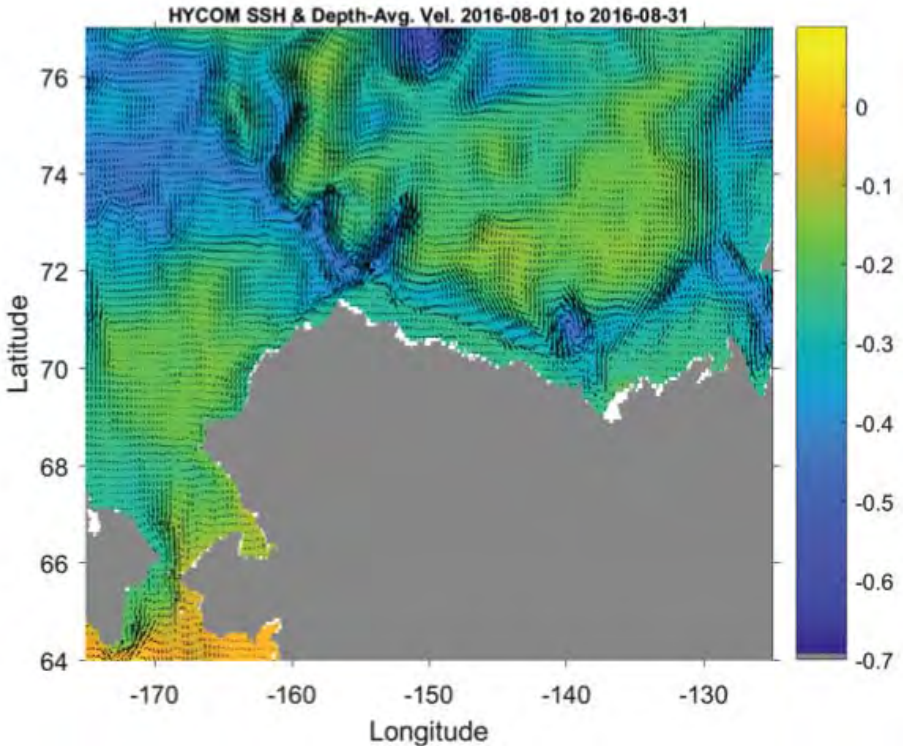


August 2016

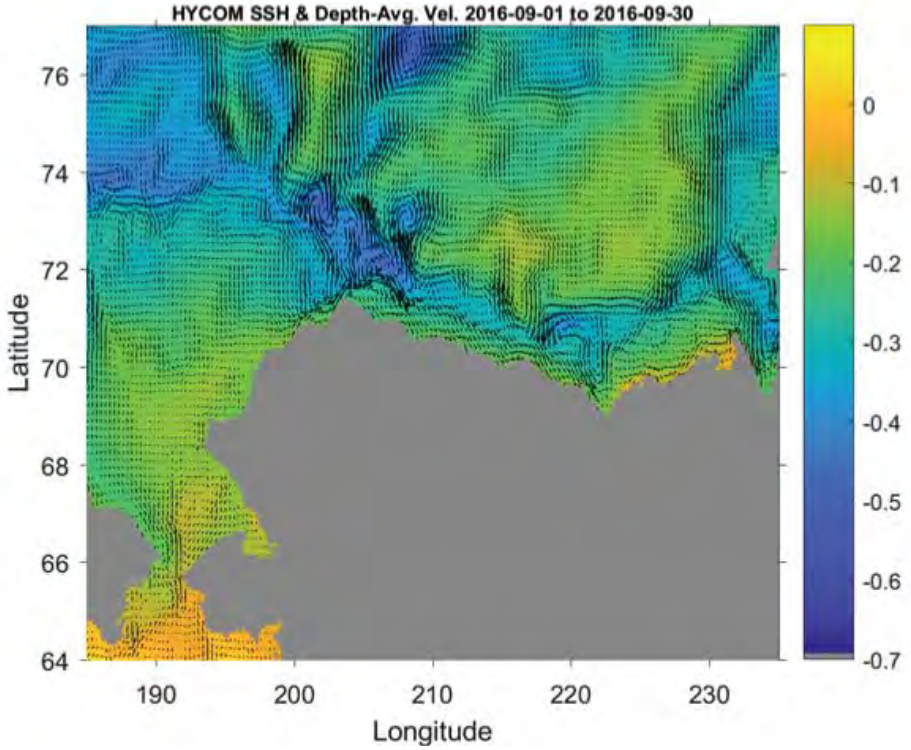


September 2016

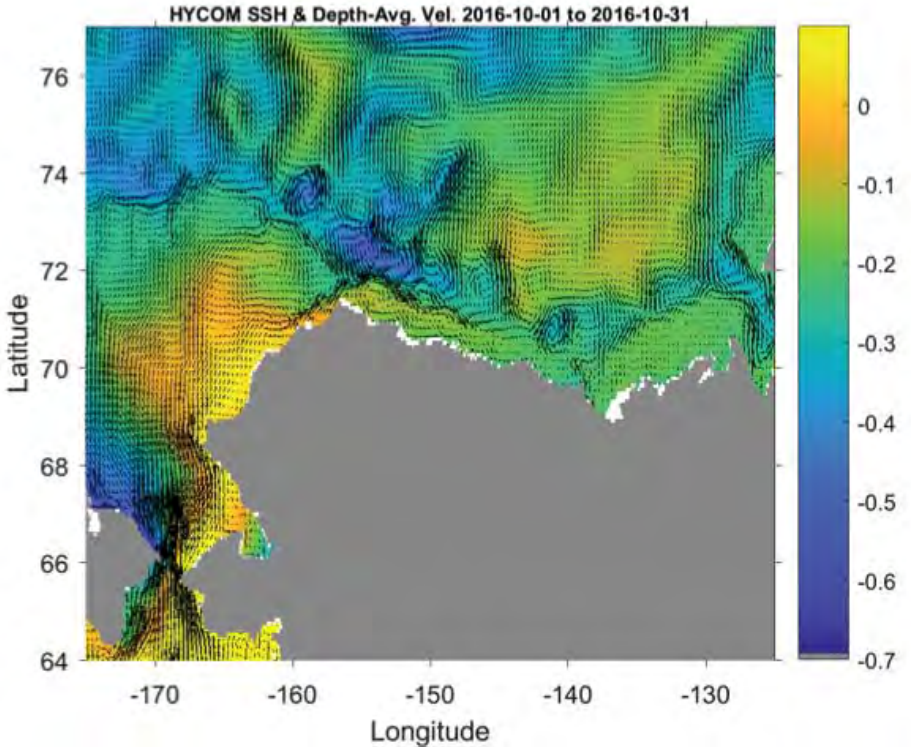


October 2016

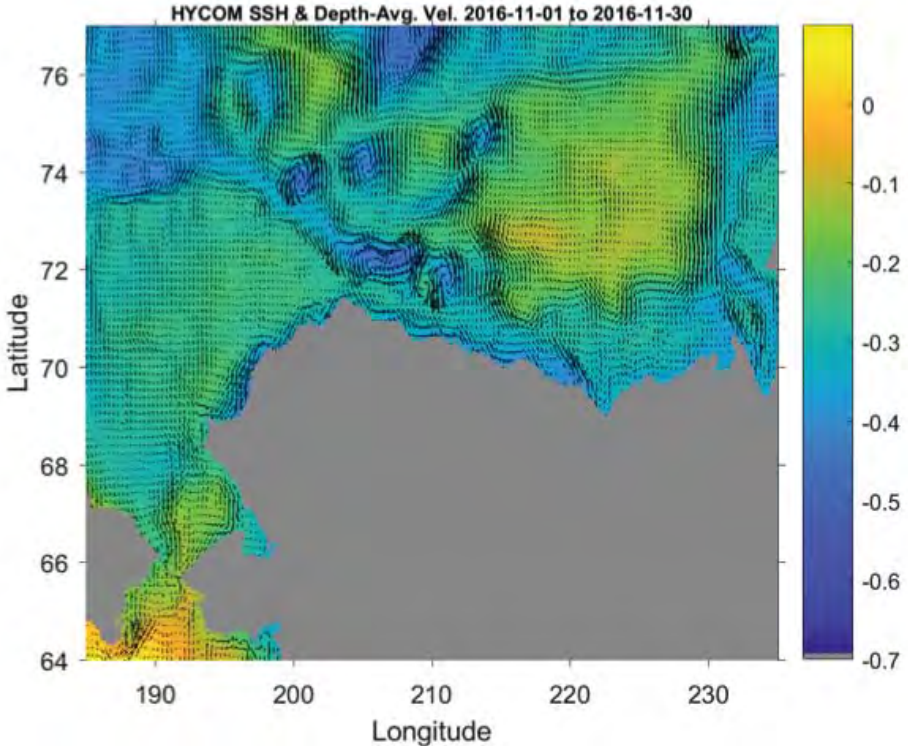


November 2016

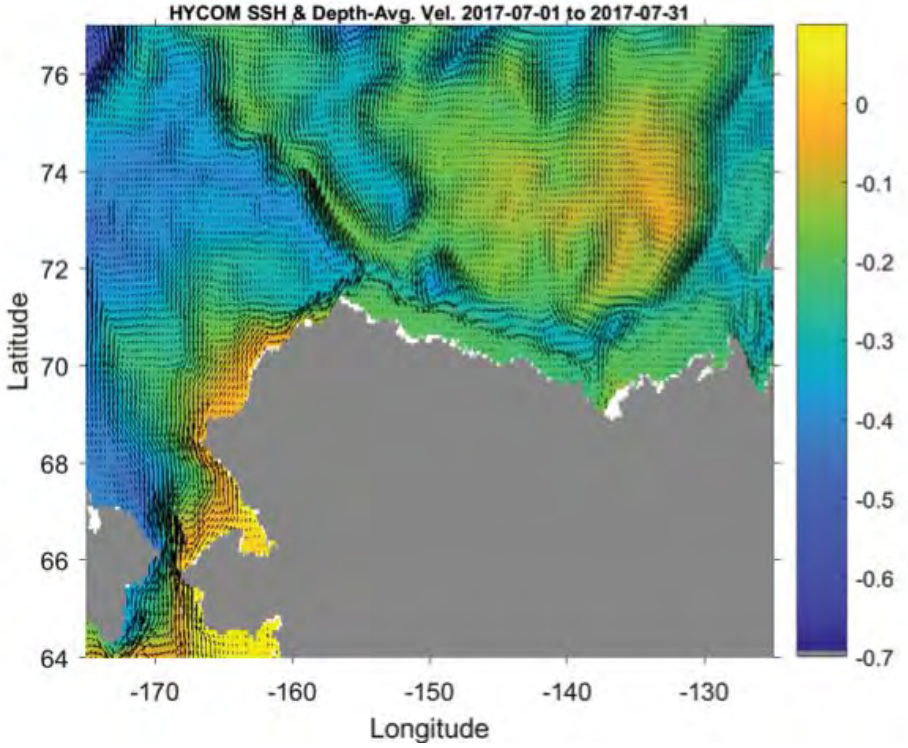


July 2017

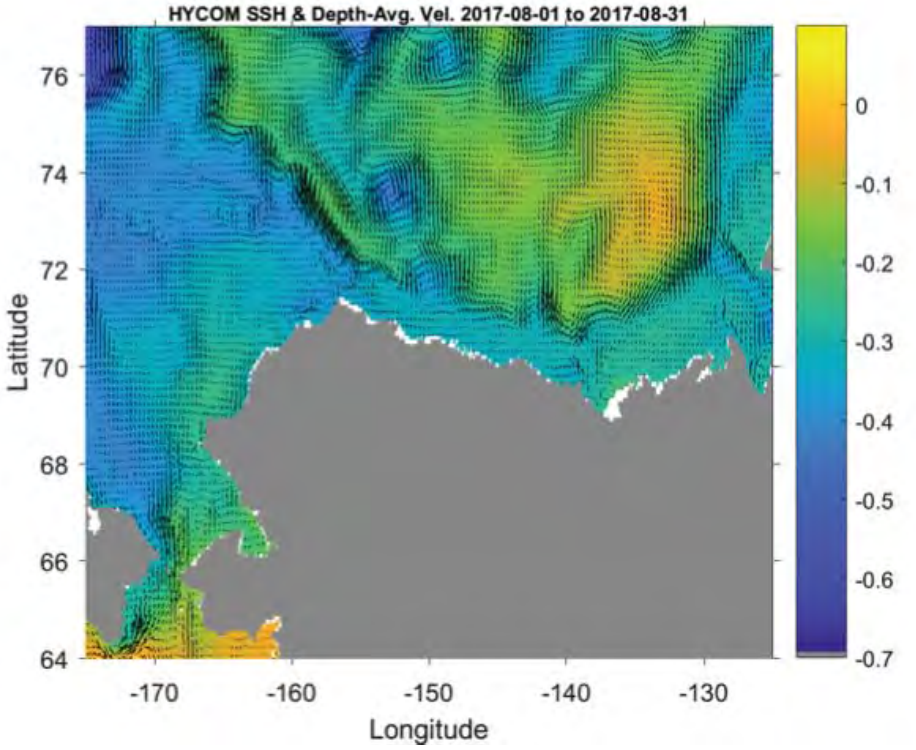


August 2017

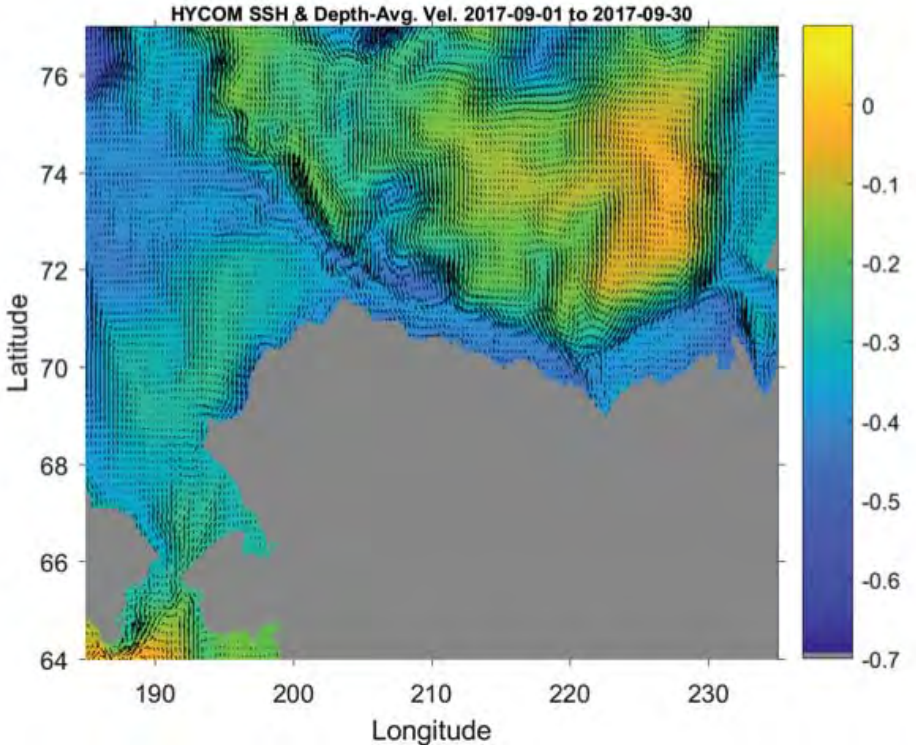


September 2016

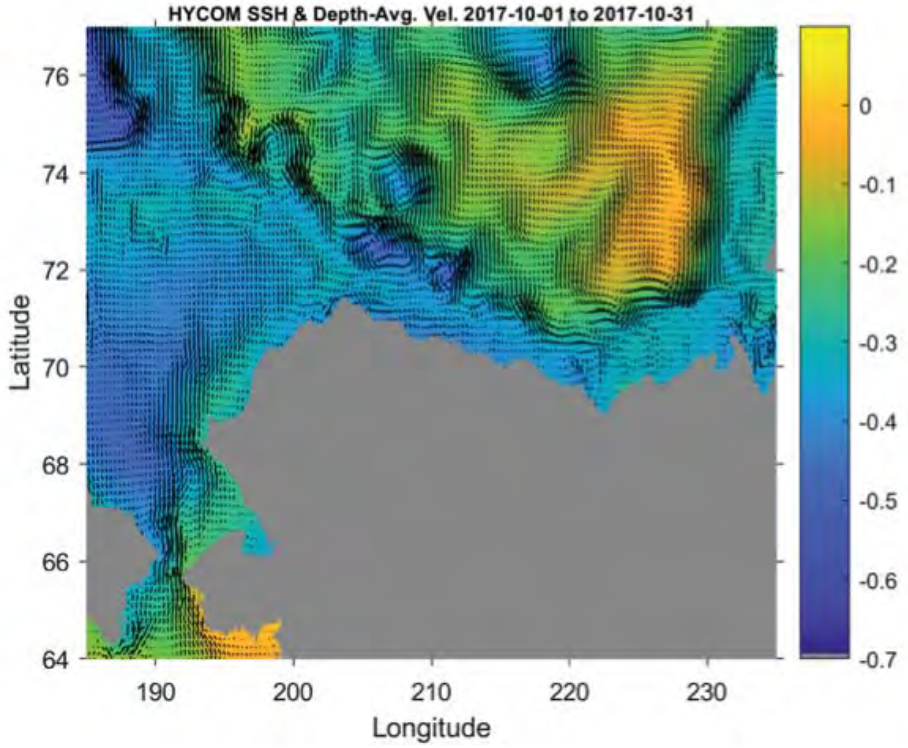


October 2017

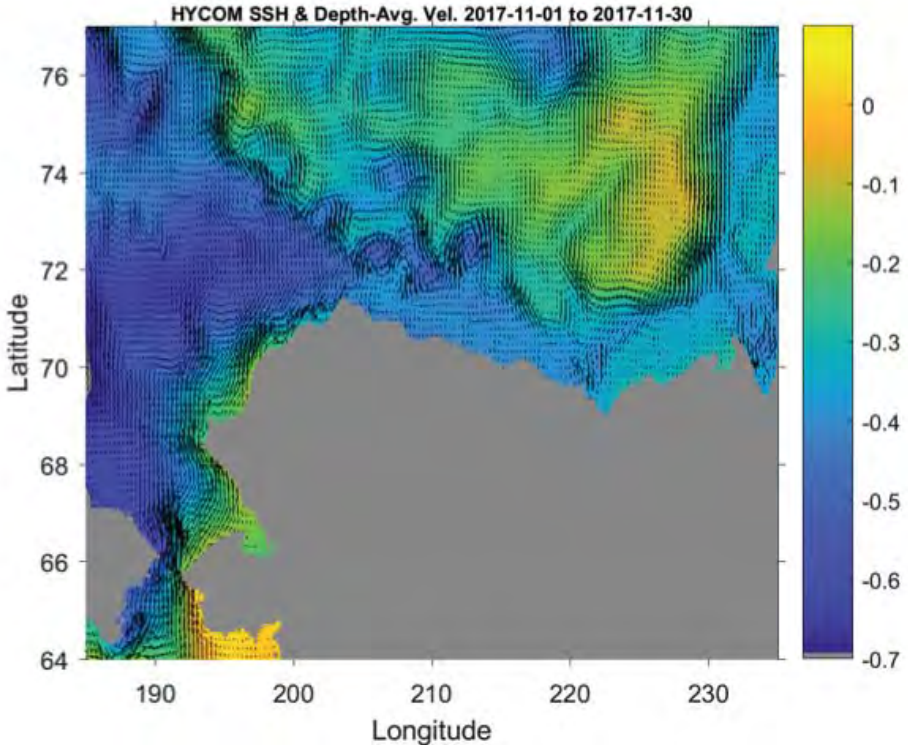


November 2017

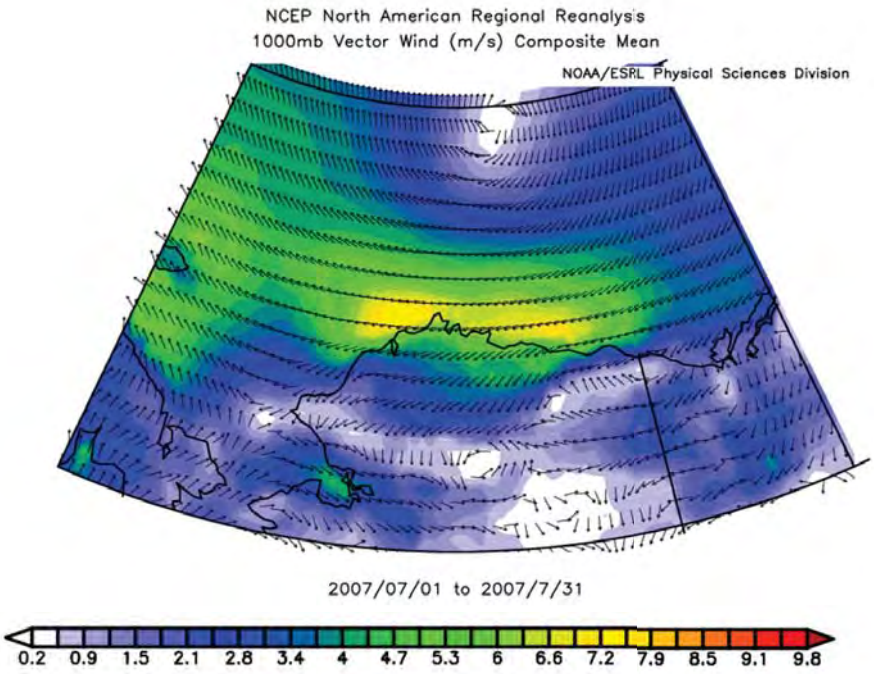


July 2007

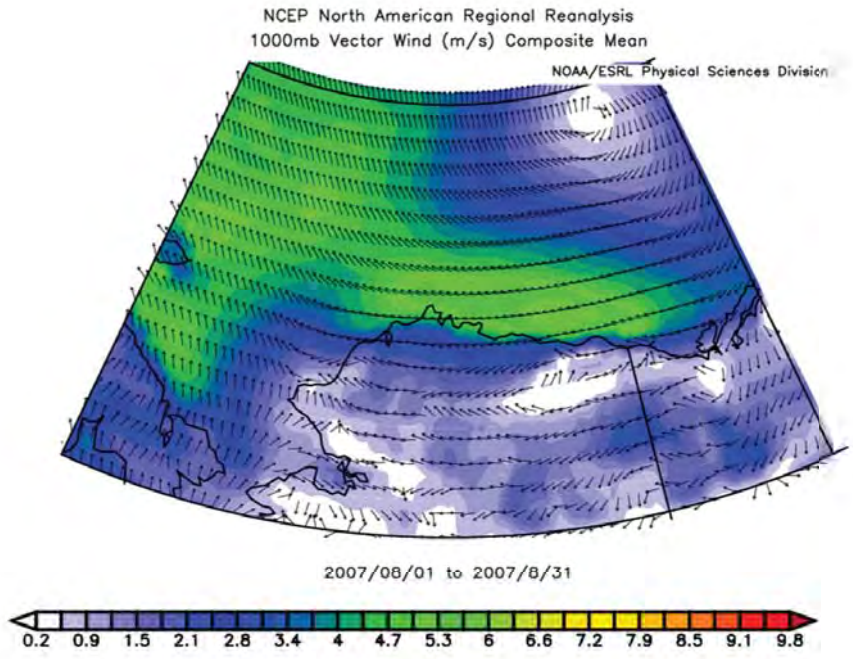


August 2007

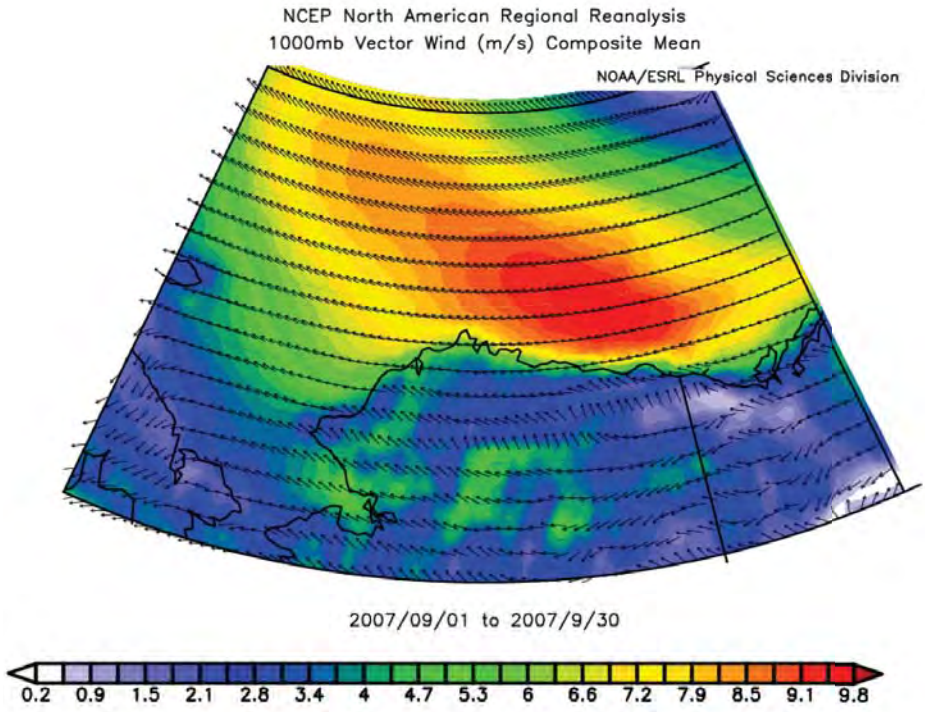


September 2007

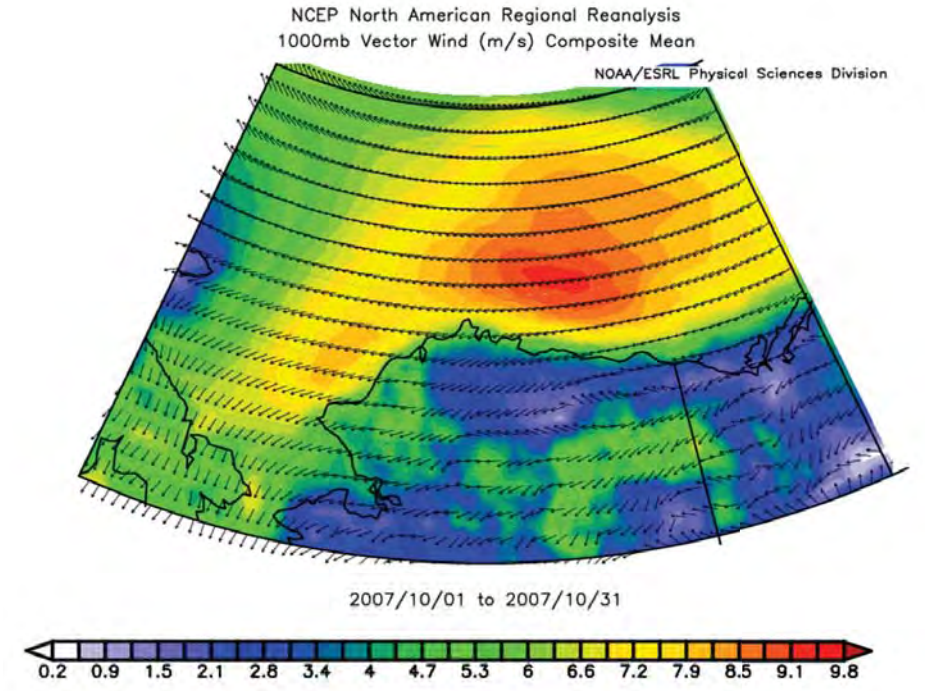


October 2007

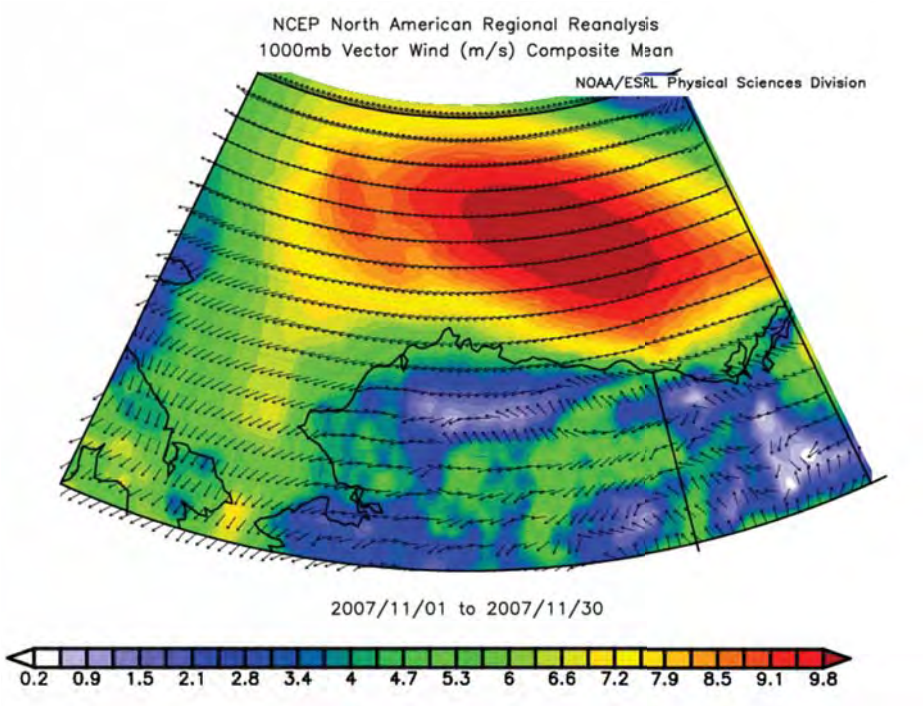


November 2007

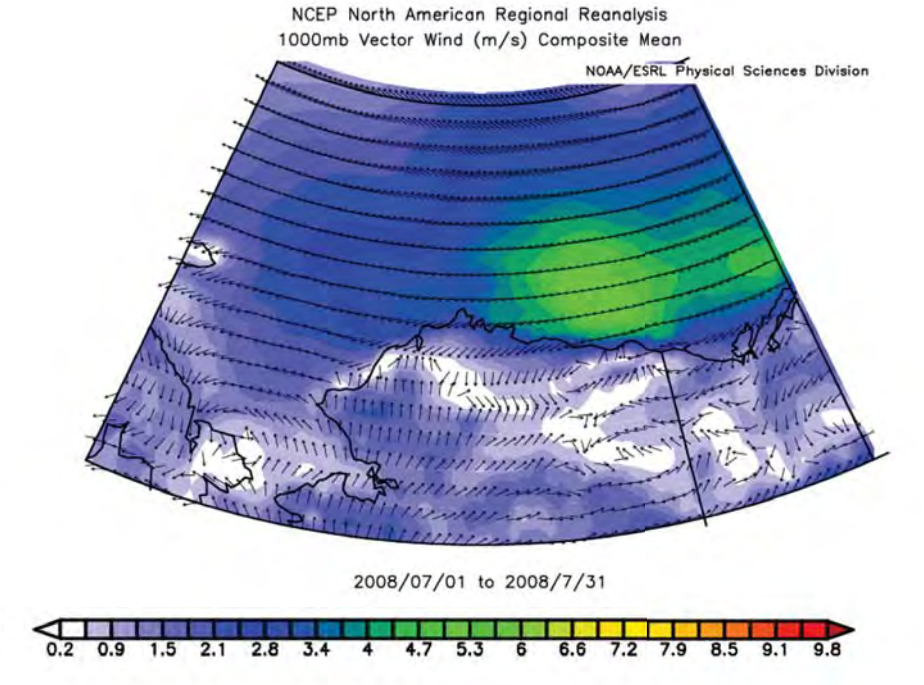


July 2008

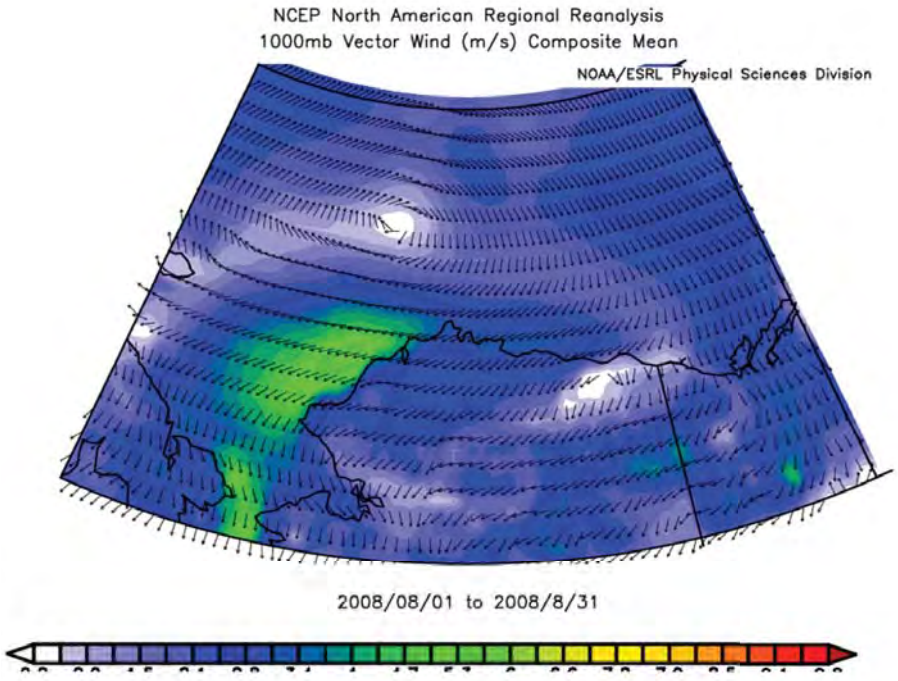


August 2008

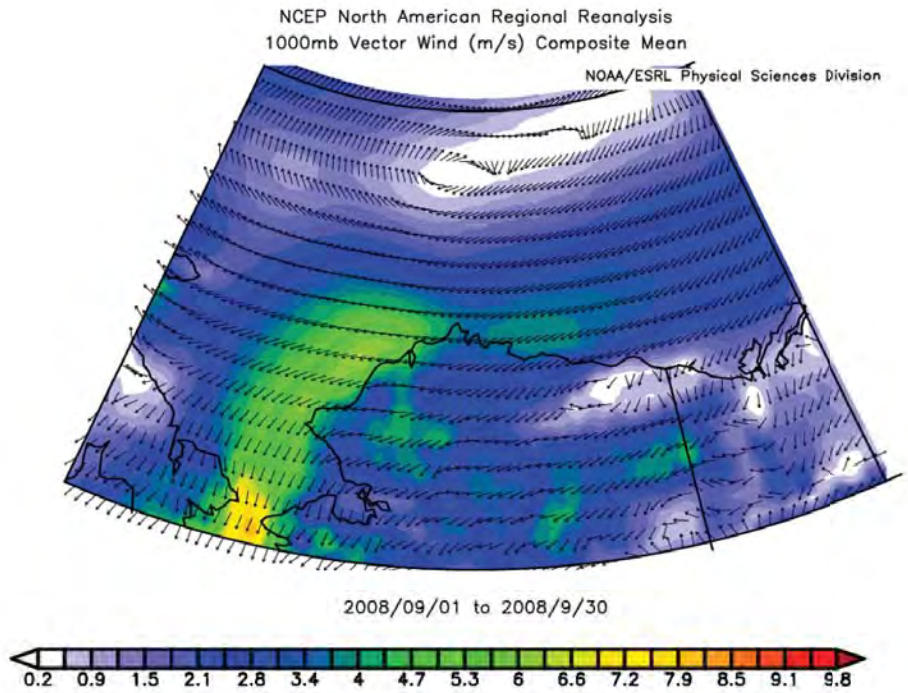


September 2008

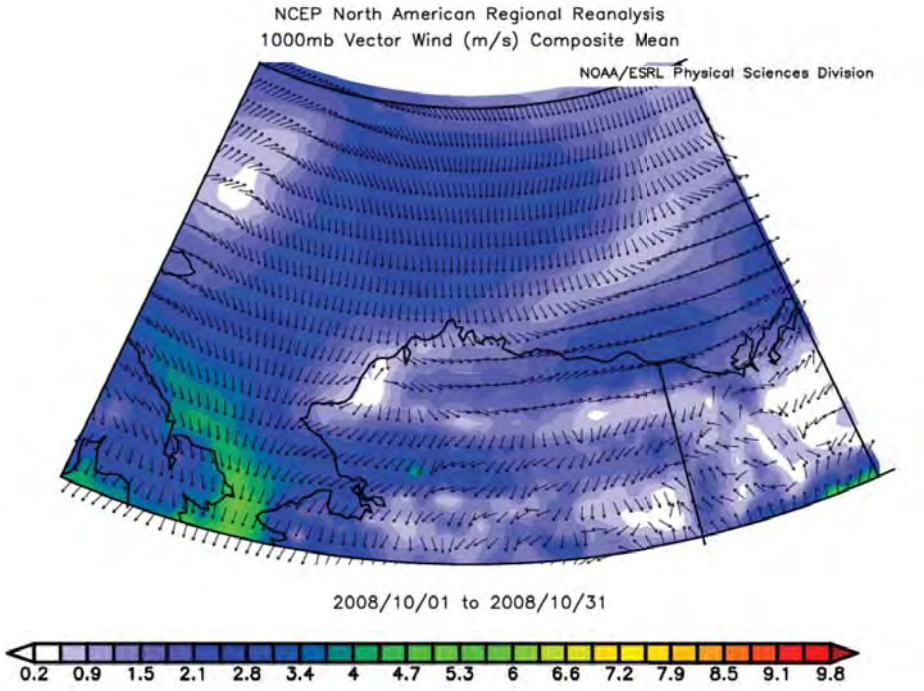


October 2008

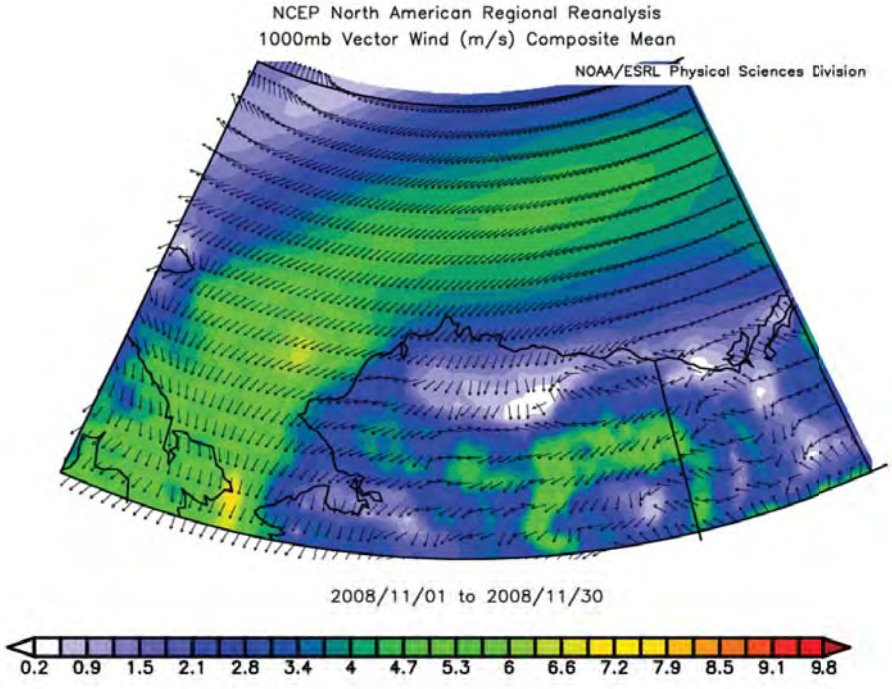


November 2008

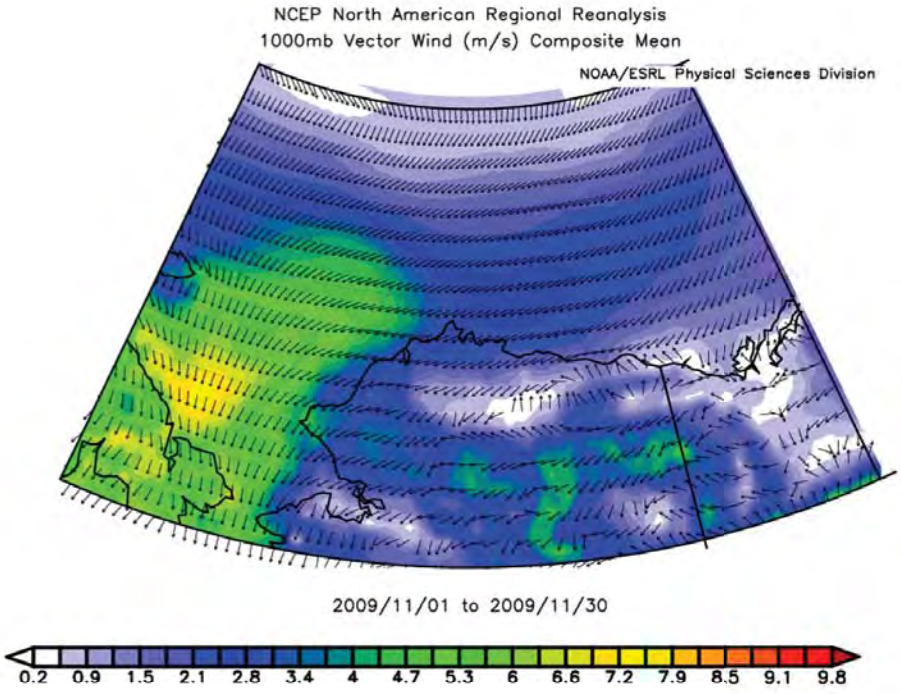


November 2009

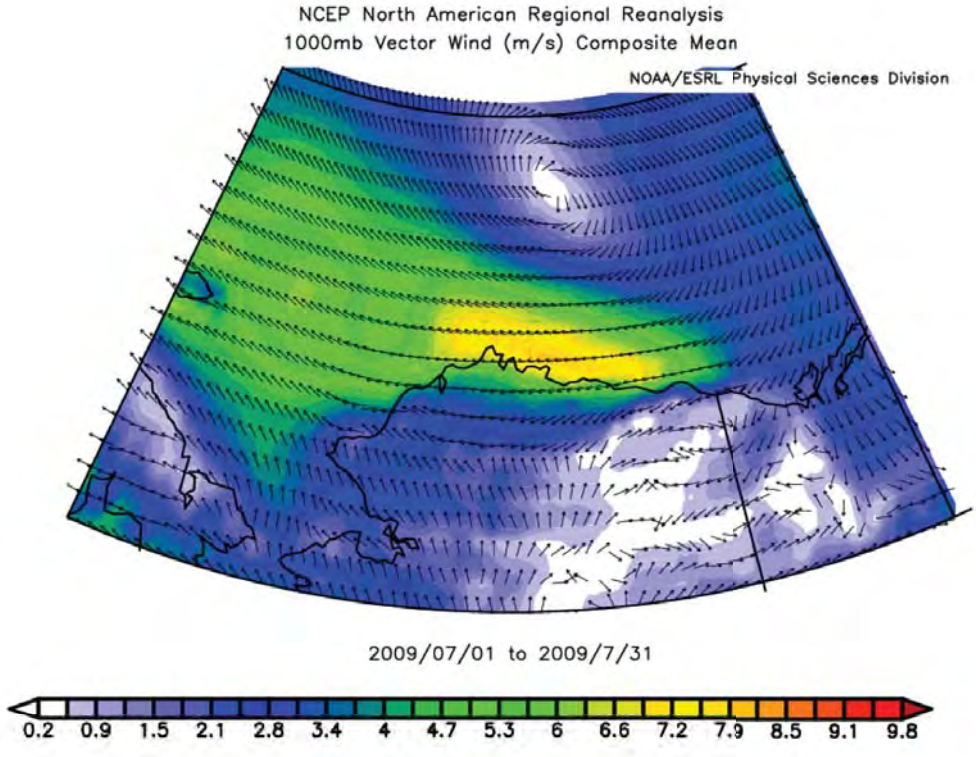

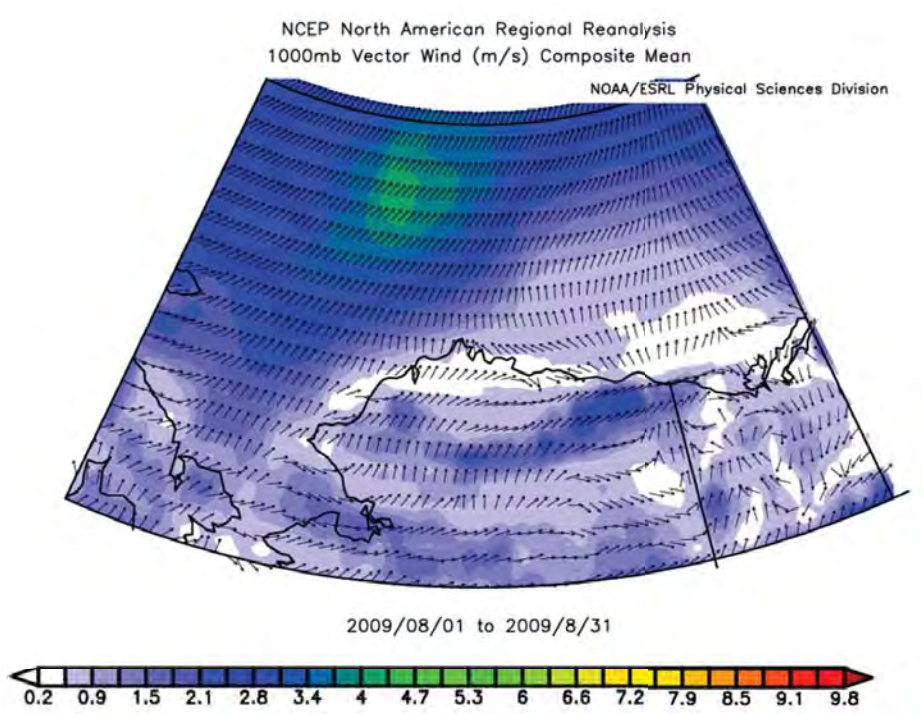


August 2009

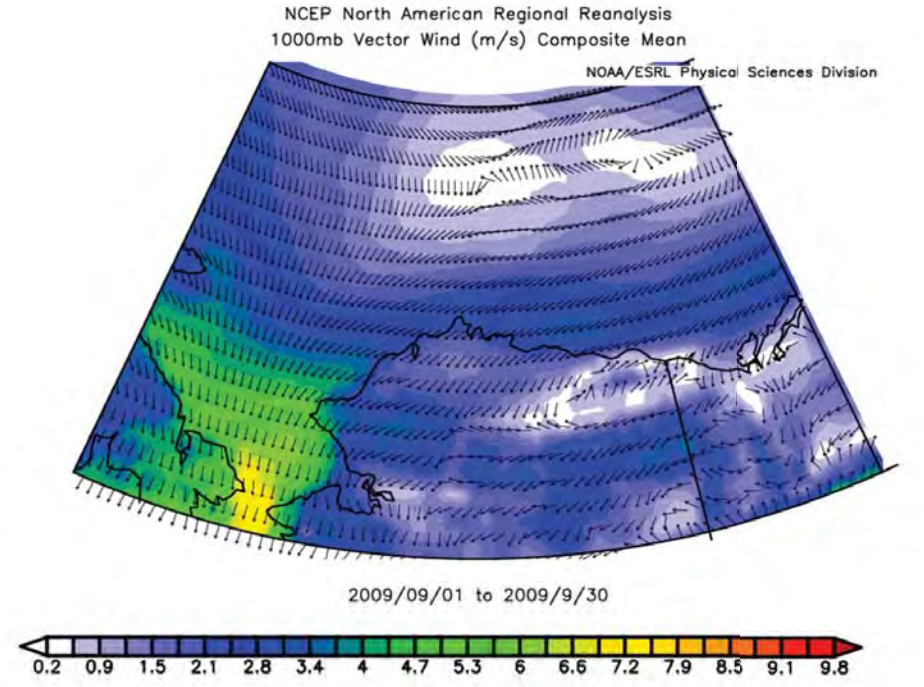


September 2009

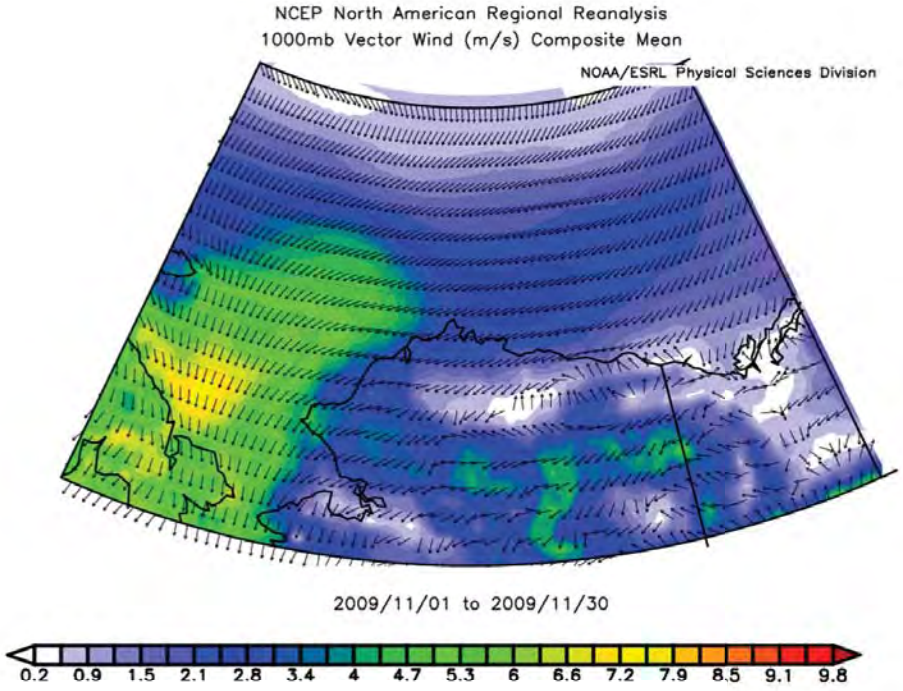


November 2009

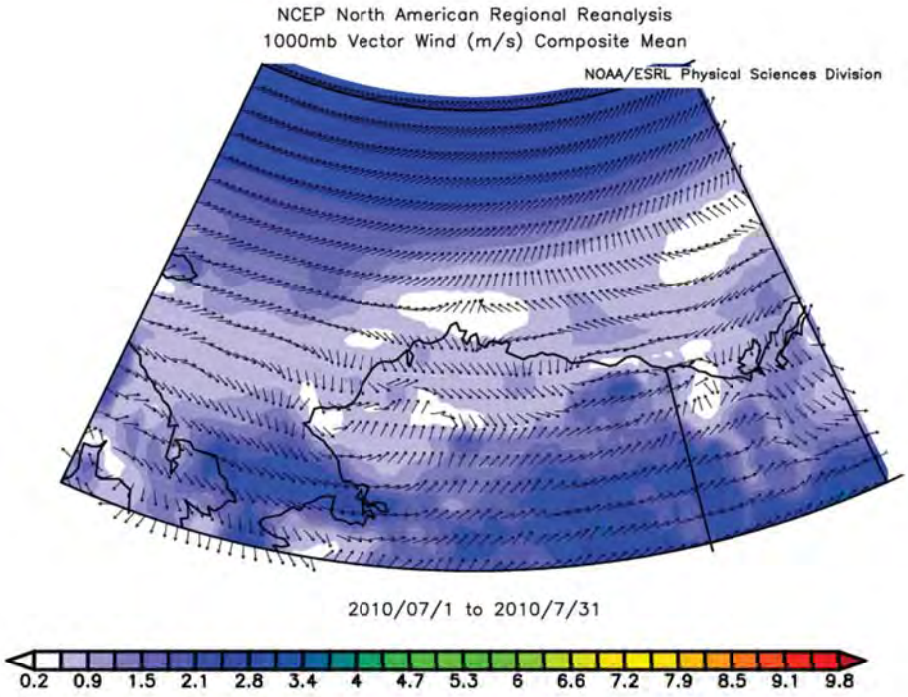


July 2010

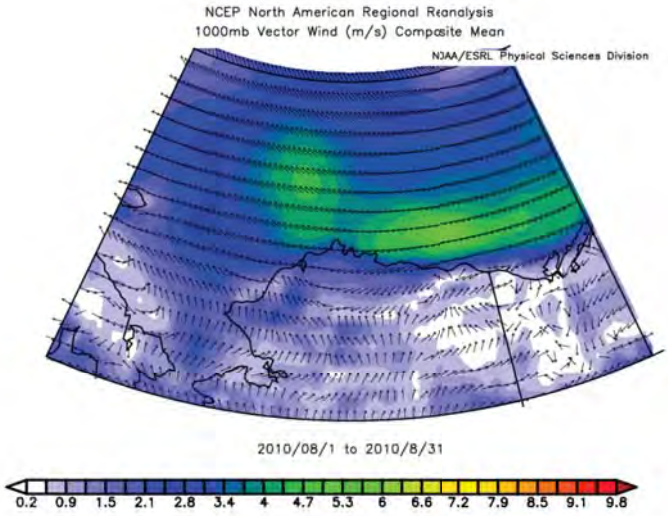


August 2010

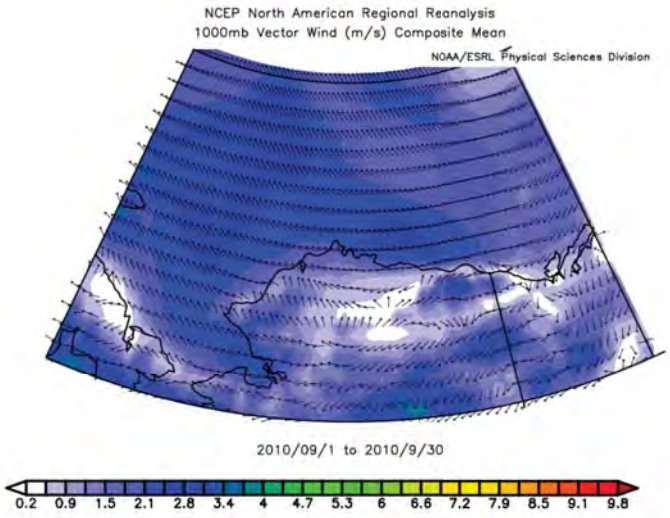


September 2010

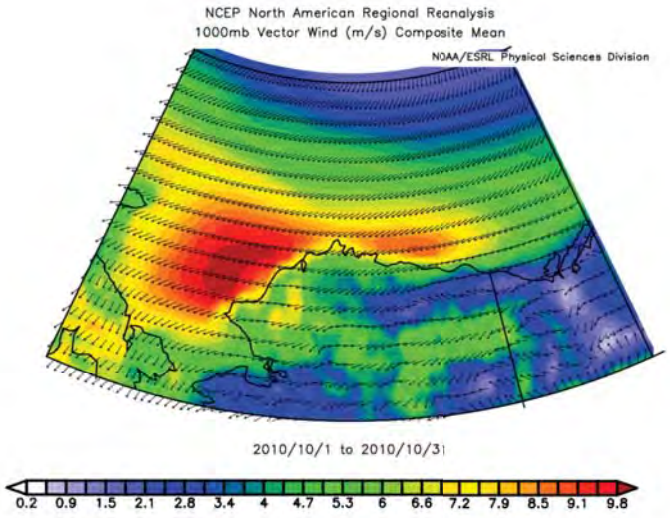


October 2010

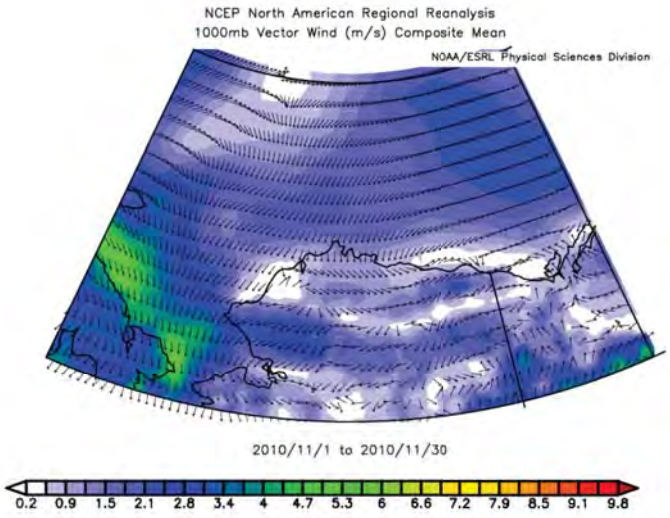


November 2010

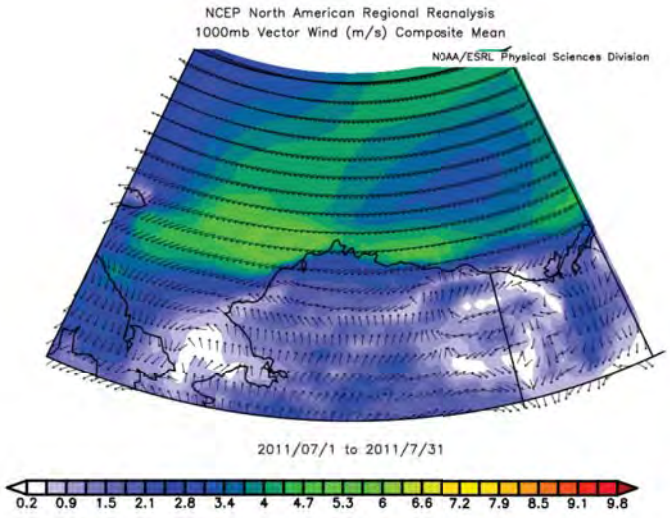


July 2011

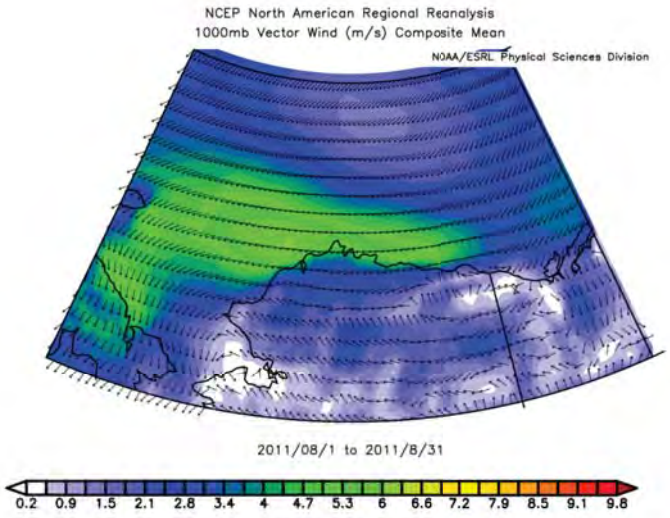


August 2011

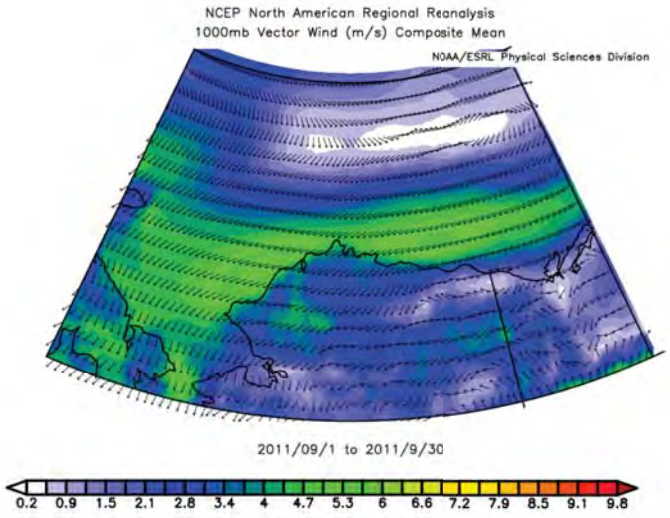


September 2011

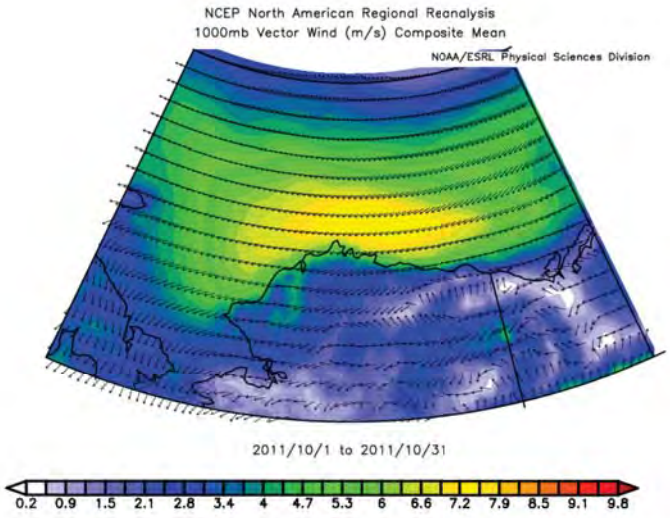


November 2011

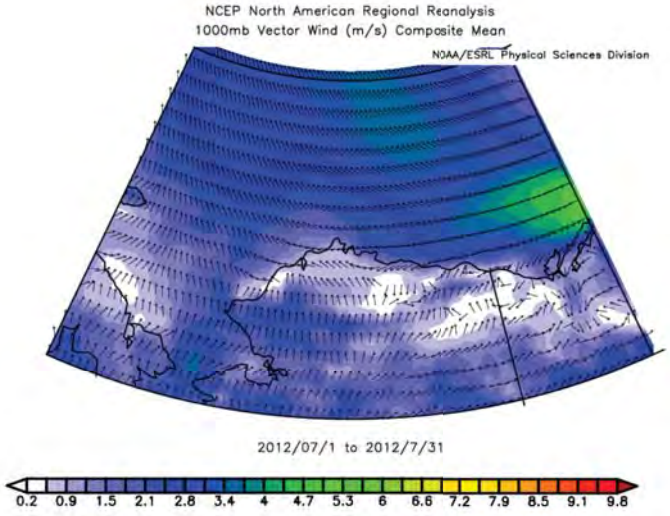


July 2012

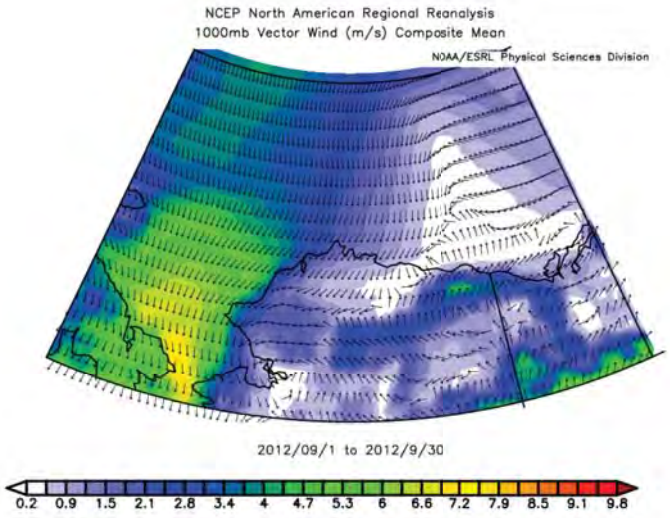


September 2012

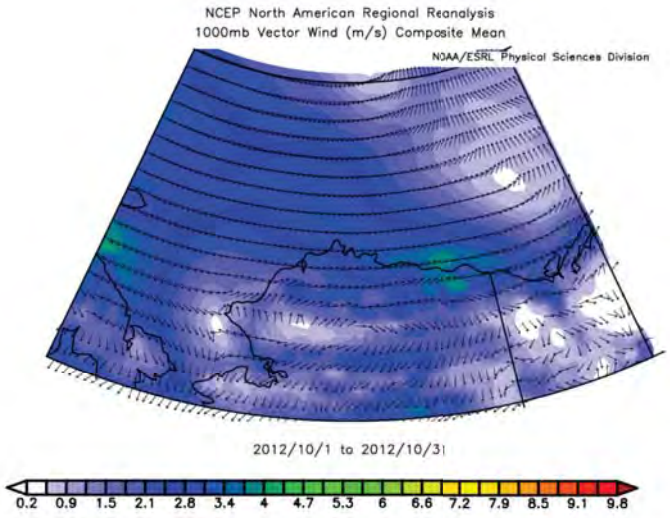


October 2012

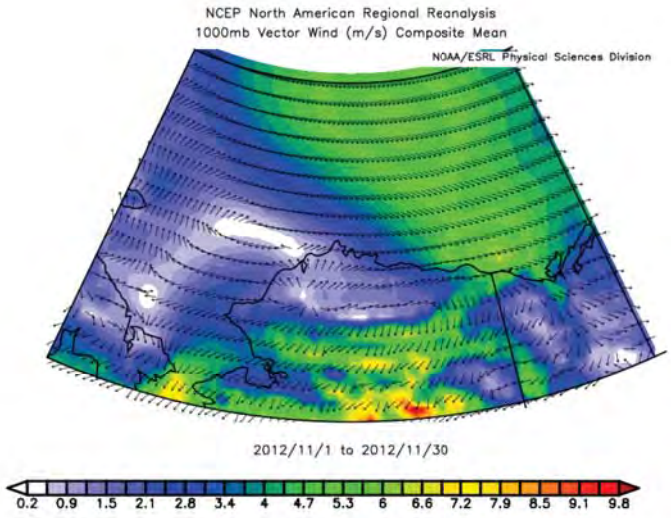


November 2012

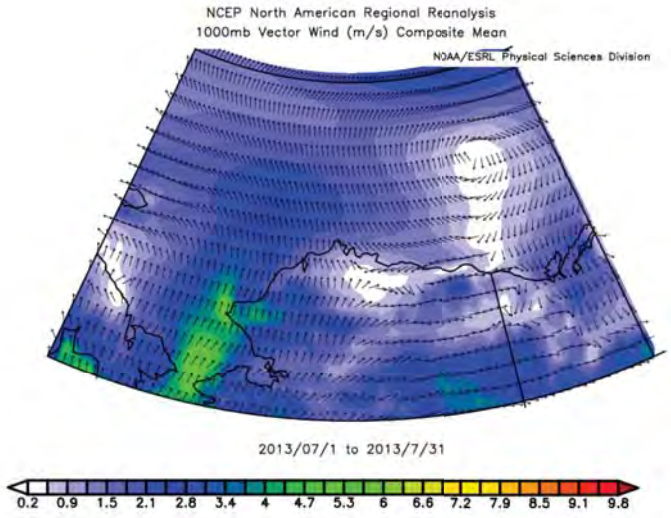


July 2013

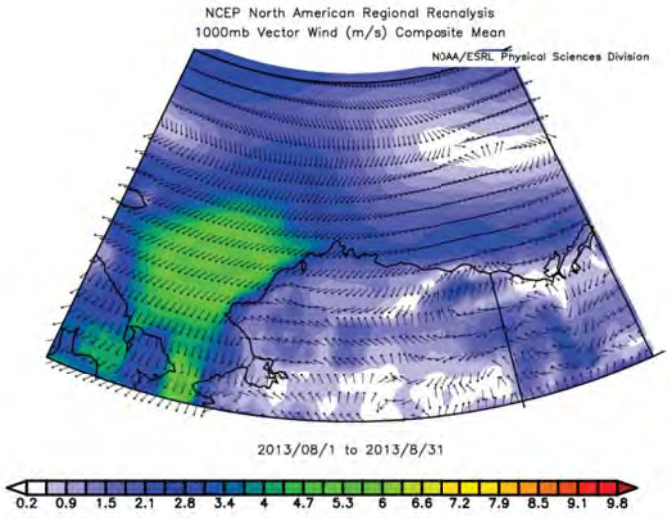


August 2013

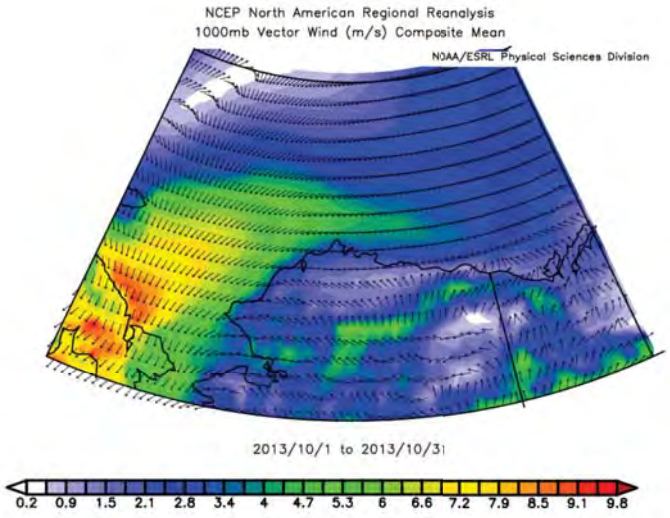


October 2013

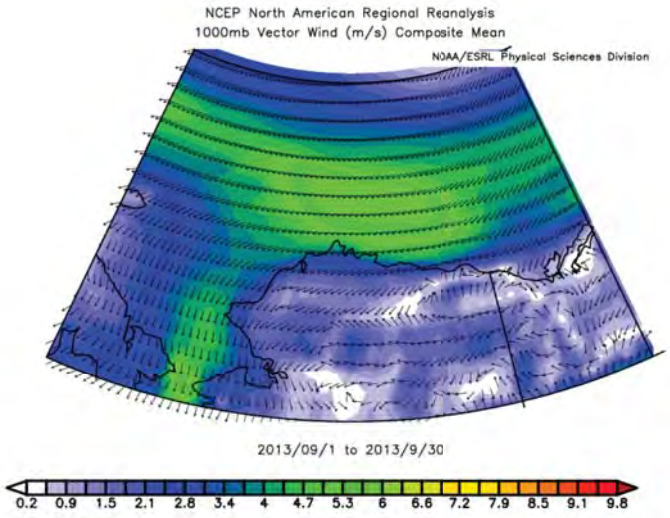


September 2013

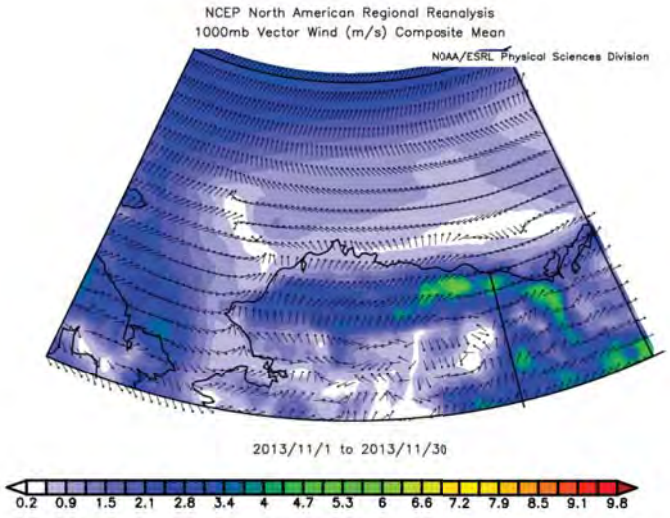


November 2013

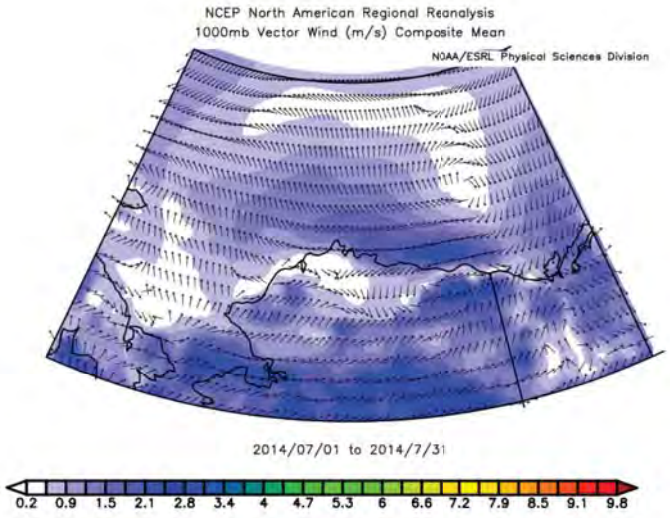


July 2014

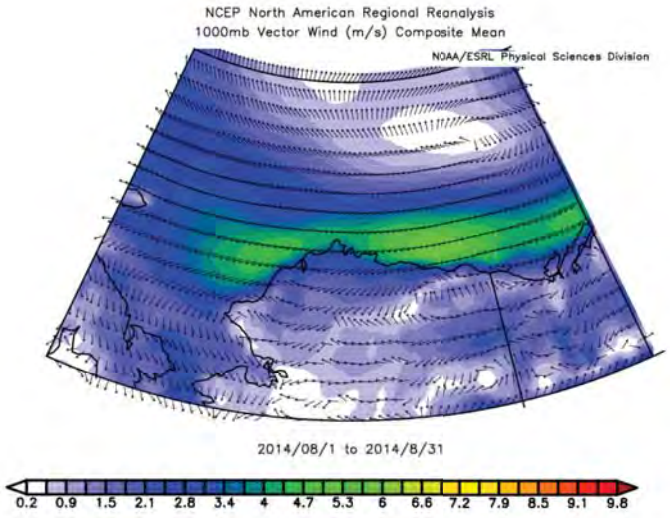


August 2014

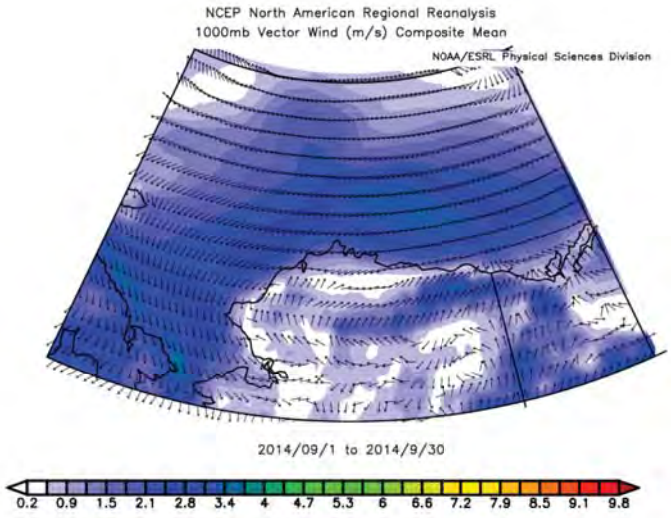


September 2014

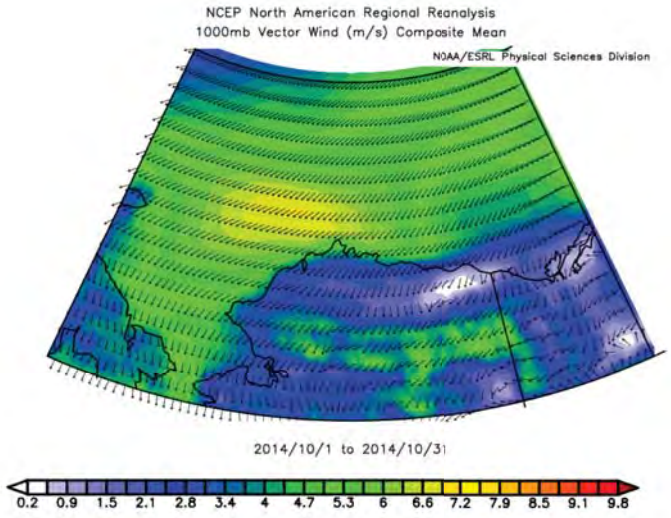


October 2014

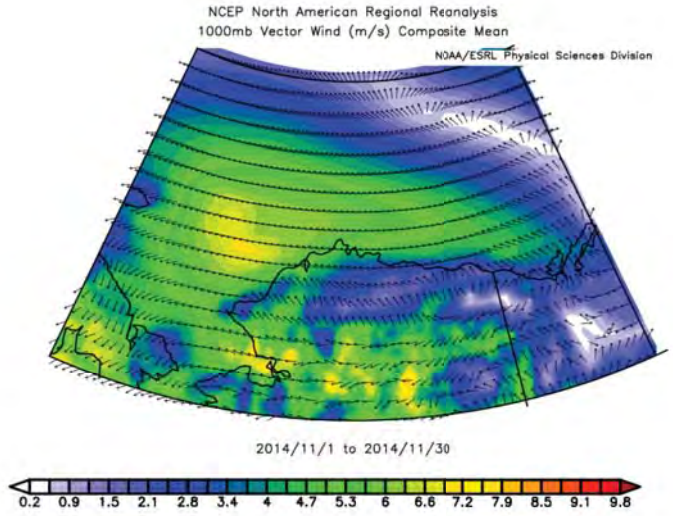


November 2014

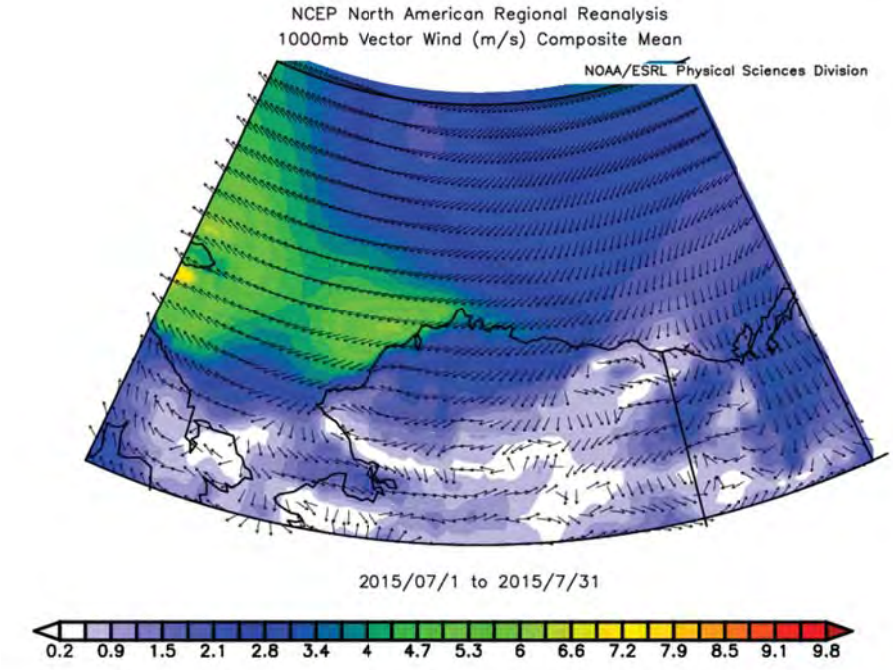


July 2014

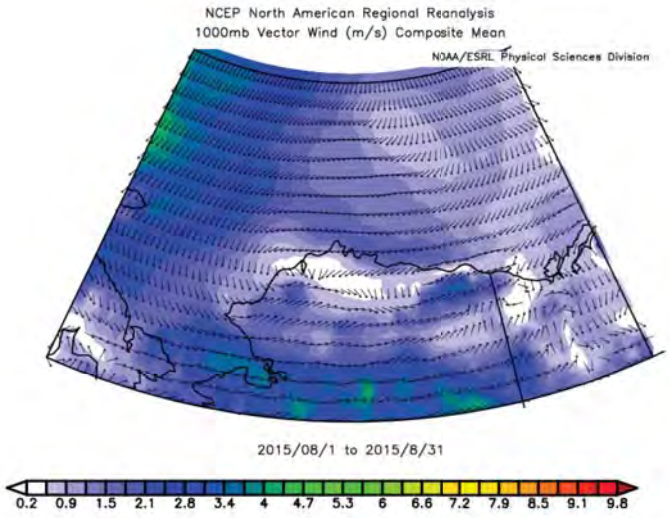


August 2015

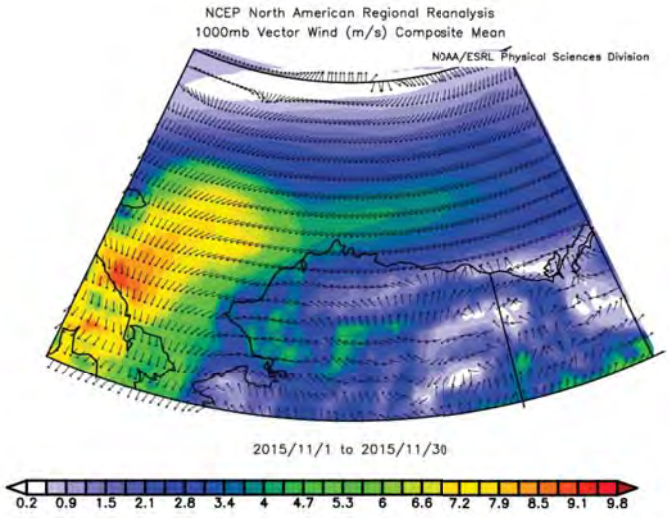


November 2015

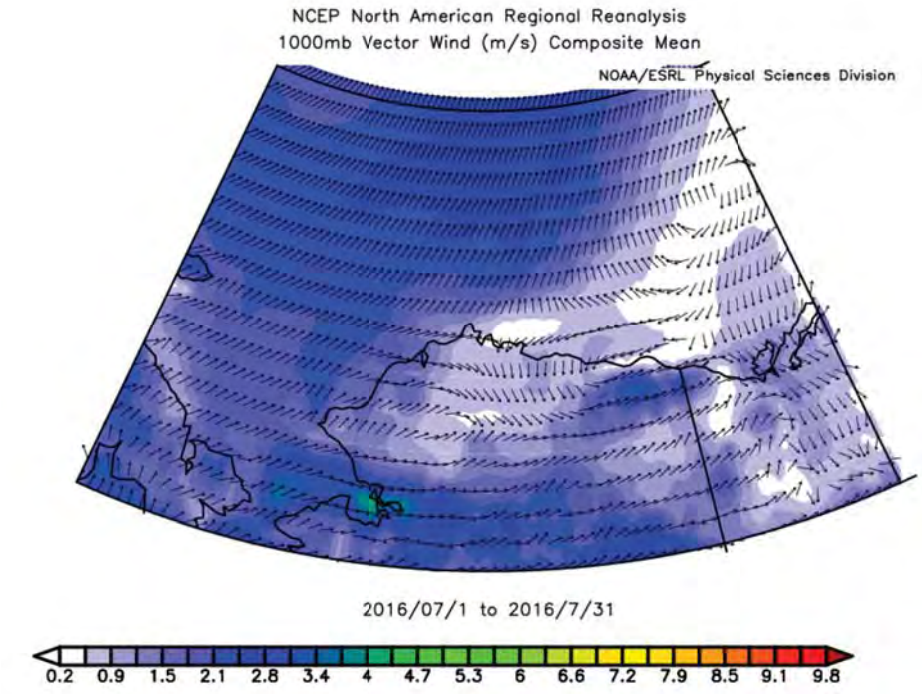


July 2016

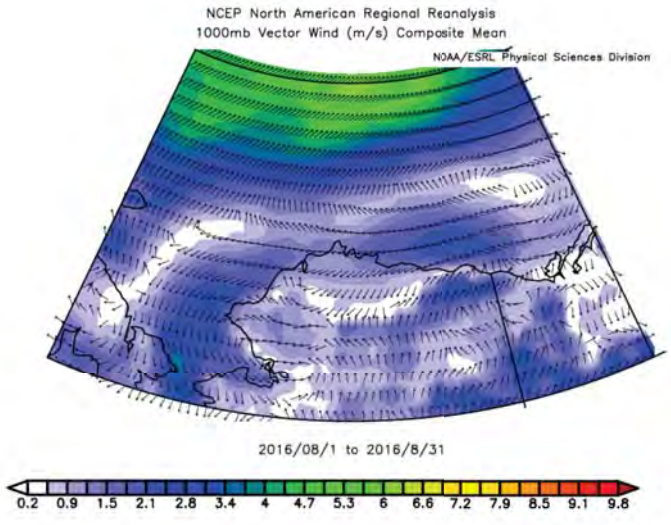


August 2016

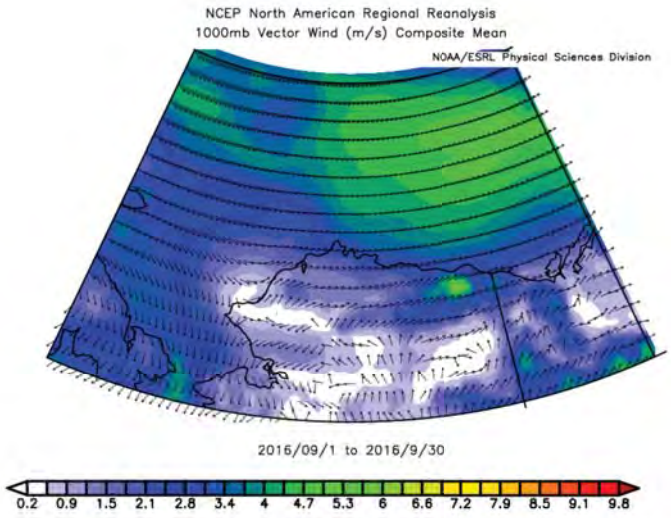


September 2016

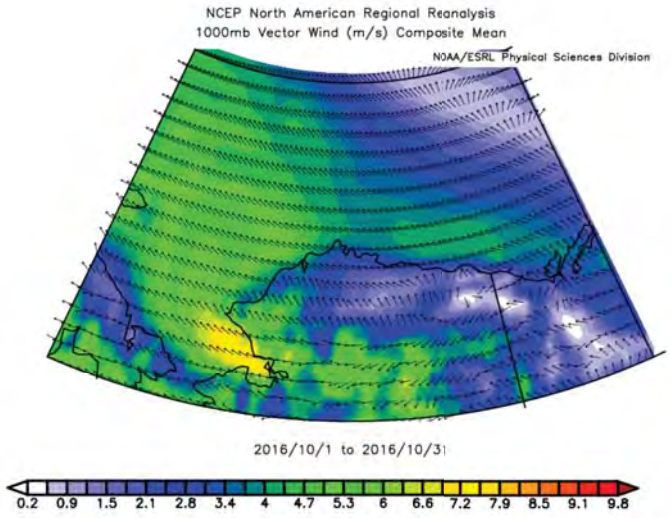


October 2016

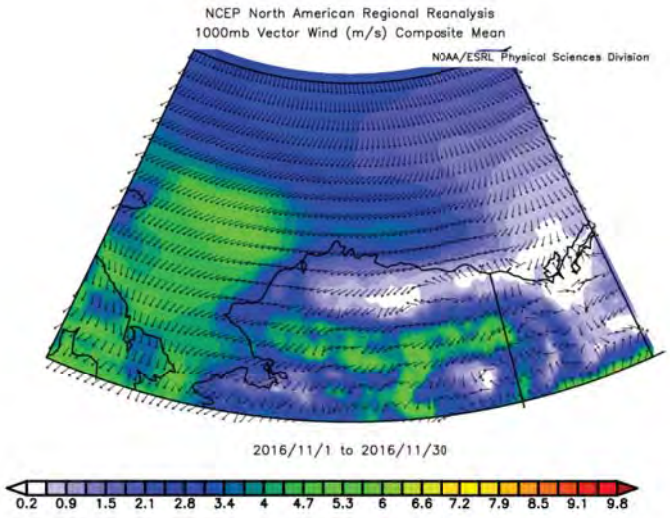


November 2016

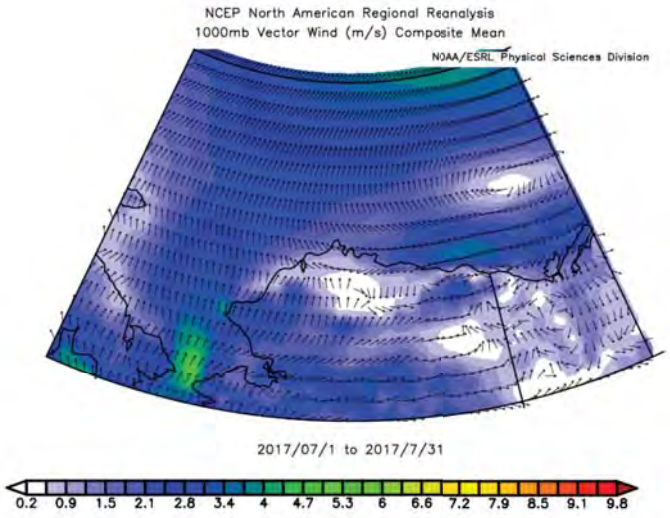


July 2017

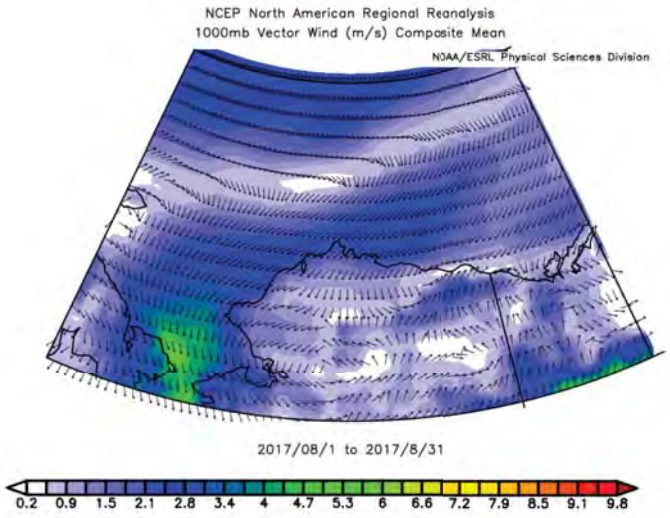


August 2017

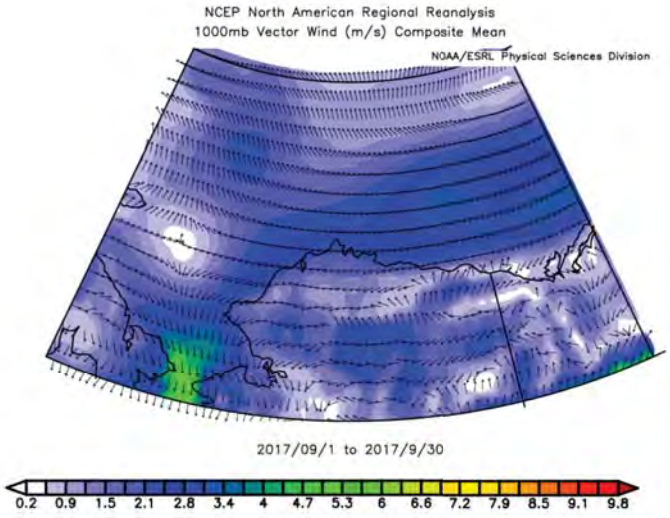


September 2016

# Appendix A

# In-Situ Data - Monthly Average Volume Transport Through Bering Strait

Note: The monthly mean inflow is displayed in Sv.

### A.0.1 Monthly Mean Transport through Bering Strait

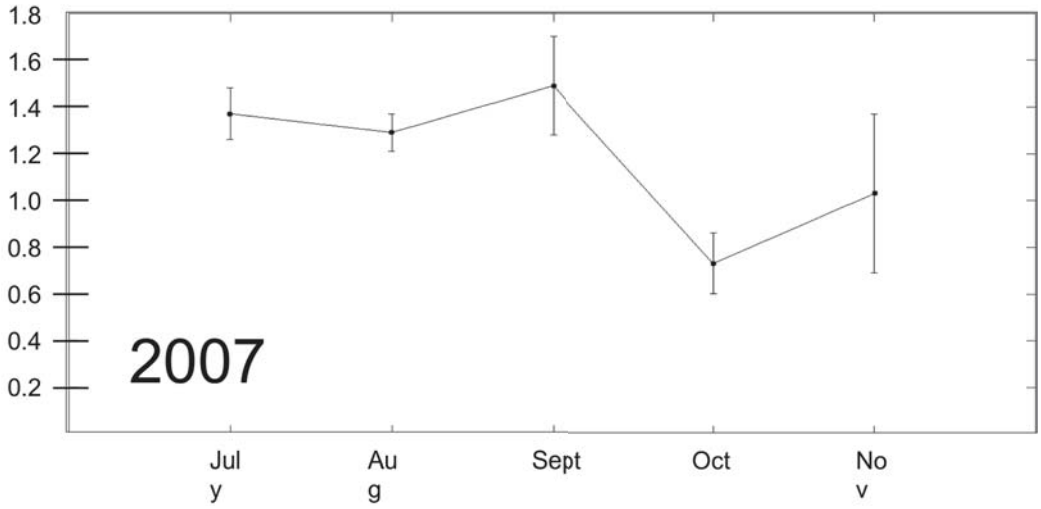
1.8
1.6
1.4
1.2
1.0
0.8
0.6
0.4
0.2
2007
July
Aug
Sept
Oct
Nov

2007

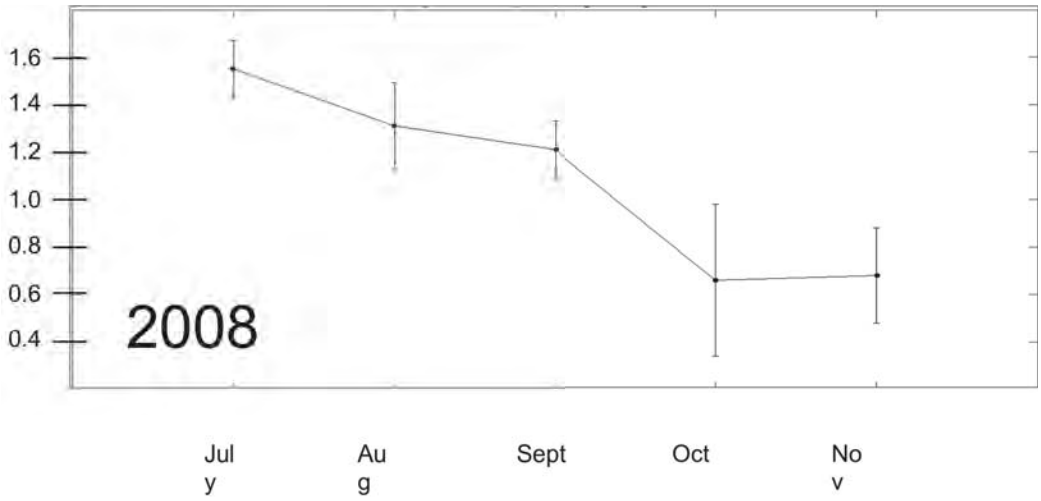
1.6
1.4
1.2
1.0
0.8
0.6
0.4
2008
July
Aug
Sept
Oct
Nov

2008

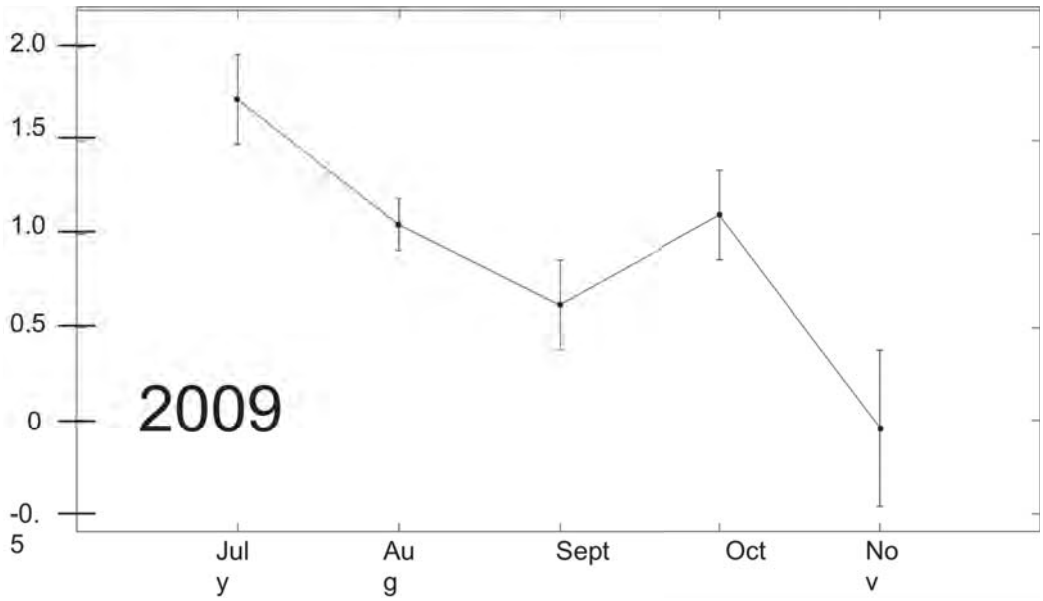
2.0
1.5
1.0
0.5
0
-0.5
2009
July
Aug
Sept
Oct
Nov

2009

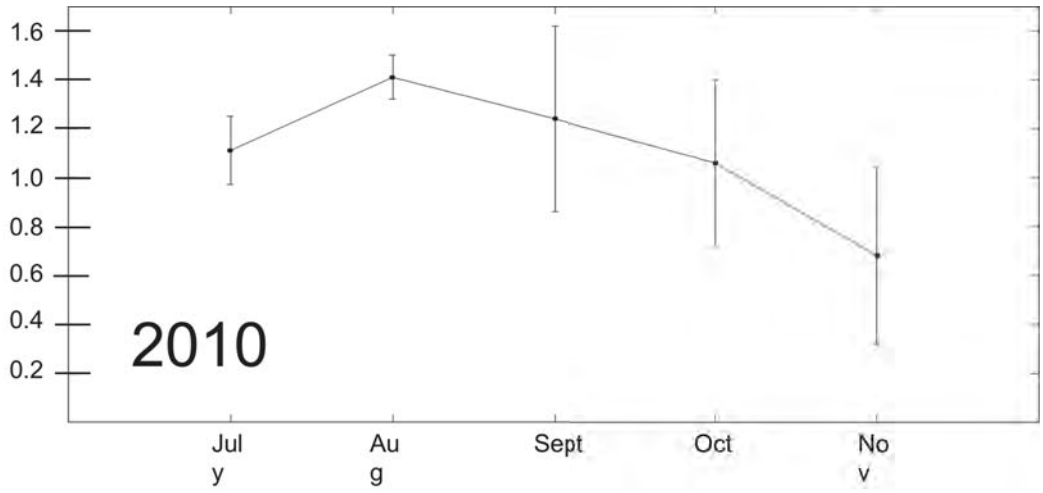
1.6
1.4
1.2
1.0
0.8
0.6
0.4
0.2
2010
July
Aug
Sept
Oct
Nov

2010

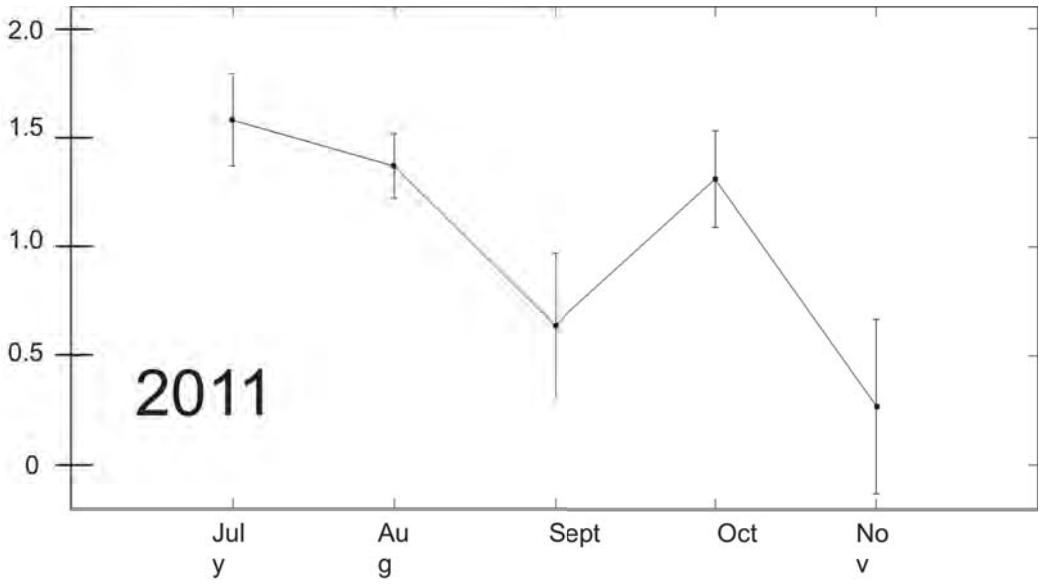
2.0
1.5
1.0
0.5
0
2011
July
Aug
Sept
Oct
Nov

2011

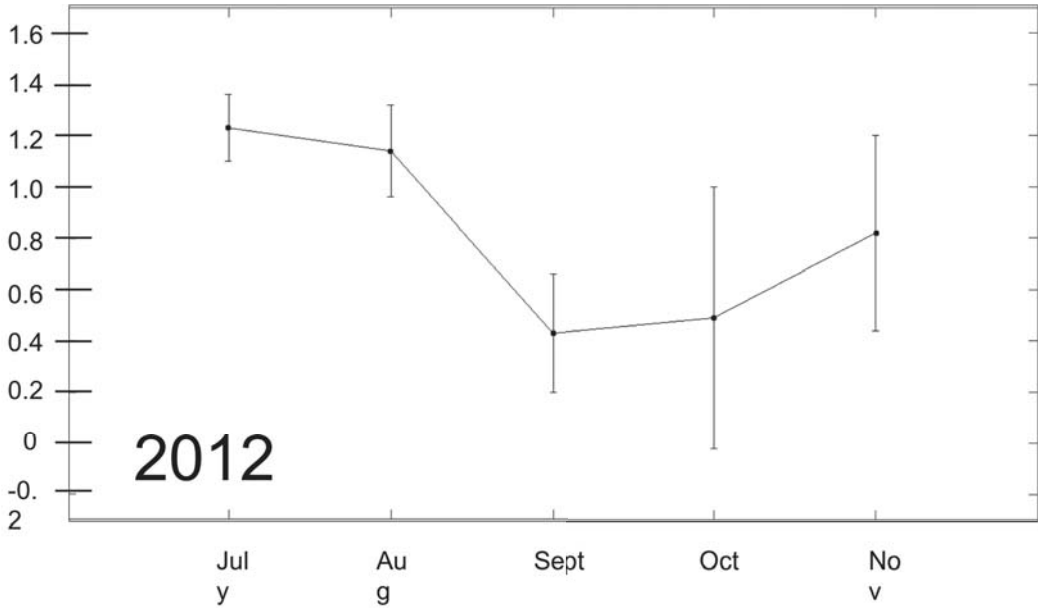
1.6
1.4
1.2
1.0
0.8
0.6
0.4
0.2
0
-0.2
2012
July
Aug
Sept
Oct
Nov

2012

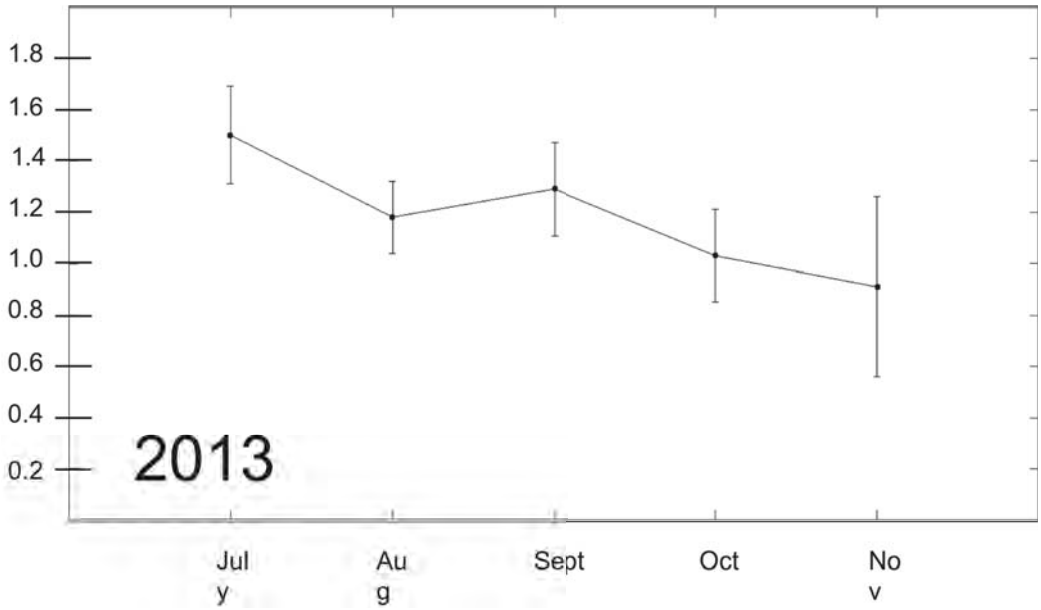
1.8
1.6
1.4
1.2
1.0
0.8
0.6
0.4
0.2
2013
Jul
y
Au
g
Sept
Oct
No
v

2013

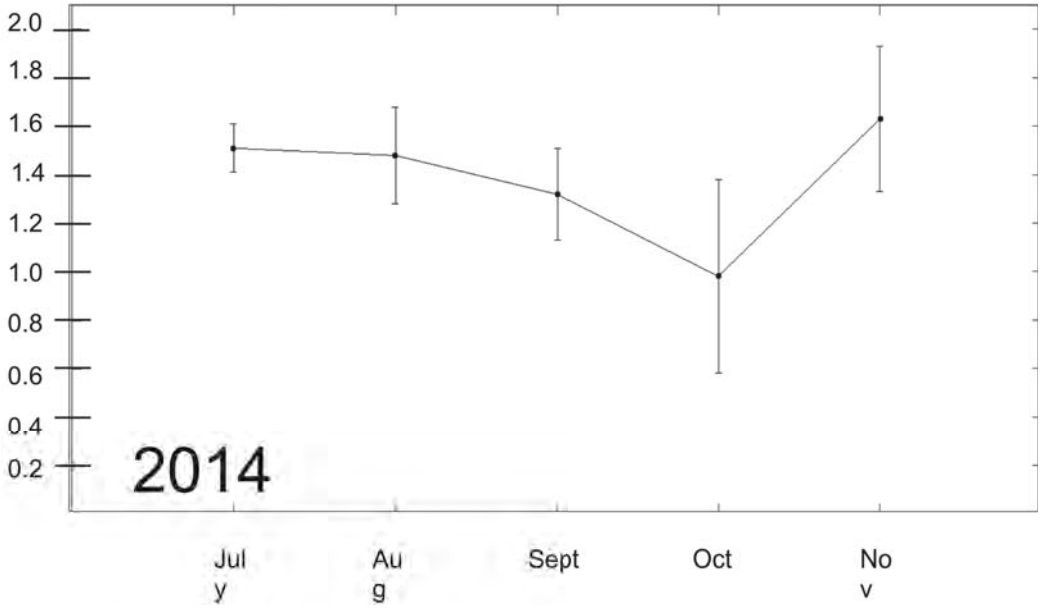
2.0
1.8
1.6
1.4
1.2
1.0
0.8
0.6
0.4
0.2
2014
Jul
y
Au
g
Sept
Oct
No
v

2014

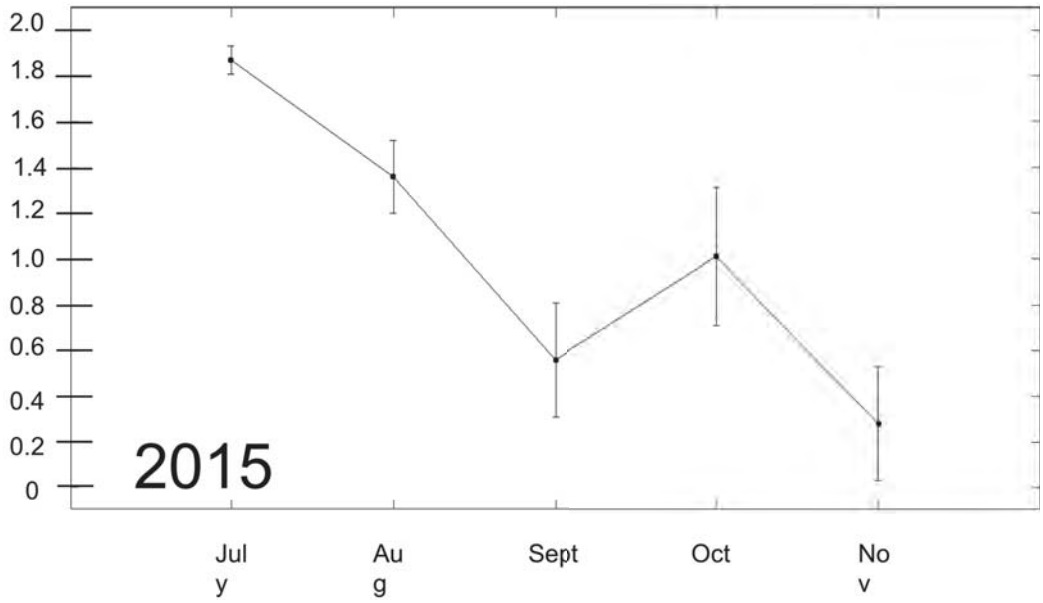


2015

# Bibliography

[1] Aagaard, Ko, and Ee C. Carmack. "The role of sea ice and other freshwater in the Arctic circulation." Journal of Geophysical Research: Oceans 94.C10 (1989): 14485-14498.

[2] Arctic Monitoring and Assessment Program, AMAP assessment report: Arctic pollution issues. Arctic Monitoring and Assessment Programme (AMAP), 1998.

[3] Brugler, Eric T., et al. "Seasonal to interannual variability of the Pacific water boundary current in the Beaufort Sea." Progress in Oceanography 127 (2014): 1-20.

[4] Danielson, Seth L., et al. "Coupled wind-forced controls of the BeringChukchi shelf circulation and the Bering Strait throughflow: Ekman transport, continental shelf waves, and variations of the PacificArctic sea surface height gradient." Progress in Oceanography 125 (2014): 40-61.

[5] Gong, Donglai, and Robert S. Pickart. "Summertime circulation in the eastern Chukchi Sea." Deep Sea Research Part II: Topical Studies in Oceanography 118 (2015): 18-31.

[6] Lewis, Edward Lyn, et al., eds. The freshwater budget of the Arctic Ocean. Vol. 70. Springer Science  Business Media, 2012.

[7] Lin, Peigen, et al. "Seasonal variation of the Beaufort shelfbreak jet and its relationship to Arctic cetacean occurrence." Journal of Geophysical Research: Oceans121.12 (2016): 8434-8454.

[8] Lin, Peigen, et al. "Characteristics and dynamics of wind-driven upwelling in the Alaskan Beaufort Sea based on six years of mooring data." Deep Sea Research Part II: Topical Studies in Oceanography (2018).

[9] Ma, Barry, Michael Steele, and Craig M. Lee. "Ekman circulation in the Arctic Ocean: Beyond the Beaufort Gyre." Journal of Geophysical Research: Oceans 122.4 (2017): 3358-3374.

[10] Morison, James, et al. "Changing arctic ocean freshwater pathways." Nature 481.7379 (2012): 66.

[11] National Research Council. The Arctic in the Anthropocene: Emerging research questions. National Academies Press, 2014.

[12] Lindstrom, Eric J. Ocean Motion and Surface Currents. Ocean Motion : Definition : Ocean in Motion - Ocean Conveyor Belt, NASA Physical Oceanography Program , oceanmotion.org/.

[13] Pickart, Robert S. "Shelfbreak circulation in the Alaskan Beaufort Sea: Mean structure and variability." Journal of Geophysical Research: Oceans 109.C4 (2004).

[14] Pickart, Robert S., et al. "Upwelling in the Alaskan Beaufort Sea: Atmospheric forcing and local versus non-local response." Progress in Oceanography 88.1-4 (2011): 78-100.

[15] Proshutinsky, Andrey, et al. "Beaufort Gyre freshwater reservoir: State and variability from observations." Journal of Geophysical Research: Oceans 114.C1 (2009).

[16] Proshutinsky, A., R. H. Bourke, and F. A. McLaughlin. "The role of the Beaufort Gyre in Arctic climate variability: Seasonal to decadal climate scales." Geophysical Research Letters 29.23 (2002).

[17] Proshutinsky, Andrey, et al. "Arctic circulation regimes." Phil. Trans. R. Soc. A 373.2052 (2015): 20140160.

[18] Proshutinsky, Andrei Y., and Mark A. Johnson. "Two circulation regimes of the winddriven Arctic Ocean." Journal of Geophysical Research: Oceans 102.C6 (1997): 12493-12514.

[19] Stabeno, Phyllis, et al. "Flow Patterns in the Eastern Chukchi Sea: 20102015." Journal of Geophysical Research: Oceans(2018).

[20] Wallcraft, A. J., E. J. Metzger, and S. N. Carroll. Software design description for the hybrid coordinate ocean model (HYCOM), Version 2.2. No. NRL/MR/7320–09-9166. NAVAL RESEARCH LAB STENNIS SPACE CENTER MS OCEANOGRAPHY DIV, 2009.

[21] Woodgate, Rebecca A. "Increases in the Pacific inflow to the Arctic from 1990 to 2015, and insights into seasonal trends and driving mechanisms from year-round Bering Strait mooring data." Progress in Oceanography (2017).